OPTICAL DATA TRANSMISSION THROUGH SCATTERING MEDIA IN FREE SPACE WITH SINGLE-PIXEL DETECTION

PAN ZILAN

PhD

The Hong Kong Polytechnic University

2023

The Hong Kong Polytechnic University
Department of Electronic and Information Engineering

Optical Data Transmission through Scattering Media in Free Space with Single-Pixel Detection

PAN ZILAN

A thesis submitted in partial fulfillment of the requirements
for the degree of Doctor of Philosophy

February 2023

CERTIFICATE OF ORIGINALITY

I hereby declare that this thesis is my own work and that, to the best of my knowledge and belief, it reproduces no material previously published or written, nor material that has been accepted for the award of any degree or diploma, except where due acknowledgement has been made in the text.

_____(Signed)

____PAN Zilan____(Name of Student)

Abstract

Optical data transmission through scattering media is challenging, which has attracted much interest in many fields, such as marine ecology and biomedical science. The existing methods suffer from huge computational cost and limited application ranges, which cannot be effectively applied to complex environment, especially in strongly and randomly scattering media. In this thesis, high-fidelity and high-robustness optical analog-signal transmission through scattering media is proposed and systematically studied, e.g., turbid water and biological tissue.

The first challenging task is how to realize high-fidelity and high-efficiency optical analog-signal transmission in static and turbid water. I have proposed a new method to optically transmit analog signals in free space through static and turbid water. Each pixel of original signal is sequentially encoded into random amplitude-only patterns as information carrier. A single-pixel detector is utilized to collect light intensities at the receiving end. Experimental results demonstrate that the proposed method shows high robustness against different propagation distances through turbid water and resists the effect of various turbulence factors. The proposed method is easy to operate and is cost-effective, which could open up a novel insight into optical signal transmission in free space through turbid water.

The second challenging task is to deal with the obstacles in the optical path, e.g., walls, rocks, suspended particles and organic matters or planktonic organisms in water. A non-line-of-sight (NLOS) optical transmission system is built to realize high-fidelity optical analog-signal transmission through turbid water around a corner. Optical experimental results demonstrate the feasibility of the proposed method when there is an obstacle

behind turbid water. In addition, the proposed method possesses a wide detection range at the receiving end, which is of great significance in practical applications.

The third challenging task is how to achieve high-accuracy optical analog-signal transmission in free-space through non-static scattering media, e.g., dynamic and turbid water. I have proposed an effective method by using a series of dynamic scaling factors to temporally correct light intensities recorded by a single-pixel bucket detector. A fixed reference pattern is utilized to obtain the series of dynamic scaling factors during optical data transmission in free space. It is demonstrated that the proposed scheme is robust against water-flow-induced turbulence and turbid water, and high-fidelity free-space optical information transmission is realized at wavelengths of 658.0 nm and 520.0 nm.

The fourth challenging task is how to realize accurate optical information transmission and achieve large penetration depth through thick biological tissues. The proposed method utilizes zero-frequency modulation to generate a series of 2D random amplitude-only patterns. The proposed method realizes accurate optical information transmission through thick biological tissues, and can overcome the challenges, e.g., penetration through small-thickness tissues and low quality of the retrieved signals.

My study in this thesis opens up a new research perspective for theoretical understanding and experimental verifications of high-fidelity free space optical analog-signal transmission through complex scattering media including static and dynamic environment. My research work will benefit the development of optical wireless data transmission in various research fields, e.g., marine ecology and biomedical science.

Publications

Journal Papers

(1) **Zilan Pan**, Yin Xiao, Yonggui Cao, Lina Zhou, and Wen Chen, "Optical analog-signal transmission and retrieval through turbid water," Applied Optics, 60 (34), 10704–10713, 2021. (**Editors' Pick**)

(2) **Zilan Pan**, Yin Xiao, Lina Zhou, Yonggui Cao, Mo Yang, and Wen Chen, "Non-line-of-sight optical information transmission through turbid water," Optics Express, 29 (24), 39498–39510, 2021.

(3) **Zilan Pan,** Yin Xiao, Yonggui Cao, Lina Zhou, and Wen Chen, "Optical data transmission through highly dynamic and turbid water using dynamic scaling factors and single-pixel detector," Opt. Express 30(24), 43480–43490 (2022).

(4) **Zilan Pan,** Yin Xiao, Yonggui Cao, Lina Zhou, and Wen Chen, "Accurate optical information transmission through thick tissues using zero-frequency modulation and single-pixel detection," Optics and Lasers in Engineering, 158, 107133(7pp), 2022.

(5) Lina Zhou, Yin Xiao, **Zilan Pan**, Yonggui Cao, and Wen Chen, "Optical hiding based on single-input multiple-output and binary amplitude-only holograms via the modified Gerchberg-Saxton algorithm," Optics Express, 29 (16), 25675–25696, 2021.

(6) Yin Xiao, Lina Zhou, **Zilan Pan**, Yonggui Cao, Mo Yang, and Wen Chen, "Analog ghost hidden in 2D random binary patterns for free-space optical data transmission," Optics and Lasers in Engineering, 150, 106880 (5pp), 2022.

(7) Yin Xiao, Lina Zhou, **Zilan Pan**, Yonggui Cao, and Wen Chen, "Physically-enhanced ghost encoding," Optics Letters, 47 (2), 433–436, 2022.

(8) Lina Zhou, Yin Xiao, **Zilan Pan**, Yonggui Cao, and Wen Chen, "Visual cryptography using binary amplitude-only holograms," Frontiers in Photonics, 2, 821304 (10pp), 2022.

(9) Yin Xiao, Lina Zhou, **Zilan Pan**, Yonggui Cao, and Wen Chen, "Physically-secured high-fidelity free-space optical data transmission through scattering media using dynamic scaling factors," Optics Express, 30 (5), 8186–8198, 2022.

(10) Yonggui Cao, Yin Xiao, **Zilan Pan**, Lina Zhou, and Wen Chen, "Direct generation of 2D arrays of random numbers for high-fidelity optical ghost diffraction and information transmission through scattering media," Optics and Lasers in Engineering, 158, 107141 (8pp), 2022.

(11) Yonggui Cao, Yin Xiao, **Zilan Pan**, Lina Zhou, and Wen Chen, "High-fidelity temporally-corrected transmission through dynamic smoke via pixel-to-plane data encoding," Optics Express, 30 (20), 36464–36477, 2022.

(12) Yonggui Cao, Yin Xiao, **Zilan Pan**, Lina Zhou, and Wen Chen, "Physically-secured ghost diffraction and transmission," IEEE Photonics Technology Letters, 34 (22), 1238–1241, 2022.

Conference Papers

(1) **Zilan Pan**, Yin Xiao, Lina Zhou, and Wen Chen, "Optical transmission through thick biological tissue using optical modulation," International Conference on Optical and Photonic Engineering (icOPEN 2022), Proceedings of SPIE, 24–27 November 2022, Nanjing, China (BEST STUDENT PRESENTATION AWARD-3rd Prize).

(2) Yonggui Cao, Yin Xiao, **Zilan Pan**, and Wen Chen, "2D arrays of random numbers as holograms for optical data transmission through scattering media in free space," Optica

Imaging and Applied Optics Congress, OPTICA, 11–15 July 2022, Vancouver, British Columbia, Canada.

Acknowledgments

First and foremost, I would like to express my heartfelt thanks to my supervisor, Dr. Chen Wen, for providing me with this unique opportunity to broaden my horizon and purse my PhD study at The Hong Kong Polytechnic University. With his priceless guidance and great patience, I learned how to conduct research and the importance of persistence when facing obstacles. Dr. Chen provided me with enormous help and advice in research and scientific writing, which benefited me throughout my PhD journey. I also benefited greatly from his rigorous attitude towards work, with which I will keep in my future path. Besides, I am deeply grateful to my co-supervisor Prof. Yu Changyuan, the expert in optical fiber. His positive and encouraging attitude towards research and life inspired me and I will try to follow in his footsteps to become a researcher with true passion.

Second, special thanks also go to the members from our lab. It was enjoyable for having inspiring discussions and working with them. Dr. Xiao Yin helped me build up my basis in experimental and theoretical optics. He also provided me with enormous help and advice in life. Dr. Zhou Lina shared many innovative designs with me. She also helped me through the days when I was depressed and impatient. Our footprint across the mountains, beaches, and rivers in Hong Kong have always been my cherished memory. Mr. Cao Yonggui provided his valuable knowledge, technical help, and suggestions to me. Many thanks to other members in our lab, Ms. Hao Yining, Ms. Peng Yang, Ms. Song Qian, Mr. Xu Zhihan for making my time at the Hong Kong Polytechnic University pleasingly colorful.

Third, I would like to show my utmost gratefulness to Mrs. Annie Law, my life mentor for their kind help. Her family provided warm-hearted guidance and support for me to

accommodate life here when I first came to Hong Kong. It would be a highly significant, extremely lucky, and meaningful experience to my life.

Finally, I would like to express my deepest gratitude to my parents and brother who have been giving me the greatest and everlasting love and support throughout my education. Family is always my strongest support and greatest pride. This thesis is dedicated to them with all my love.

Pan Zilan, Hong Kong, February 2023.

Table of Contents

List of Figures

List of Tables

Chapter 1 Introduction

1.1 Background

Optics plays a vital role in our daily life, and has accompanied us for a long time. Light-based systems or devices have experienced a great evolution from copper mirrors, simple lenses, and prism to microscopy and photography systems [1–14]. The aforementioned systems are mostly applied in free space or transparent media, such as glass or air. In many cases, there are no opaque materials in the optical systems, and light propagates along a straight line.

However, as optical systems are implemented in the broader areas, scattering problems exist in many disciplines, e.g., radar, sonar, acoustics, electromagnetics, medical science, optics and so on [15–29]. The presence of scattering media breaks the assumption of free space or transparent media assumption. Here, water medium is taken as an example. When optical information is transmitted in water environments, it is challenging to obtain accurate information. Since the light is scattered or absorbed by the water particles in the transmission path between the transmitter and the receiver, and it no longer follows the straight-line propagation in certain levels. The particles existing in water conditions are a type of scattering media preventing the optical system from transmitting the information correctly. This scattering problem exists in many research areas, e.g., marine ecology, remote sensing, and biomedical science.

In this Chapter, the interaction between light and scattering media including absorption and scattering is discussed. The statistical properties of the scattered light, i.e., speckle patterns, are described. After that, transmission matrix theory is introduced to model the

relationship between the input and output light in scattering environments. Finally, the physics of light absorption is also explained.

1.1.1 Light Scattering

The interactions between light and matter holds a great significance in science and technology. The scattering and absorption of light, by bound electrons in atoms, molecules, and solids, as well as by free electrons, form the direct basis [30–35]. In terms of scattering, there are various kinds of scattering including elastic scattering, inelastic scattering, quasi-elastic scattering, nonlinear process and so on. Here, our discussion is limited to elastic scattering. Elastic scattering can lead to light diffusion, when light waves propagate in scattering media. A single particle scattering model is first given, and then a collection of particles is introduced. Finally, the properties of scattering media based on the model are discussed.

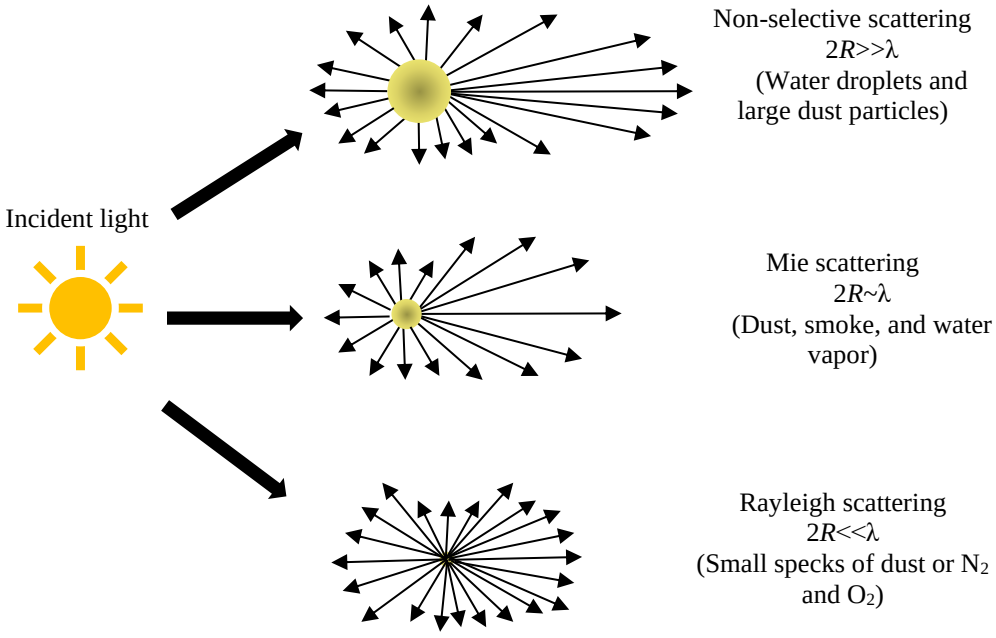

Figure 1.1 The angular distribution of the scattered light for the different types of scattering including Rayleigh scattering, Mie scattering and non-selective scattering [36]. *R* represents the radius of particle size.

Single particle scattering

Rayleigh scattering or Mie scattering can simply model the scattering of a single small particle [36–39], as shown in Fig. 1.1. Rayleigh scattering can be applied when particles are much smaller than the wavelength of the incident light, which is derived from the phenomenon when light interacts with a dipole. For the particle size is on the order of the wavelength, the scattering can be explained by Mie scattering. It is an approximation derived by tackling the challenge in Maxwell's equation of the monochromatic plane wave irradiated homogeneous and isotropic spherical scatter. To characterize the single particle scattering, the scattering anisotropy, g, is used to model the physics of single particles [39].

$$g = \int_0^{\pi} p(\theta) 2\pi \sin(\theta) d\theta \times \cos\theta = \langle \cos\theta \rangle, \tag{1.1}$$

where $p(\theta)$ denotes density distribution of the scattering field, θ denotes the photon scattering angle and < > denotes an ensemble average. The range of anisotropy parameter is [-1, 1]. Here, backward scattering is represented by -1, and forward scattering is represented by 1. Biotissues undergo Rayleigh scattering and Mie scattering due to the heterogeneous structures. For most biotissues, anisotropy factor g is approximately 0.9, which means that forward scattering dominates over backward scattering. In addition to scattering anisotropy, another important parameter for single particle scattering is scattering cross section σ_s, which represents the capability of particle's scattering. It is deemed as the effective scattering area that a photon impinges. σ_s is the product of scattering efficiency Q_s and geometric cross-sectional area A_s, which can be described by

$$\sigma_s = Q_s A_s. \tag{1.2}$$

A collection of particles scattering

Scattering media in real applications are always a collection of scatterers that are distributed in a random way within a finite three-dimensional space. It is necessary to

apply a statistical model to explain the interaction between light and scattering media. It is based on an assumption that only scattering exists in this process. Scattering coefficient μ_s and the scattering mean free path (MFP) l_s with units of mm^{-1} are employed to describe the scattering effect, which can be described by

$$\mu_s = \sigma_s N_s, \tag{1.3}$$

$$l_s = \frac{1}{\mu_s}, \tag{1.4}$$

where N_s denotes the total number of scatters per units of mm^{-3}. The intensity of ballistic light can be derived based on l_s when light propagates through the sample, which can be described by

$$I(l) = I_0 e^{-\frac{l}{l_s}} = I_0 e^{-\mu_s l}, \tag{1.5}$$

where I_0 denotes the incident light intensity, l denotes optical path length. It is found that ballistic light intensity experiences exponential decay in the process of scattering. To further quantify how much of the light still follows the straight line, the parameters of reduced scattering coefficient μ_s' (mm^{-1}) and transport mean free path l_s' (mm) are used to describe the scattering media.

$$\mu_s' = (1-g)\mu_s m, \tag{1.6}$$

$$l_s' = \frac{1}{\mu_s'}. \tag{1.7}$$

The multiple scattering process is described in Eqs. (1.6) and (1.7). The particle model is an approximation for a real scattering medium. Ballistic photons also exist which is useful and applied in many applications e.g., imaging in biological field.

Speckle

When monochromatic light is shone onto scattering media, light experiences the diffusion inside scattering media and the output is uncorrelated in the spatial domain as shown in Fig. 1.2. The scattered light field is termed speckle field [40–44]. According to the principle of Huygens, the complex field is the phasor summation of the output plane of the scattering medium as described by

$$E(x,y)=\sum_{p=1}^{N}a_p(x,y)=\sum_{p=1}^{N}\left|a_p(x,y)\right|e^{i\theta_p}, \tag{1.8}$$

where $E(x,y)$ denotes the output electric field at an arbitrary point, $a_p(x,y)$ denotes each beamlet of output wavefront at an arbitrary point on the output surface, and $\left|a_p(x,y)\right|$ and θ_p denote amplitude and phase information of $a_p(x,y)$, respectively. It is known that a_p is generated by incident light with limited energy. Only five beamlets are shown in Fig. 1.2, and are used as an example to show the phasor summation process. *N* is large in the diffusive propagation of light in the scattering medium. According to central limit theory, $E(x,y)$ follows complex normal distribution if *p* is enough large. The corresponding imaginary part (*I*) and real part (*R*) of $E(x,y)$ can be derived based on transformation as follows,

$$\mathrm{A}=\sqrt{R^2+I^2}, \tag{1.9}$$

$$\theta_p=\arctan\left(\frac{I}{R}\right), \tag{1.10}$$

$$R=A\cos\theta_p, \tag{1.11}$$

$$I=A\sin\theta_p. \tag{1.12}$$

The probability density function (PDF) of R and I follows a Gaussian distribution described by

$$Y(R,I)=\frac{1}{2\pi\sigma^2}\exp\left(-\frac{R^2+I^2}{2\sigma^2}\right), \tag{1.13}$$

where σ denotes the standard deviation. Based on Eq. (1.13), the PDF is a circular Gaussian density function and $E(x,y)$ in Eq. (1.8) can also be regarded as a complex circular Gaussian random variable.

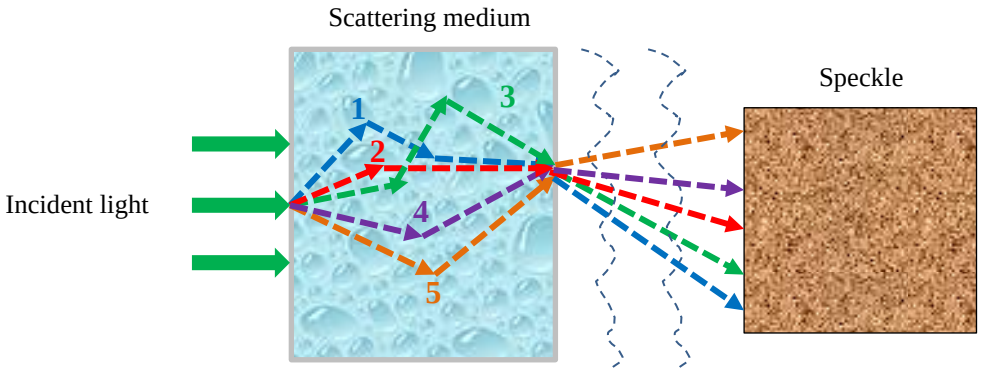

Figure 1.2 Illustration of light's diffusive propagation and output wavefront through a scattering medium. The incident light beam propagates through a scattering medium and a speckle is generated.

Transmission matrix

It is assumed that the interaction of light and scattering medium is regarded as a linear lossless process. Therefore, a scattering medium is a linear system that transforms the input light field to the output light field. According to the speckle theory, the input and output wavefronts can be discretized as elementwise arrays of optical modes. Supposed that array E_x and array E_y respectively represent the input and output wavefront and have m and n elements, every element of E_x and E_y is complex value of the corresponding optical mode. The transform can be represented by a transmission matrix T_{xy}, which describes how phase and amplitude of the input field are modified by the medium to be

presented on the output plane. The mathematical equation is given in Eq. (1.14), and an elementwise expression based on Eq. (1.14) is given in Eq. (1.15) to make the process easy to understand [45–50].

$$E_y = T_{xy} E_x, \tag{1.14}$$

$$\begin{bmatrix} E_{y,1} \\ E_{y,2} \\ \cdots \\ E_{y,m} \end{bmatrix} = \begin{bmatrix} T_{11} & T_{12} & \cdots & T_{1n} \\ \cdots & & & \cdots \\ T_{m1} & T_{m2} & T_{m3} & T_{mn} \end{bmatrix} \begin{bmatrix} E_{x,1} \\ E_{x,2} \\ \cdots \\ E_{x,n} \end{bmatrix}. \tag{1.15}$$

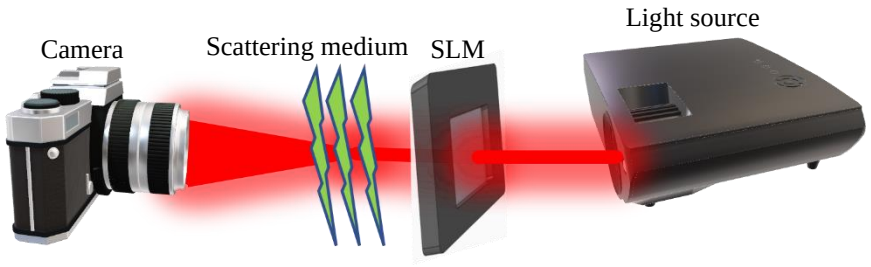

$$\underbrace{\begin{bmatrix} E_{y,1} \\ E_{y,2} \\ \cdots \\ E_{y,m} \end{bmatrix}}_{\text{output}} = \underbrace{\begin{bmatrix} T_{11} & T_{12} & \cdots & T_{1n} \\ \cdots & & & \cdots \\ T_{m1} & T_{m2} & T_{m3} & T_{mn} \end{bmatrix}}_{\text{transmission matrix}} \underbrace{\begin{bmatrix} E_{x,1} \\ E_{x,2} \\ \cdots \\ E_{x,n} \end{bmatrix}}_{\text{input}}$$

Figure 1.3 A schematic of shaping the transmission matrix in scattering media. The process for performing wavefront shaping in complex medium by using a spatial light modulator (SLM) and free-space optics to tailor the incoming beamlet.

A schematic of shaping the transmission matrix is shown in Fig. 1.3. Transmission matrix theory is widely used in the analysis of wavefront shaping (WFS) [51–56] and phase conjugation [57–61].

1.1.2 Light Absorption

Absorption of light takes place when matter captures electromagnetic radiation, converting the energy of photons to internal energy. The absorption of a bulky macroscopic material can be characterized by a coefficient termed absorption coefficient μ_a. According to the Beer-Lambert-Bouguer law, light intensity along the propagation direction can be described by

$$I(l) = I_0 e^{-\mu_a l}, \tag{1.16}$$

where I_0 denotes the incident light intensity and l denotes the propagation distance in scattering media. It can be found that there is an exponential decay towards the light intensity with the propagation inside scattering media. The absorption coefficient has a connection with wavelength. In typical applications of biology, major components of biological tissue induce absorption effect, e.g., water and hemoglobin. The optical window of 650–950 nm has relatively low absorption from biological tissue, and therefore enables light to penetrate tissue with less loss. For water in the sea, blue–green window (400–520 nm) has a low water absorption coefficient. Therefore, in most biomedical and underwater applications, these optical windows are opted to acquire more scattered signal light. In a word, the absorption level can be varied with different ranges of wavelengths in biological tissue and water.

1.2 Literature Review

Seeing through turbid water or fog, looking around corners, and focusing deep into biological tissue [62–72] have been treated as challenging tasks in optics. Disordered optical scattering which scrambles the light distribution of optical field from different optical directions is the main reason. Random scattering media can significantly increase

system complexity that impedes useful information to be transmitted. Therefore, it is desirable to develop feasible solutions to realize high-fidelity information transmission when light travels through complex scattering media. Optical information transmission in free space through complex scattering media has attracted much attention, and is of great significance in applications, e.g., marine ecology and biomedical science.

WFS in the disordered environments has been widely studied to control the wavefront of input light in complex scattering media. A. P. Mosk and I. M. Vellekoop proposed and demonstrated the WFS in 2007 via iteration algorithm [46]. They have provided an insightful perspective for controlling light through complex scattering media in optical focusing and transmission. Based on the transmission matrix, the corresponding wavefront can be measured according to the scattering medium to generate specific patterns through or inside the scattering medium. In the WFS, optical phase or complex field of light from different scattering paths is first calculated, and then the output field is actively manipulated by shaping an input wavefront. It has become an efficient and systematic method to actively control optical wavefronts and further manipulate light through complex scattering media. Thanks to the development of electronic devices, optical wavefront shaping can be realized by using spatial light modulator (SLM) or digital micromirror devices (DMD). The SLM can be used to impose spatially-varying modulation on the incident wave, where the modulation can realize amplitude, phase, and polarization modulation. A DMD can realize phase modulation, binary phase modulation, or binary amplitude modulation, respectively. In general, iterative optimization [73–81], transmission matrix measurement [82–93], or phase conjugation [94–103] are powerful to obtain correct wavefronts.

Iterative optimization requires measurement of the focusing light intensity on the target modes by using a feedback signal. A large number of feedback signals can be employed including photoacoustic wave [105,106], second-harmonic generation [107], fluorescent light from a probe particle [108–110], or light intensity in the corresponding modes measured by a photodetector [45]. Due to the requirement of a relatively long time of convergence by finding solutions through trial and error, iterative methods have some inherent limitations in practice.

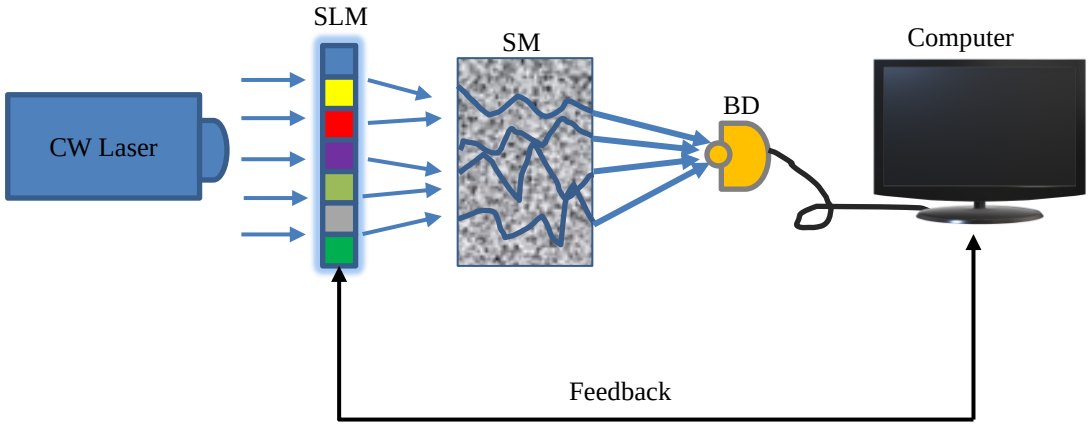

Figure 1.4 A diagram of WFS in scattering media [104]. CW Laser: continuous-wave (CW) laser; SM: Scattering medium; BD: Bucket detector.

Transmission matrix measurement [82–93] can be considered as a supplement of iteration optimization. Transmission matrix can be obtained via calculating the output wavefronts based on a *prior* knowledge of input wavefronts. It requires more time for transmission matrix measurement than iterative optimization. Furthermore, only part of the modes of the incident field and the output field can be accessed in practice. The part of modes that is not accessible is regarded as a loss. Therefore, transmission matrix measurement requires a direct access to the output plane in most situations.

Phase conjugation gives a description of light propagation in a linear and lossless medium based on time reverse of the electrical field [94–104]. In the input plane, a randomly selected point of light source propagates through scattering media, and scattered light can be obtained in the output plane. According to the principle of phase conjugation, wavefront at the output field can be reflected off with a conjugate phase, and scattered light will retrace its propagation and focus back on the target mode as if time is reversed. However, it is challenging to locate the desired focus spot inside a scattering medium. To address these issues, a promising avenue is guide-star WFS [56] which could be small fluorescent particles or second-harmonic particles embedded in the scattering media. The general principle of guide-star WFS is shown in Fig. 1.5.

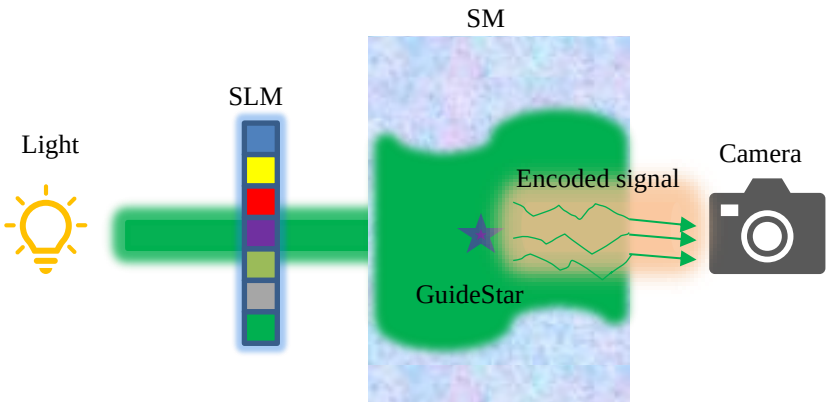

Figure 1.5 Principle of guide-star WFS [54].

The guide-star, which is typically located at the desired focus spot inside a scattering medium, interacts with the scattered photons and encodes its location in the scattered light. The measurement system detects the exiting scattered light and identifies the components that originate from the location of guide-star. The system then determines a wavefront modulation map to be presented on a SLM to tailor the wavefront of the incident. Guide-star WFS is an attractive technique for deep penetration light focusing and efficient delivery of light energy beyond the diffusion limit. Due to the limitation of system latency

and guide-star mechanism of current WFS methods, progress in science and technology is showing a great potential to gradually solve these limitations.

The WFS techniques have been continuously developed and improved [111–113]. Phase measurement and spatial light modulation are essential parts in these WFS schemes to achieve correct wavefront. For phase measurement, three kinds of methods are developed to solve the problem. Various forms of interferometry are utilized in the phase measurement process for extracting phase information of the scattered light. Holographic method is another powerful and mature method which can extract phase information directly [111,112]. In addition to these two methods, different kinds of phase retrieval techniques are feasible to acquire corresponding phase information indirectly. A SLM is used to display a pattern based on the knowledge of phase information. The SLM controls light propagation through complex scattering media in parallel and then a desired optical pattern is obtained through scattering media according to interference of all modulated optical paths. It is worth noticing that various WFS techniques always take advantage of phase connection among different optical channels to generate the desired output pattern due to interference. It is indicated that the main principle of optical WFS is *priori* knowledge of the phase relationship between the input and output wavefront. The perspective of mathematic, transmission matrix connects the optical fields on the input plane and the output plane as discussed in Section 1.1. There are millions of entries in a transmission matrix and it is challenging to measure real and imaginary parts of all the entries since only intensity information can be obtained by the detectors. The phase is required and obtained by using interferometric techniques e.g., phase-shifting or off-axis holography.

The WFS methods are based on an assumption that knowledge of the phase is a necessity for optical control through scattering media. The dependence on phase information makes the system vulnerable as the phase is sensitive to external perturbations. H. W. Ruan and C. H. Yang challenged this assumption by proposing a novel method called optical-channel-based intensity streaming (OCIS) [113]. The method employs an intensity-only approach for controlling light through a scattering medium. Instead of actively tuning the interference between the optical paths via WFS, OCIS can manipulate light and transmit optical information through scattering media with linear intensity operation. They demonstrated that OCIS could generate distinct energy null points which are distinct from WFS. It is demonstrated that the intensity-only scheme is feasible for information transmission through disordered scattering media.

1.3 Motivations and Objectives

As mentioned above, there are many challenges in optical information transmission through complex scattering media. These challenges are briefly described as follows:

(1) It is a desirable task to overcome the challenges that exist in optical signal transmission through turbid water. WFS has been developed to analyze the propagation of electromagnetic waves through scattering media. However, WFS needs a feedback control by iterative algorithms when dealing with scattering. Transmission matrix has also been established to describe scattering media. In transmission matrix measurement, random scattering media are considered as a matrix to complete transformation on light waves. However, measurement of the scattering matrix in real applications could be complicated and time-consuming, since it requires a priori calibration process. Another potential approach to dealing with the effect of scattering is adaptive optics (AO) which relies on calibrated distortions of light beam. Digital signal processing (DSP) is also feasible to

tackle the scattering effect. To obtain effective results, AO and DSP require high cost, and rely on the complexity of optical system. Therefore, it is highly desirable to design new optical systems to transmit analog signals in free space and simultaneously achieve high fidelity and high robustness through static scattering media.

(2) It is challenging to realize high-fidelity optical analog-signal transmission in free-space through turbid water, when there are obstacles in the optical path, e.g., walls, rocks, large-suspended particles and organic matters or planktonic organisms in the water. Traditional line-of-sight scheme is not suitable, since a strict alignment between the transmitter and the receiver is requested. WFS has been developed to mitigate the attenuation problem by controlling the wavefront. However, WFS needs a feedback control using an iterative algorithm which is complicated and time-consuming. Therefore, it is highly desirable to establish a simple NLOS free-space optical information transmission system to transmit optical signals through turbid water.

(3) It is a key scientific problem that many scattering media are dynamic, and many studies are conducted based on an assumption that scattering media are static. Complex and dynamic water environment could hinder applications of optical wireless communication. There is a severe power loss of optical waves in highly dynamic and turbid water environment, and the power loss is mainly due to absorption, scattering and turbulence. The turbulence also imposes a limit on the propagating wave due to the fluctuation in the refractive index of water in the presence of air bubbles, temperature, and salinity, and could induce beam wandering and wavefront distortion. The water turbidity variation in the sea is also an important factor to affect the received light intensity. The variation of water turbidity in turbulent water conditions is considered as dynamic environment. The existing methods are not easy to implement with high cost. Therefore, it is desirable to

develop new approaches to retrieving accurate signals, when optical wave propagates through highly dynamic and turbid water.

(4) It is challenging to realize high-fidelity optical information transmission through thick biological tissues with low light intensity owing to complex structures and strong scattering characteristics of biological tissues. Conventional methods are focused on high-resolution biomedical imaging using invisible light. It is difficult to realize deep-penetration optical information transmission with low light intensity using visible light. This issue is still open for research. In many medical applications, it is feasible to transmit data using optical light source, and it is highly desirable that delivering accurate information through thick tissues can be fully explored by using optical light source with low illumination power.

Figure 1.6 My key research work.

The main objective of this thesis is to develop advanced methods which can realize high-fidelity optical information transmission in static and complex scattering medium, e.g., turbid water and turbid water with obstacles in propagation path. In addition, an effective method using a series of dynamic scaling factors to correct light intensities is proposed to realize high-fidelity and high-robustness free-space optical data transmission through highly dynamic and turbid water. Furthermore, it is promising to verify the feasibility and efficiency of optical information transmission through biological tissues. The key research work of this thesis is shown in Fig. 1.6.

1.4 Outline of Thesis

This Ph.D. thesis consists of six chapters, and Chapters 2, 3, 4 and 5 are based on my published papers. The rest of this thesis is organized as follows:

In Chapter 2, a new approach based on zero-frequency modulation and single-pixel detection is presented. A series of 2D random amplitude-only patterns are generated by using zero-frequency modulation method and are used as optical information carriers. In addition, a noise suppression strategy, i.e., differential operation, is developed to obtain high-quality signal reconstruction. The proposed method can achieve high-accuracy analog-signal transmission in various turbid water environments.

In Chapter 3, more complex water environments are introduced, i.e.., obstacles between the transmitter and the receiver. It is experimentally demonstrated that the proposed method can achieve high fidelity and high robustness for free-space optical information transmission through turbid water. In addition, the proposed method possesses a wide detection range at the receiving end.

In Chapter 4, an effective method is developed to realize high-fidelity optical information transmission in dynamic and complex water conditions. A series of dynamic scaling

factors are calculated to correct light intensities recorded by a single-pixel bucket detector. A fixed reference pattern is utilized before each illumination pattern to obtain the series of dynamic scaling factors during optical data transmission in free space. Different kinds of analog signals can be retrieved with high fidelity based on the proposed method in different dynamic and turbid water environment.

In Chapter 5, optical wireless information transmission is studied based on the proposed method in free space through different thickness of biological tissues. The proposed method can achieve high-fidelity data transmission through thick biological tissue with low power consumption. Different visible light wavelengths are also tested and verified.

In Chapter 6, the research findings are summarized, and the main contributions of this thesis are described. Then, future work is discussed, and potential research directions are described.

Chapter 2 Optical Analog-signal Transmission and Retrieval Through Turbid Water with Single-Pixel Detector

2.1 Introduction

As information carrier, optical wave has attracted much attention in recent years [114,115]. The high-bandwidth optical wave offers an opportunity for data transmission. Different from optical fiber communication, optical communication in free space has its own advantages and application background [116–118]. However, light wave propagating in free space usually encounters scattering media, e.g., turbid water or opaque materials in which scattering and absorption are unavoidable [119–123]. As a result, spatial information of the incident light is scrambled, and partially or completely ballistic photons are lost. In general, optical system through scattering media yields speckle due to the interference inside the scrambled light beams [119–121], which makes it difficult to deliver accurate information of signal in the field of data transmission. Hence, there is strong interest in the investigation of high-robustness and high-fidelity optical signal transmission in free space through scattering media [122,123]. Several approaches have been proposed in the literature to analyze the propagation of electromagnetic waves, e.g., WFS [122] and transmission matrix measurement [123]. However, WFS needs a feedback control by iterative algorithms when dealing with the scattering modifications. In transmission matrix measurement, random scattering media are considered as a matrix to complete transformation on light waves. However, measurement of the scattering matrix in real applications could be complicated and time-consuming, since it requires a priori calibration process. Another potential approach to dealing with the effect of scattering is adaptive optics (AO) which relies on calibrated distortions of light beam [124]. Digital

signal processing (DSP) is also feasible to tackle the scattering effect [125]. To obtain effective results, AO and DSP require high cost and rely on the complexity of system. Therefore, it is highly desirable to design new optical systems to easily transmit the signal in free space and simultaneously achieve high fidelity and high robustness through scattering media.

As one kind of scattering media, turbid water is still a great obstacle for transmitting analog signal in free space, since the property of scattering in turbid water is complicated. In the environment with turbid water, various turbulence and attenuation factors affect the transmission efficiency and accuracy between the transmitter and the receiver. The approaches for transmitting information through turbid water using optical waves could be restricted by low robustness, low transmission quality, and complicated devices [126–131]. How to overcome the challenges that exist in optical analog-signal transmission through turbid water remains an open question.

In this Chapter, a new and robust method that takes advantage of a series of random amplitude-only patterns is proposed to build up a high-fidelity transmission channel in free space through turbid water and transmit analog signals by utilizing visible and coherent light source. In the proposed approach, analog signal is considered as independent pixel values, and each pixel value is encoded into a random amplitude-only pattern which is a two-dimensional matrix. Then, these patterns are sequentially embedded into SLM and are illuminated to propagate through turbid water. At the receiving end, a single-pixel detector is utilized to detect the light intensity. By employing the proposed method, the receiver can obtain high-fidelity signal information. Different water conditions are studied, and experimental results in each case are quantitatively evaluated. The main contributions of this Chapter are described as follows: (1) It realizes

optical signal transmission in free space through turbid water utilizing a series of random amplitude-only patterns as information carrier. (2) The proposed approach is easy to operate, and is robust against highly scattering and absorption effect in turbid water, which can realize high-fidelity transmission in free space through turbid water and can be applied to the field of underwater communication. Moreover, *priori* knowledge about turbid water is not needed for signal retrieval. (3) At the receiving end, light intensity is detected by a single-pixel (bucket) detector [132–136], which makes the proposed method advantageous for analog-signal transmission. The corresponding publication is as follows: **Zilan Pan**, Yin Xiao, Yonggui Cao, Lina Zhou, and Wen Chen, "Optical analog-signal transmission and retrieval through turbid water," Applied Optics, 60 (34), 10704–10713, 2021.

2.2 Methodology

A detailed description of our approach is given, and a schematic optical experimental setup is shown in Fig. 2.1.

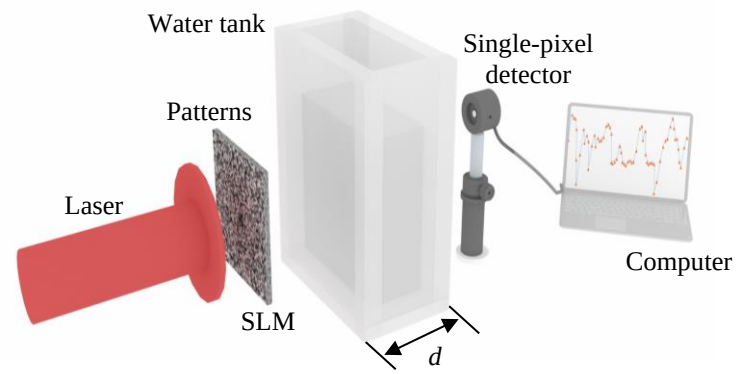

Figure 2.1 A schematic experimental setup for the proposed method to optically transmit analog signal in free space through turbid water. *d*, axial distance in water tank.

In the proposed method, a series of computer-generated random amplitude-only patterns are sequentially embedded into the SLM and then are illuminated to propagate in

free space. The 2D patterns displayed by the SLM are fully covered by the laser beam. The propagating wave is scattered and absorbed through turbid water. At the receiving end, light intensity is collected by a single-pixel detector as shown in Fig. 2.1.

The procedure for encoding analog signals into random amplitude-only patterns is called zero-frequency modulation and described as follows:

(1) Generate a random amplitude-only pattern *g* with real values by computer;

(2) Apply fast Fourier Transform (FFT) to *g* and obtain its spectrum *G*;

(3) In the Fourier spectrum *G*, zero frequency is substituted by one pixel value of the analog signal and a new spectrum *G'* is generated;

(4) Inverse fast Fourier transform (IFFT) is applied to *G'* to obtain an updated amplitude-only pattern *P*;

(5) Repeat the above steps until each point of original analog signal is processed.

2.2.1 Mathematical Tools for Analyzing Zero-Frequency Modulation

Fourier analysis is a powerful analytical tool in digital signal processing and has a wide range of applications in engineering and physics, such as image processing, RADAR, and so on. J. Fourier proposed the theory of Fourier analysis in 1807 and pointed out that any continuous-time signal can be decomposed into a finite sequence of complex-valued function of frequency. The two-dimensional (2D) Fourier transform and inverse Fourier transform are described by

$$G\left(f_x, f_y\right) = \int_{-\infty}^{\infty}\int_{-\infty}^{\infty} g\left(x, y\right)\exp\left[-j\cdot 2\pi\left(f_x x + f_y y\right)\right]dxdy, \tag{2.1}$$

$$g\left(x, y\right) = \int_{-\infty}^{\infty}\int_{-\infty}^{\infty} G\left(f_x, f_y\right)\exp\left[j\cdot 2\pi\left(f_x x + f_y y\right)\right]df_x df_y, \tag{2.2}$$

where $j = \sqrt{-1}$, (x,y) denotes the coordinate in spatial domain, (f_x,f_y) denotes the coordinate in frequency domain, $g(x,y)$ denotes 2D image, $G(f_x,f_y)$ denotes Fourier

spectrum of $g(x,y)$. Later, Fourier analysis can be applied to discrete signals and digital images. The discrete 2D Fourier transform and inverse Fourier transform can be described by

$$G(u,v)=\sum_{x=-M/2}^{M/2-1}\sum_{y=-N/2}^{N/2-1} g(x,y)\exp\left[-j\cdot 2\pi\left(\frac{ux}{M}+\frac{vy}{N}\right)\right], \tag{2.3}$$

$$g(x,y)=\frac{1}{MN}\sum_{u=-M/2}^{M/2-1}\sum_{v=-N/2}^{N/2-1} G(u,v)\exp\left[j\cdot 2\pi\left(\frac{ux}{M}+\frac{vy}{N}\right)\right], \tag{2.4}$$

where (u,v) denotes the discrete form of (f_x,f_y), $\frac{1}{MN}$ denotes the scaling factor to preserve accuracy when retrieving information. The discrete 2-D Fourier transform indicates that an M×N digital image in the spatial domain can be expressed as a sum of Fourier coefficients, $G(u,v)$, and a finite sequence of complex-valued function of frequency as shown in Fig. 2.2.

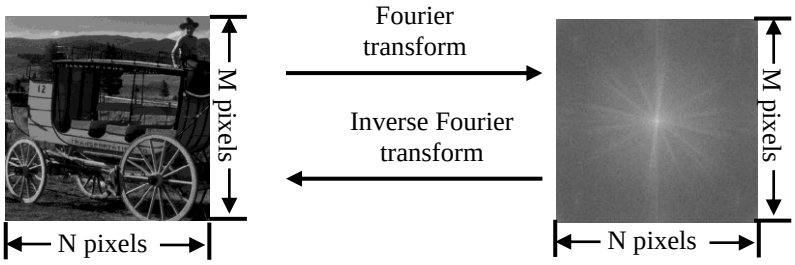

Figure 2.2 The Fourier transform and inverse Fourier transform for 2D image. The red area in the Fourier spectrum figure is the zero-frequency area.

According to the theory of Fourier transform, it is found that the value of zero-frequency in $G(u,v)$ is equal to the sum of elements in $g(x,y)$, which can be described by

$$\begin{aligned} G(0,0) &= \sum_{x=-M/2}^{M/2-1}\sum_{y=-N/2}^{N/2-1} g(x,y)\exp\left[-j\cdot 2\pi\left(\frac{0x}{M}+\frac{0y}{N}\right)\right] \\ &= \sum_{x=-M/2}^{M/2-1}\sum_{y=-N/2}^{N/2-1} g(x,y) \end{aligned}. \tag{2.5}$$

It is the principle of zero-frequency modulation. Based on Eq. (2.5), Eq. (2.3) can be further described by

$$\begin{aligned} G(u,v) &= \sum_{x=-M/2}^{M/2-1}\sum_{y=-N/2}^{N/2-1} g(x,y)\exp\left[-j\cdot 2\pi\left(\frac{ux}{M}+\frac{vy}{N}\right)\right] \\ &= G(0,0)+G(u,v)_{u\neq 0,v\neq 0} \\ &= \sum_{x=-M/2}^{M/2-1}\sum_{y=-N/2}^{N/2-1} g(x,y)+\sum_{x=-M/2}^{M/2-1}\sum_{y=-N/2}^{N/2-1} g(x,y)\exp\left[-j\cdot 2\pi\left(\frac{ux}{M}+\frac{vy}{N}\right)\right]_{u\neq 0,v\neq 0} \end{aligned} \tag{2.6}$$

When zero-frequency value is substituted by each pixel value of the transmitted data, a new Fourier spectrum, $G'(u,v)$, can be obtained. The process can be described by

$$\begin{aligned} G'(u,v) &= \sum_{x=-M/2}^{M/2-1}\sum_{y=-N/2}^{N/2-1} g(x,y)+\sum_{x=-M/2}^{M/2-1}\sum_{y=-N/2}^{N/2-1} g(x,y)\exp\left[-j\cdot 2\pi\left(\frac{ux}{M}+\frac{vy}{N}\right)\right]_{u\neq 0,v\neq 0} \\ &= G'(0,0)+\sum_{x=-M/2}^{M/2-1}\sum_{y=-N/2}^{N/2-1} g(x,y)\exp\left[-j\cdot 2\pi\left(\frac{ux}{M}+\frac{vy}{N}\right)\right]_{u\neq 0,v\neq 0} \\ &= G'(0,0)+G(u,v)-G(0,0) \end{aligned} \tag{2.7}$$

According to Eq. (2.4), $P(x,y)$ can be obtained after inverse Fourier transform for $G'(u,v)$ and described by

$$\begin{aligned} P(x,y) &= \frac{1}{MN}G'(0,0)+g(x,y)-\frac{1}{MN}G(0,0) \\ &= \frac{G'(0,0)-G(0,0)}{MN}+g(x,y) \end{aligned} . \tag{2.8}$$

When the pixel value of the transmitted data is lower than $G(0,0)$, there are negative values in the updated Fourier spectrum matrix, also called illumination pattern (P), which are not suitable to be embedded into the SLM. To overcome this challenge, the illumination pattern P is further transformed into two independent patterns, i.e., $t+P$ and $t-P$ where t denotes a positive constant to eliminate negative values. The positive constant value of m depends on the maximum and minimum values of P as described in Eqs. (2.11) and (2.12),

$$\max\left[P(x,y)\right]=\frac{G^{'}(0,0)-G(0,0)}{MN}+\max\left[g(x,y)\right], \tag{2.9}$$

$$\min\left[P(x,y)\right]=\frac{G^{'}(0,0)-G(0,0)}{MN}+\min\left[g(x,y)\right], \tag{2.10}$$

$$t>\max\left[P(x,y)\right], \tag{2.11}$$

$$\text{and } t>abs\left\{\min\left[P(x,y)\right]\right\}. \tag{2.12}$$

It is observed that when optical wave propagates through turbid water, the illumination pattern *P* which is considered as an information carrier has ultra-high robustness against scattering and absorption [134–136]. Another feature is that we can flexibly adjust the pattern size according to practical conditions. In other words, each pixel of original signal can be projected onto one random amplitude-only pattern with any size, e.g., 512×512 or 256×256 pixels. However, the size of the patterns may affect quality of the retrieved signal. In practice, compressed sensing can also be applied to reduce the number of 2D patterns to be generated.

A flow chart to illustrate the proposed method is shown in Fig. 2.3. In Fig. 2.3, a 2D image is used as original signal, and each pixel of this 2D image is converted into one amplitude-only pattern according to the proposed principle. In optical experiments, random amplitude-only patterns generated correspondingly to each pixel of original signal are sequentially embedded into the SLM.

When optical wave propagates through turbid water, the light intensity $I(l)$ decays due to the scattering and absorption effect. According to Beer-Lambert law [137], the light intensity attenuates exponentially which can be described by

$$I=I_0\exp(-\mu l), \tag{2.13}$$

where I_0 denotes the incident light intensity, $I(l)$ denotes the transmitted light intensity, l denotes the path length, and $\mu(\lambda)$ is also called Beer's coefficient, In turbid water condition, the turbidity of water can affect light propagation, and can lead to partial or complete attenuation of light intensity. In addition, salinity in-homogeneity also leads to irregular change in the refractive index of water, and eventually influences data transmission. The different turbulence factors are tested and verified from the perspective of optical experiments in Section 2.3 which gives a detailed description of experimental process and experimental results.

2.2.2 Single-Pixel Detection

After wave propagation through turbid water, a single-pixel detector is used to collect the light intensity. The recording and retrieval process is described by [134–136]

$$\begin{aligned} \mathrm{B1} &= \delta \iint \left[t + P(x,y) \right] e^{-2\pi j(x\xi + y\eta)} dxdy \Big|_{\xi=0,\eta=0}, \\ &= \delta \iint \left[t + P(x,y) \right] dxdy \end{aligned} \tag{2.14}$$

$$\begin{aligned} \mathrm{B2} &= \delta \iint \left[t - P(x,y) \right] e^{-2\pi j(x\xi + y\eta)} dxdy \Big|_{\xi=0,\eta=0}, \\ &= \delta \iint \left[t - P(x,y) \right] dxdy \end{aligned} \tag{2.15}$$

$$\mathrm{B} = \mathrm{B1} - \mathrm{B2} = 2\delta \iint P(x,y) dxdy. \tag{2.16}$$

where $j = \sqrt{-1}$, (x,y) denotes the coordinate in spatial domain, (ξ,η) denotes the coordinate in frequency domain, $t+P(x,y)$ and $t-P(x,y)$ denote 2D random patterns with 512×512 pixels, t denotes a matrix with a positive constant, B1 and B2 denote the recorded intensity values, B denotes the retrieved value, and δ denotes a scaling factor. The detailed process is shown in Fig. 2.3. When the first pixel of original signal is transmitted, the first and second measurements by using single-pixel detector are respectively denoted by B11 and B12, where B11 denotes the intensity obtained from the pattern $t+P_1$, and B12 denotes

the intensity obtained from the pattern t-P_1. Then, differential operation is applied and the value B1 is equal to B11-B12, and is proportional to the first pixel value of original signal as described in Eq. (2.16). Therefore, after all pixel values of the signal are transmitted, intensity values collected by single-pixel detector can be directly used for signal retrieval. Differential operation can be suppressed noise including environmental noise and thermal noise produced by electrical equipment. In conclusion, the proposed method has high-robustness against noise.

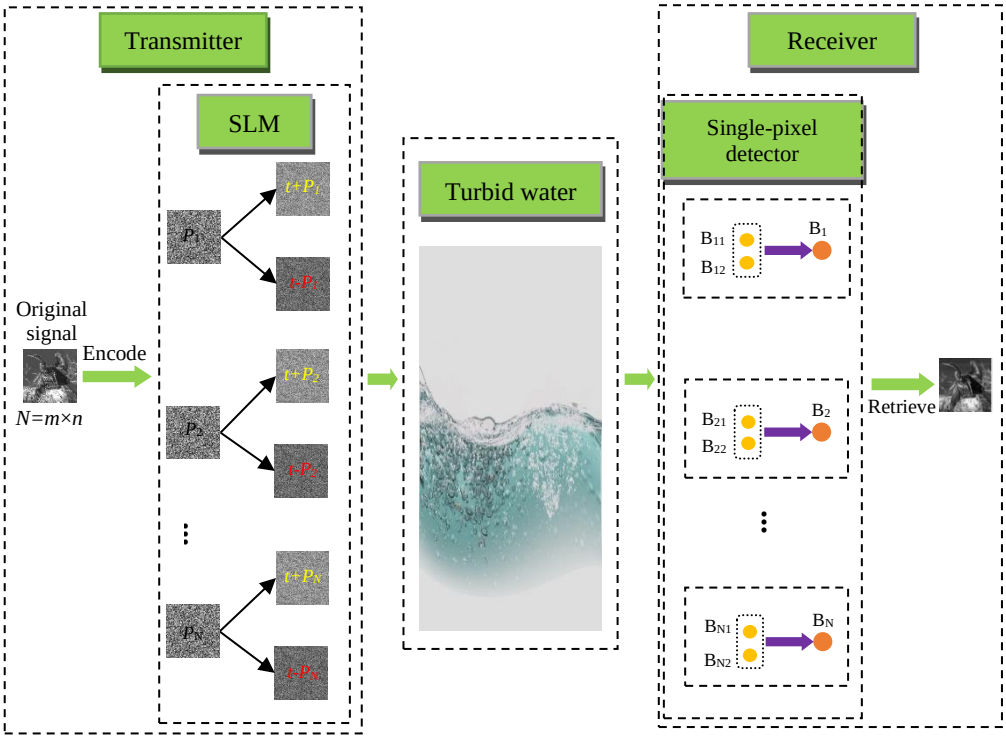

Figure 2.3 A schematic procedure for the proposed optical transmission in free space through turbid water: a 2D image is used as a typical signal here, and a single-pixel (bucket) detector collects light intensity in the detection stage.

According to the flow chart in Fig. 2.3, high-fidelity signal transmission through complex environment can be realized. This realizes high-fidelity optical transmission in free space through turbid water by taking random amplitude-only patterns as information carrier. In addition, the designed experimental setup has the advantage of cost-effective, and is easy to implement.

2.3 Experimental Results and Discussion

A number of optical experiments are conducted to evaluate performance of the proposed method. The proposed method is verified in different water conditions, i.e., clean water, water mixed with milk, water with salt (salinity in-homogeneity), and water with milk and salt. In addition, real seawater samples are also tested in our optical experiments. In Fig. 2.1, a laser beam (He-Ne laser, 17.0 mW) with wavelength of 633.0 nm is utilized, and the laser is collimated to be a plane wave. It is worth noting that the proposed approach can be applied by using other wavelengths in practice. The collimated light illuminates the SLM (Holoeye, LC-R720) with pixel size of 20.0 μm. In this study, a modulation rate of 1.25 Hz is used to conduct a proof-of-principle experiment and verify the proposed method. Different kinds of analog signals, including 1D signals and 2D images, are tested. Temperature in the laboratory for the whole optical experiments is set as 24℃.

2.3.1 Clean Water

The proposed method is first used to transmit analog signals through clean water, and different wave propagation distances in the water tank, i.e., *d* in Fig. 2.1, are studied. With the increase of wave propagation distances through clean water, intensity of optical wave attenuates gradually. In this case, three typical propagation distances (i.e., 110 mm, 160 mm and 310 mm) through clean water are tested to verify the proposed approach. For each propagation distance *d*, three irregular analog signals are utilized and tested for optical transmission in free space.

Three different signals are respectively encoded into a series of random amplitude-only patterns according to the principle introduced in Section 2.2, and the patterns carrying signal information are first illuminated to propagate through clean water with axial

distance *d* of 110 mm. After the light intensity behind the water tank is collected by single-pixel detector, the results retrieved at the receiving end are shown in Figs. 2.4(a)–2.4(c). As can be seen in Figs. 2.4(a)–2.4(c), three signals experimentally retrieved at the receiving end almost overlap with original signals, indicating that high-fidelity optical signal transmission through clean water is realized.

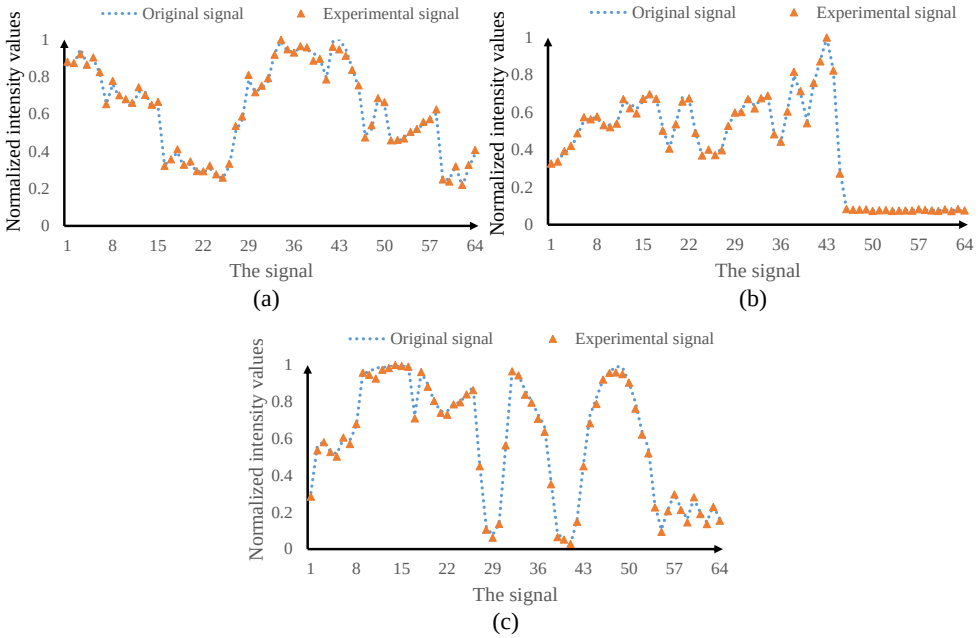

Figure 2.4 (a)–(c) Comparisons between three different kinds of original analog signals and the signals experimentally obtained at the receiving end, when the propagation distance *d* in Fig. 2.1 is 110 mm.

When the propagation distance *d* in water tank increases to 160 mm, the generated amplitude-only patterns corresponding to the three different analog signals are still used and tested. In this case, the signals retrieved at the receiving end are shown in Figs. 2.5(a)–2.5(c). As can be seen in Figs. 2.5(a)–2.5(c), high-fidelity signal transmission is still realized when the longer propagation distance *d* is used. Although the longer distance decays the light intensity to be collected by single-pixel detector, the results shown in Figs. 2.5(a)–2.5(c) demonstrate that the proposed method is robust against propagation distance *d* in Fig. 2.1, which is meaningful and significant in practical applications.

To test robustness of the proposed method through clean water, a propagation distance *d* of 310 mm is also tested in optical experiment. In this case, original signals to be tested are the same as those used in Figs. 2.4 and 2.5, which can be useful for a comparison about performance of the proposed method when different wave propagation distances are used. After random amplitude-only patterns embedded into the SLM are illuminated to propagate through clean water, the experimentally retrieved signals are shown in Figs. 2.6(a)–2.6(c).

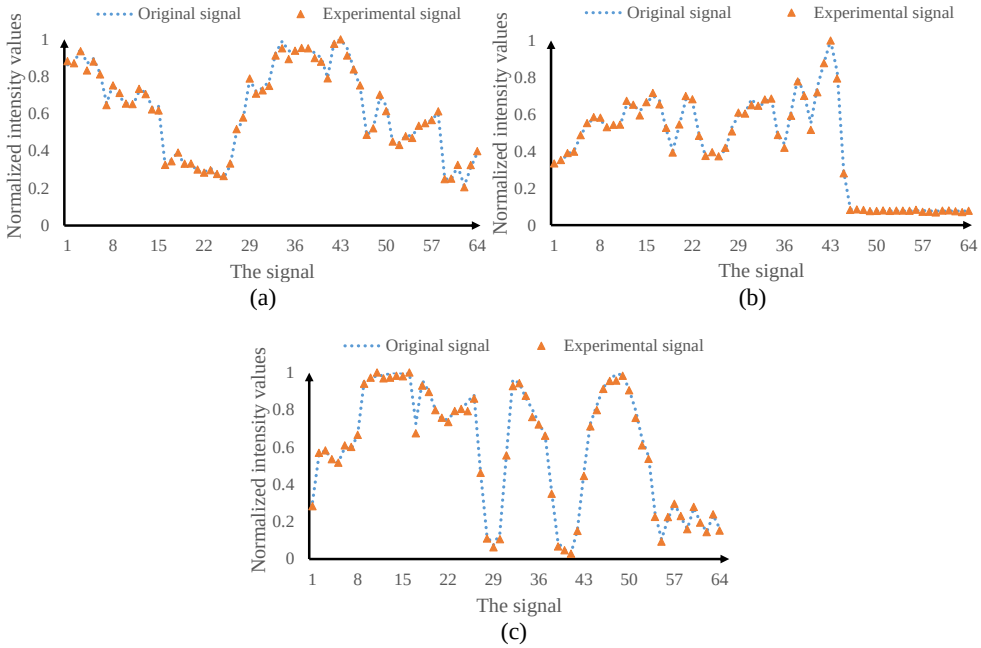

Figure 2.5 (a)–(c) Comparisons between three different kinds of original analog signals and the signals experimentally obtained at the receiving end, when the propagation distance *d* in Fig. 2.1 is 160 mm.

As can be seen in Figs. 2.6(a)–2.6(c), the signals experimentally obtained at the receiving end are highly close to original signals, indicating that the proposed method can realize high-fidelity and high-robustness optical signal transmission when different propagation distances through water medium are used. It is worth noting that other wave propagation distances can also be tested in our experiments, and for the sake of brevity the results are not presented here.

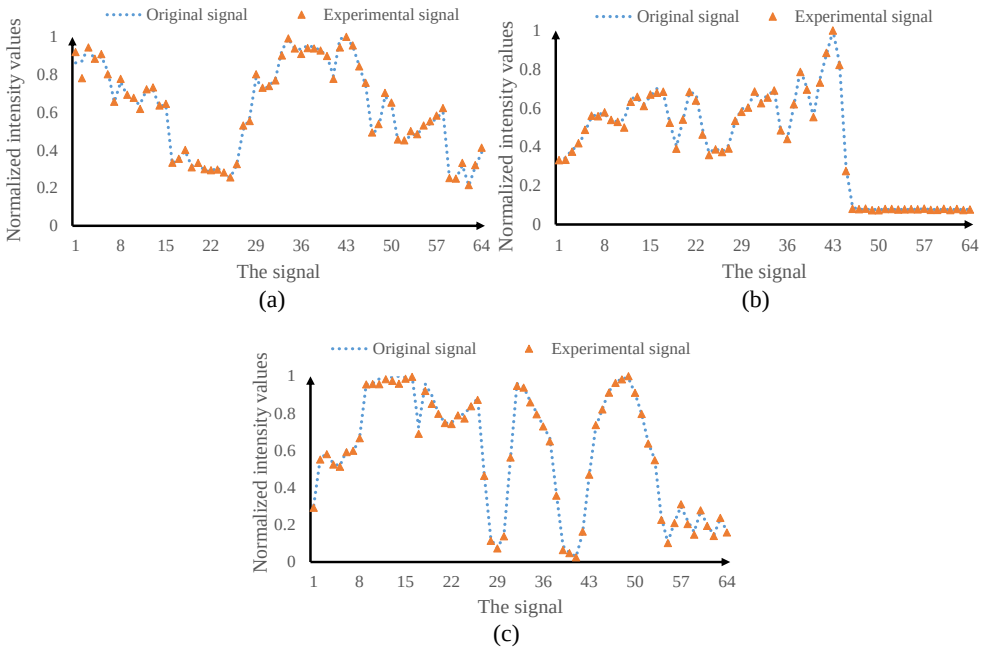

Figure 2.6 (a)–(c) Comparisons between three different kinds of original analog signals and the signals experimentally obtained at the receiving end, when the propagation distance *d* in Fig. 2.1 is 310 mm.

It is found that the propagation distance *d* in our experiments does not affect performance of the proposed approach. Although the long propagation distance can attenuate light intensity dramatically, the data collected by single-pixel detector can still be used for high-fidelity signal retrieval as long as the light intensity can be effectively detected and the laser power is properly controlled. However, light intensity is attenuated when a long transmission distance is used, which is also explained in Eq. (2.13). It was found that attenuation coefficient through clean water is close to 0.071 m^{-1} [138]. For instance, in this study, the transmitted power before turbid water is 3.5 mW, and the lower limit of received power is 600.0 nW. According to the attenuation coefficient and Beer-Lambert law in Eq. (2.13), the estimated propagation distance through turbid water could be less than 122.0 m in practice.

To quantitatively evaluate performance of the proposed method, signal-to-noise ratio (SNR) and mean squared error (MSE) are respectively calculated by

$$\mathrm{SNR} = 10 \times \log_{10}\left[\frac{\sum S_{ori}^2}{\sum \left(S_{ori} - S_{re}\right)^2}\right], \tag{2.17}$$

$$\mathrm{MSE} = \frac{1}{N}\sum \left(S_{ori} - S_{re}\right)^2, \tag{2.18}$$

where S_{ori} denotes original signal, S_{re} denotes the retrieved signal, and N denotes the total number of pixels in original signal. The calculated MSE and SNR values in different cases are shown in Table 2.1, signal *a* denotes the signals in Figs. 2.4(a), 2.5(a) and 2.6(a); signal *b* denotes the signals in Figs. 2.4(b), 2.5(b) and 2.6(b); signal *c* denotes the signals in Figs. 2.4(c), 2.5(c) and 2.6(c). The low MSE values and high SNR values further illustrate that the proposed method can realize high-fidelity optical signal transmission in free space through clean water when different propagation distances are used. In addition, as can be seen in Table 2.1, with different propagation distances, the MSE and SNR values always keep steady, which means the proposed method is robust against wave propagation distance through clean water.

Table 2.1 Quantitative comparisons using clean water with different wave propagation distances.

Signal	Distance *d*	MSE	SNR (dB)
Signal *a*	110 mm	2.94×10^{-4}	31.82
	160 mm	2.31×10^{-4}	32.87
	310 mm	3.49×10^{-4}	31.07
Signal *b*	110 mm	8.60×10^{-5}	34.59
	160 mm	1.68×10^{-4}	31.71
	310 mm	1.24×10^{-4}	33.01
Signal *c*	110 mm	3.17×10^{-4}	31.65
	160 mm	3.35×10^{-4}	31.42
	310 mm	1.95×10^{-4}	33.77

From the experimental results in Figs. 2.4–2.6 and Table 2.1, it can be summarized that the propagation distance through water medium does not affect the quality of signal

transmission in free space, since amplitude-only patterns are generated as information carrier and single-pixel detector is used to record light intensity. This kind of information carrier is a powerful tool, and single-pixel detector has the feature of stability and sensitiveness to light intensity.

2.3.2 Water Mixed with Milk

Since clean water shows relatively low capability in absorption and scattering when the light wave propagates, the effect of turbid water on transmission efficiency and accuracy is further studied. In the experiments, clean water of 850 mL is mixed with different volumes of milk (i.e., 80 mL, 90 mL, and 100 mL). To quantify the turbidity level, milk in water is used in our optical experiments. Attenuation coefficient based on Beer-Lambert law can also be calculated [137,139–141]. Then, complex environment with different turbidities is constructed. It is well recognized that the milk can effectively increase the turbidity of water, and makes wave propagation in murky water difficult. Owing to this reason, milk is considered as a suitable candidate for altering the turbidity of water. In this case, light wave propagating through turbid water encounters strong scattering and absorption which usually destroy information carrier drastically. In conventional methods, it is impossible or difficult to effectively transmit the desired signal to the receiver in free space through such a complicated environment. In our method, information carrier, i.e., the generated random amplitude-only patterns, can still serve as a robust tool to transmit information. Although the murky water makes it impossible to accurately control amplitude-only patterns through complicated environment, the data collected by single-pixel detector are still effective for retrieving the signal with high fidelity. Performance of the proposed method is also verified from the perspective of optical experiments.

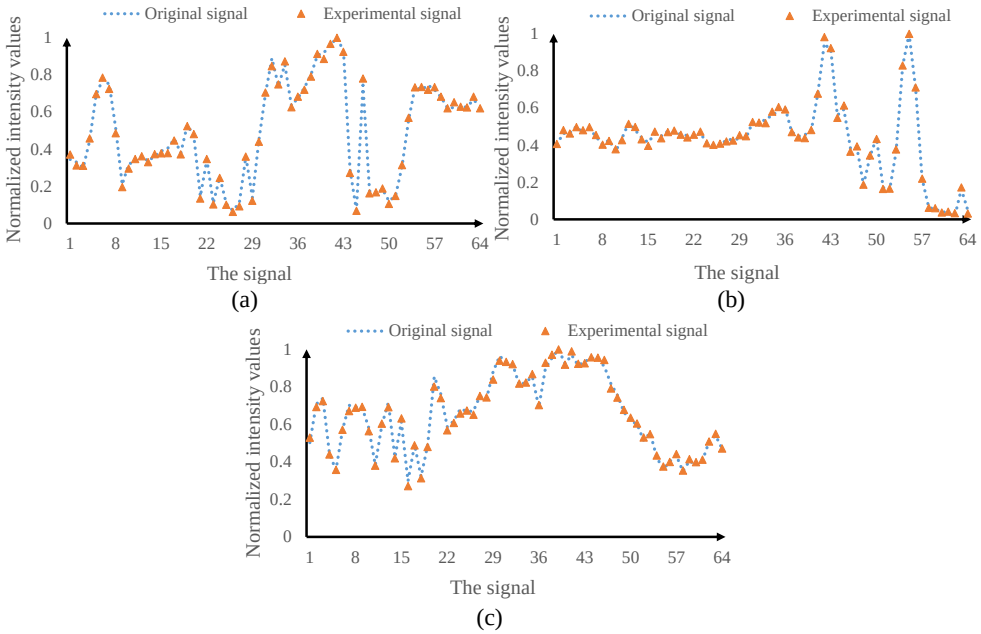

Figure 2.7 (a)–(c) Comparisons between three different kinds of original analog signals and the signals experimentally obtained at the receiving end when milk of 80 mL and clean water of 850 mL are placed in the water tank.

In Fig. 2.1, the propagation distance *d* through murky water is fixed as 160 mm in order to make a comparison due to different turbidities in the water tank. The single-pixel detector is placed 30 mm away from water tank and 240 mm away from the SLM. The only variable in this case is the turbidity which is controlled by different volumes of milk, i.e., 80 mL, 90 mL and 100 mL. Here, another three different irregular analog signals are employed for optical transmission, and in each case these signals are tested independently. Optical experimental results obtained at the receiving end are shown in Figs. 2.7–2.9.

As shown in Figs. 2.7(a)–2.7(c), these signals can be experimentally retrieved with high fidelity, when turbid water is constructed by using clean water of 850 mL and milk of 80 mL. The experimental results shown in Figs. 2.7(a)–2.7(c) illustrate that our approach has the feature of high robustness against scattering. In addition, there is a dramatic attenuation in light intensity when milk is added into water owing to the absorption effect in murky water. It has been mentioned in Section 2.3.1 that as long as single-pixel detector can detect the light intensity effectively and the laser power is

properly controlled, the data recorded can be employed to retrieve the signals with high fidelity. The experimental results in Figs. 2.7(a)–2.7(c) further verify this finding, since the light intensity detected after murky water is an order of magnitude lower than that detected when clean water is used. The dramatic reduction in light intensity through murky water does not affect high-fidelity signal transmission, which makes the proposed method be of value in practical applications.

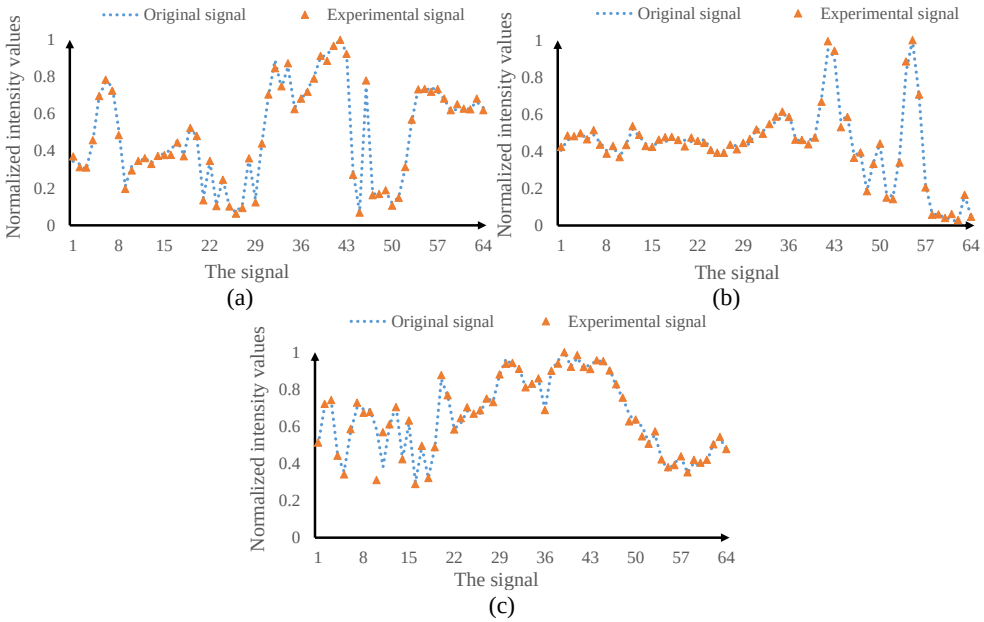

Figure 2.8 (a)–(c) Comparisons between three different kinds of original analog signals and the signals experimentally obtained at the receiving end when milk of 90 mL and clean water of 850 mL are placed in the water tank.

To further investigate performance of the proposed method, clean water of 850 mL mixed with more milk, i.e., 90 mL and 100 mL, is also studied. Obviously, these two cases increase the turbidity of murky water. When the optical wave propagates through turbid medium, by taking advantage of the characteristic of single-pixel detector which is able to detect weak light intensity, signal retrieval with high fidelity is still realized. The experimental results corresponding to these two cases are respectively shown in Figs. 2.8 and 2.9. The proposed method still performs well in these two complicated environments,

which further illustrates that the proposed scheme is a powerful tool in the field of optical transmission in free space.

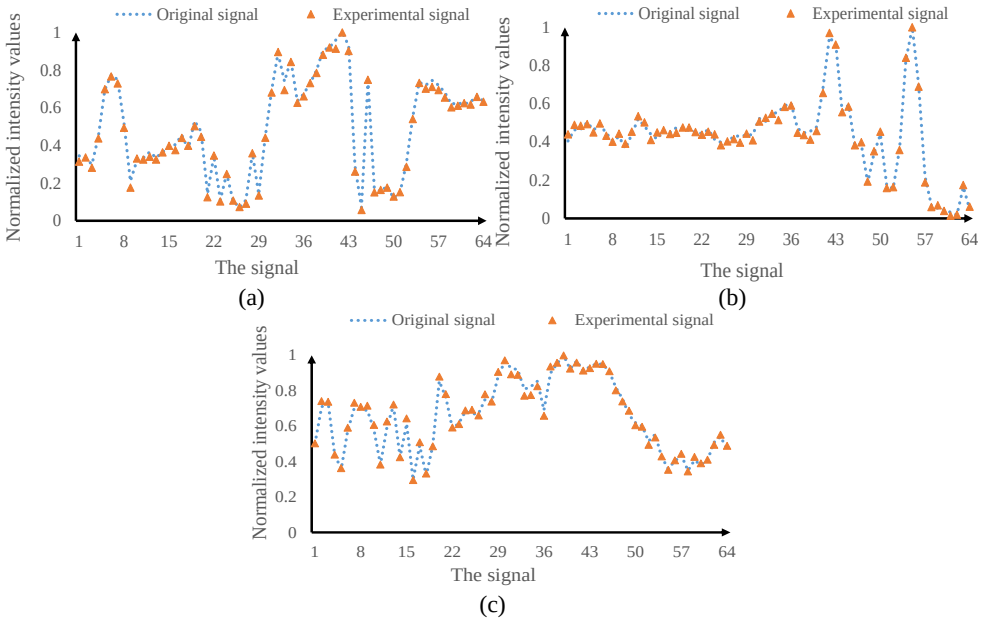

Figure 2.9 (a)–(c) Comparisons between three different kinds of original analog signals and the signals experimentally obtained at the receiving end when milk of 100 mL and clean water of 850 mL are placed in the water tank.

Table 2.2 Quantitative comparisons about the effect of the turbidity of turbid water.

Signal	Turbidity	MSE	SNR (dB)
Signal *a*	850 mL clean water + 80 mL milk	2.29×10^{-4}	31.36
	850 mL clean water + 90 mL milk	4.03×10^{-4}	28.90
	850 mL clean water + 100 mL milk	3.34×10^{-4}	29.72
Signal *b*	850 mL clean water + 80 mL milk	1.40×10^{-4}	32.12
	850 mL clean water + 90 mL milk	3.17×10^{-4}	28.58
	850 mL clean water + 100 mL milk	3.29×10^{-4}	28.42
Signal *c*	850 mL clean water + 80 mL milk	2.70×10^{-4}	32.44
	850 mL clean water + 90 mL milk	1.91×10^{-4}	23.95
	850 mL clean water + 100 mL milk	3.53×10^{-4}	31.28

Performance of the proposed method is quantitatively evaluated by SNR and MSE, and the calculated SNR and MSE values are shown in Table 2.2. In Table 2.2, signal *a* denotes the signals in Figs. 2.7(a), 2.8(a) and 2.9(a); signal *b* denotes the signals in Figs. 2.7(b), 2.8(b) and 2.9(b); signal *c* denotes the signals in Figs. 2.7(c), 2.8(c) and 2.9(c). As can be seen in Table 2.2, in more complex environment compared to clean water, the SNR and

MSE values almost maintain in the same level. These results mean that high-fidelity and high-robustness optical transmission can be realized even if the turbid medium exists in wave propagation path.

2.3.3 Water with Salt

Salinity in-homogeneity leads to irregular changes in the refractive index of water, and significantly affects signal transmission quality. Therefore, it is necessary to further study the impact of salt on the proposed method. In Fig. 2.1, the wave propagation distance *d* through water is fixed as 160 mm. The single-pixel detector is placed 50 mm away from water tank and 260 mm away from the SLM. In our experiment, clean water of 850 mL is respectively mixed with three different weights of salt, i.e., 60 g, 90 g and 120 g.

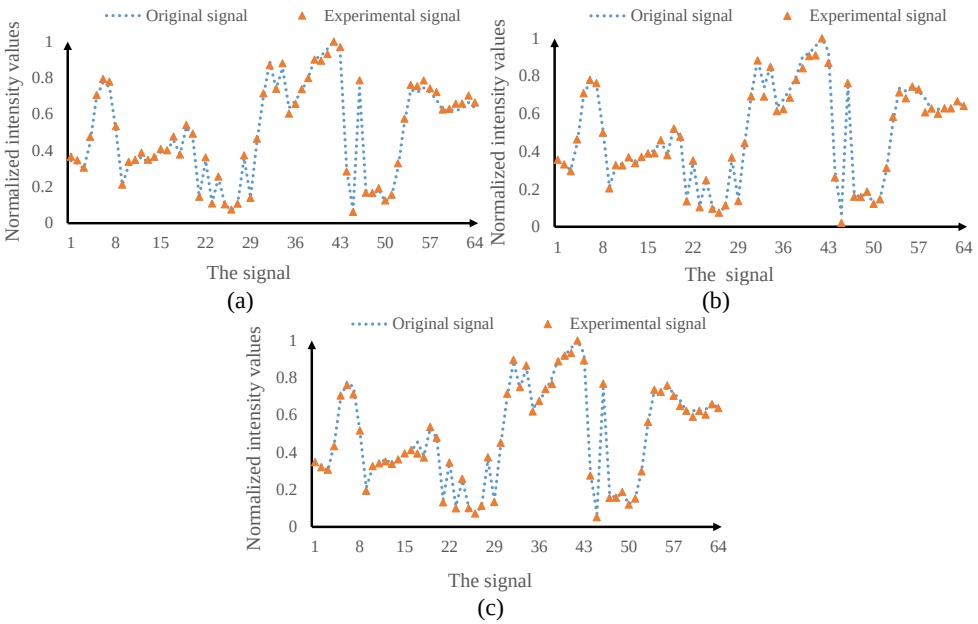

Figure 2.10 (a)–(c) Comparisons between original signal and the experimentally retrieved signals when three different weights of salt (i.e., 60 g, 90 g and 120 g) are respectively used with clean water of 850 mL. SNR values of the retrieved signals in (a)–(c) are 28.91 dB, 27.86 dB, and 30.81 dB, respectively. MSE values of the retrieved signals in (a)–(c) are 4.02×10^{-4}, 5.13×10^{-4}, and 5.10×10^{-4}, respectively.

Typical experimental results are shown in Fig. 2.10. As can be seen in Fig. 2.10, the signals are still retrieved with high fidelity. The MSE and SNR values of these retrieved

signals are calculated and shown in Fig. 2.10. In this case, the low MSE values and high SNR values also illustrate that the proposed method is feasible and effective. It can be seen in Figs. 2.10(a)–2.10(c) that salinity in-homogeneity does not affect high-fidelity signal transmission. Many kinds of signals have been tested in this study, and experimental results always illustrate that the retrieved signals overlap with original signals. With the increase of the salt, the MSE values and SNR values of the retrieved signals still keep steady.

2.3.4 Water with Milk and Salt

More complicated turbid-water environments are further studied, i.e., clean water with salt and milk. In this kind of turbid environment, the scattering medium becomes more complex and turbid, and it is found that our method can still resist the disorder of scattering media. In Fig. 2.1, light wave propagates through turbid medium with axial distance *d* of 160 mm. The single-pixel detector in Fig. 2.1 is placed 50 mm away from water tank and 260 mm away from the SLM. Typical experimental results are shown in Figs. 2.11(a)–2.11(c). To experimentally demonstrate feasibility of the proposed approach, three different kinds of irregular analog signals are used and tested through turbid medium, in which clean water of 850 mL is mixed with salt of 120 g and milk of 70 mL. It can be seen from Figs. 2.11(a)–2.11(c) that the signals retrieved at the receiving end almost overlap with original signals. Therefore, the proposed method can still realize high-fidelity optical transmission in free space even if the turbid medium becomes more complex. The calculated MSE and SNR values given in Fig. 2.1 further demonstrate that the proposed method can realize high-robustness and high-fidelity optical transmission through turbid water.

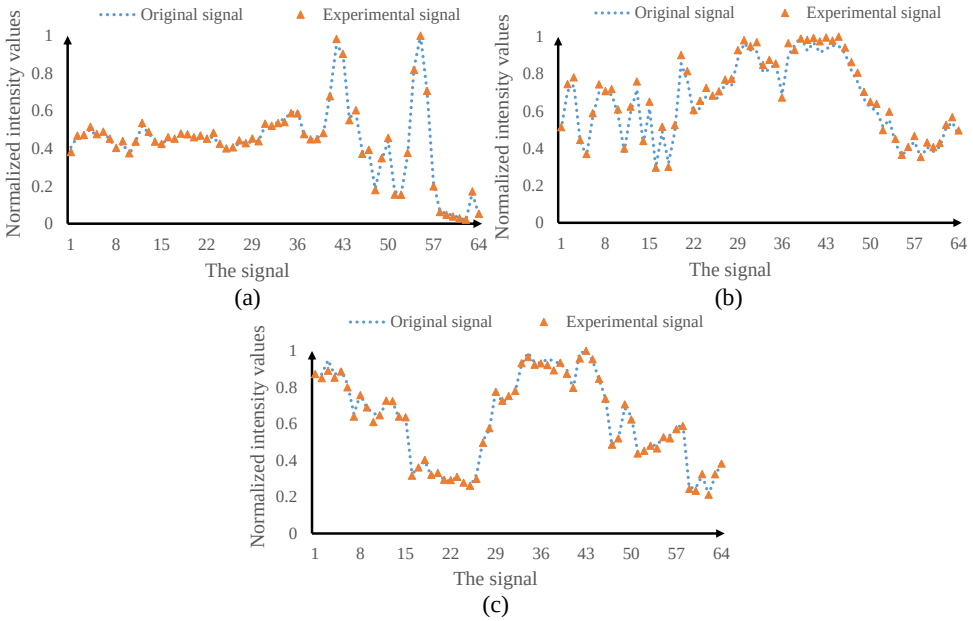

Figure 2.11 (a)–(c) Comparisons between three different kinds of original analog signals and the signals experimentally obtained at the receiving end when salt of 120 g, milk of 70 mL and clean water of 850 mL are placed in the water tank. SNR values of the retrieved signals in (a)–(c) are 32.91 dB, 26.23 dB, and 30.65 dB, respectively. MSE values of the retrieved signals in (a)–(c) are 1.17×10^{-4}, 1.13×10^{-4}, and 3.85×10^{-4}, respectively.

2.3.5 Seawater Samples

Real seawater samples which are obtained from the Star Venue in Hong Kong are also tested by using the proposed method, and several 2D images are utilized as original signals. The optical experimental setup in Fig. 2.1 is applied. The size of signal (2D image) is 64×64 pixels, and that of the generated random pattern is 512×512 pixels. The experimental results retrieved at the receiving end are shown in Figs. 2.12 and 2.13.

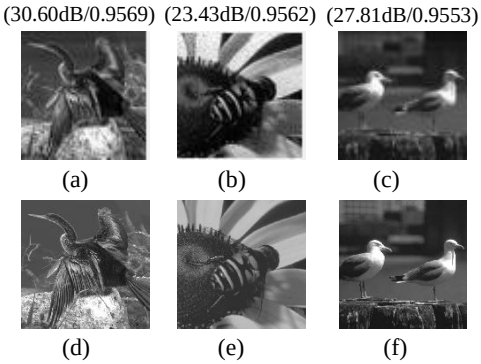

Figure 2.12 (a)–(c) 2D images obtained at the receiving end in optical experiments, and (d)-(f) original images. The PSNR and SSIM values are given inside the brackets.

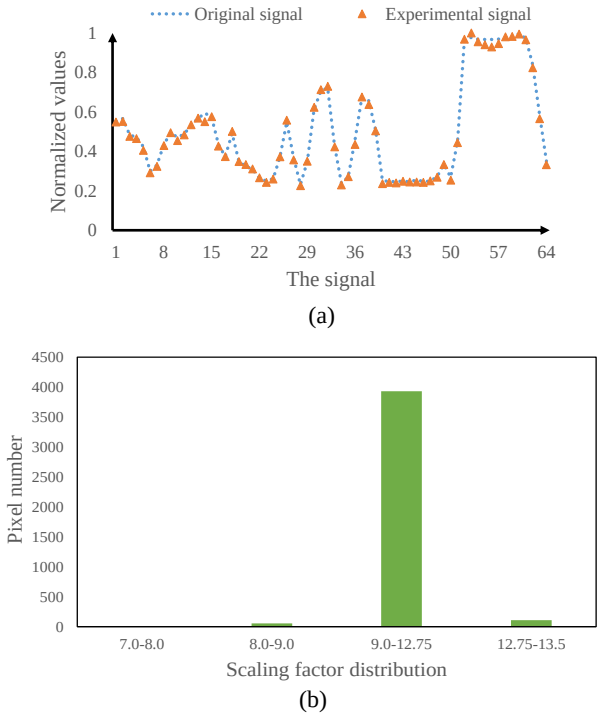

Figure 2.13 (a) A typical comparison between pixel values along the 30th row of the retrieved image in Fig. 2.12(b) and those in original image, and (b) a typically statistical result about scaling factor distribution (magnitude of the coefficients: 2.0×10^{-12}) for the retrieved image in Fig. 2.12(b).

Peak signal-to-noise ratio (PSNR) and structural similarity index measure (SSIM) [142] are used to quantitatively evaluate quality of the retrieved images, as given in Figs. 2.12(a)–2.12(c). It is also observed that there is always a steady scaling factor between original analog signal and the experimentally retrieved signal. As can be seen in Fig. 2.13(b), the scaling factor distribution is within a small range. The study demonstrates that the proposed method can resist scattering, absorption effect and environmental noise, and can realize high-robustness and high-fidelity optical signal transmission in free space through turbid water.

2.4 Summary

In this Chapter, a high-fidelity and high-robustness optical signal transmission channel has been proposed in free space through turbid water. It is demonstrated that a versatile

approach is developed to encode analog signals into random amplitude-only patterns in order to realize high-robustness and high-fidelity optical transmission in free space through turbid water. A number of experimental results have demonstrated that for different kinds of analog signals, the proposed method is able to realize high-fidelity information transmission through turbid water. Compared with conventional methods, the proposed method is easier to implement, and a *prior* knowledge about turbid water is not required. In terms of the higher data rate, other devices may be applied to replace the SLM used, e.g., digital micromirror device or LED-array. This work is meaningful to offer an insight into optical analog-signal transmission in free space through turbid water, and the proposed method could be of value in many applications.

Chapter 3 Non-Line-of-Sight Optical Information Transmission through Turbid Water

3.1 Introduction

Wireless data transmission plays an important role in various research areas, and has stimulated considerable interest in recent years. To satisfy the ever-increasing demands for various applications (e.g., communication [143–146]), wireless data transmission is expected to be continuously developed. There are many wireless data transmission technologies, e.g., radio-frequency [147], acoustic [148] and optical wireless [149–154]. Radio frequency transmission technology provides high-velocity waves, but it is not highly suitable for long-distance transmission since radio frequency waves attenuate rapidly (e.g., through turbid water). Acoustic transmission technology uses acoustic waves to carry information which can be restricted by low-bandwidth and noise pollution in turbid water environment. Recently, it has been found that optical wireless communication is a promising alternative for free-space data transmission through turbid water, which offers high bandwidth, low latency, and unlicensed optical spectra.

However, for free-space optical transmission through turbid water, one fundamental challenge is that turbid water has strong absorption and scattering effects on optical beams resulting from water molecules and suspended particles. In this case, it is difficult to realize high-fidelity and high-efficiency free-space optical information transmission through turbid water. Another significant challenge is to deal with the obstacles in the optical path, e.g., walls, rocks, large suspended particles and organic matters or planktonic organisms in the water, which block wave propagation between the transmitter and the receiver. When there are obstacles in the optical path, the light dramatically attenuates. Traditional line-of-sight scheme is not suitable in this case, since a strict alignment

between the transmitter and the receiver is requested. Therefore, non-line-of-sight (NLOS) optical wireless communication [155–158] has been developed, and can relieve the strict pointing and tracking requirements in the line-of-sight link. In addition, it is also important to address the diffusing loss resulting from obstacles. WFS has been developed to mitigate the attenuation problem by controlling the wavefront [159–162]. However, WFS needs a feedback control using an iterative algorithm which is complicated and time-consuming. Therefore, it is highly desirable to establish a simple NLOS free-space optical information transmission system to transmit optical signals through turbid water.

In this Chapter, a new method is proposed to establish a high-fidelity and high-robustness laser-based NLOS transmission channel through turbid water. This is the first investigation of encoding signal information into 2D random amplitude-only patterns to realize high-fidelity free-space optical transmission through turbid water around a corner. In the proposed method, original signal is considered as independent pixel values, and each pixel value is encoded into a 2D random amplitude-only pattern. The generated amplitude-only patterns are sequentially embedded into SLM to be illuminated to propagate through turbid water. The optical wave is diffused through turbid water. Subsequently, part of the diffused wave reflects from a scattering wall around the corner, and the rest of the wave is blocked. At the receiving end, a single-pixel detector [163–167] is used to record light intensity. At the receiver operation, high-fidelity signal information can be retrieved by using the collected light intensity without complicated post-processing algorithms. The proposed method is fully verified by using different turbid water conditions, different separation distances around the corner and different detection angles, and optical experimental results are quantitatively evaluated. In addition to free-space one-dimensional analog-signal transmission, it is also feasible to transmit grayscale images in

the designed NLOS link through turbid water. The proposed approach can effectively overcome the challenges in conventional NLOS free-space optical data transmission methods, i.e., low-fidelity analog signal retrieval through turbid water, low light detection, low mobility and high pointing errors. The corresponding publication is as follows:

Zilan Pan, Yin Xiao, Lina Zhou, Yonggui Cao, Mo Yang, and Wen Chen, "Non-line-of-sight optical information transmission through turbid water," Optics Express, 29 (24), 39498–39510, 2021.

3.2 Principle

Figure 3.1 shows a schematic experimental setup for laser-based NLOS free-space optical information transmission through turbid water around a corner. He-Ne laser with wavelength of 633.0 nm is used, and an amplitude-only SLM serves as the transmitter. Original signal is first encoded into a series of 2D computer-generated random amplitude-only patterns which are sequentially embedded into the amplitude-only SLM.

The proposed optical encoding method is described as follows: Firstly, a 2D matrix with random real values is generated. Then, FFT is applied to the 2D matrix to obtain its corresponding spectrum *G*. Zero frequency of spectrum *G* is replaced by one pixel value of original signal, and a new Fourier spectrum *G*' is correspondingly generated. Next, IFFT is applied to the Fourier spectrum *S*' to obtain an updated random amplitude-only pattern. The above steps are repeated until all the pixels of original signal are individually encoded into random amplitude-only patterns. Since the finally generated random amplitude-only pattern for each pixel value of original signal contains negative values, a positive constant *t* is further used to divide the generated random amplitude-only pattern (*P*) into two patterns (*t*+*P*) and (*t*-*P*) which are sequentially embedded into the SLM in

optical experiments. A flow chart is further shown in Fig. 3.2 to illustrate the proposed optical data encoding method.

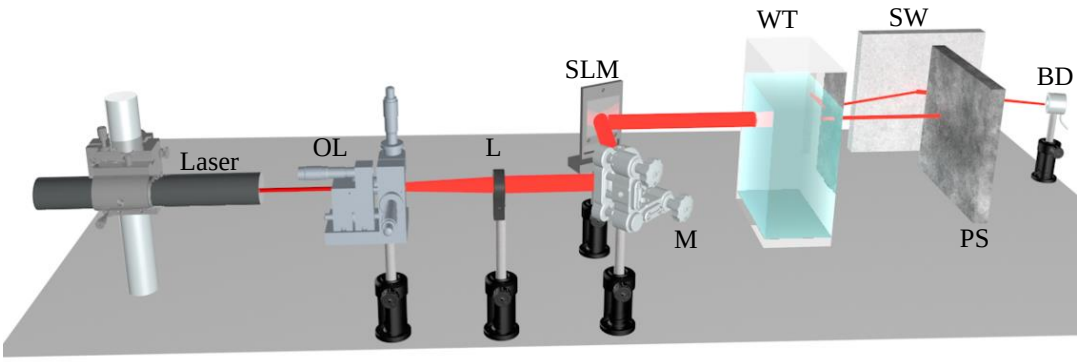

Figure 3.1 Experimental setup for the proposed NLOS free-space optical information transmission system: OL: Objective lens with magnification of 40; SLM: Amplitude-only spatial light modulator; WT: Water tank; SW: Scattering wall; BD: Single-pixel (bucket) detector; L: Lens with focal length of 100.0 mm; M: Mirror; PS: Protective screen to block the beam. An ordinarily white paper is used as the scattering wall.

As can be seen in Fig. 3.1, the wave propagates in free space through turbid water which consists of skimmed milk and clean water. The diameter of skimmed milk particles ranges from 10 to 600 nm. The particles can result in strong scattering effects, including Mie scattering and Rayleigh scattering [168]. The optical wave is attenuated rapidly by the scattering effects. In addition, when the wave propagates through turbid water, the photons encounter absorption effect. To characterize these parameters, the scattering and absorption coefficients are defined as μ_s and μ_a, respectively. The total attenuation coefficient $\mu(\lambda)$ can be represented as the sum of scattering and absorption coefficients described by

$$\mu = \mu_s + \mu_a, \tag{3.1}$$

According to Beer-Lambert law [169], the light intensity can be calculated by

$$I = I_0 \exp(-\mu l), \tag{3.2}$$

where I_0 denotes the incident light intensity, $I(l)$ denotes the transmitted light intensity, l denotes the path length, and $\mu(\lambda)$ is also called Beer's coefficient.

Behind turbid water, the diffused optical wave further propagates around a corner, as seen in Fig. 3.1. Part of the diffused optical wave is blocked by a protective screen as shown in Fig. 3.1, and other part of the diffused wave is reflected by scattering wall and then recorded by a single-pixel detector at the receiving end. The single-pixel detector is a high-sensitivity device, and is suitable for wide-range wavelength and low-light detection. Finally, the recorded light intensity is used to directly retrieve the signal. The recording and retrieval process is described by

$$\begin{aligned} \mathrm{B1} &= \delta \iint \left[t + P(x,y) \right] e^{-2\pi j(x\xi + y\eta)} dxdy \Big|_{\xi=0,\eta=0}, \\ &= \delta \iint \left[t + P(x,y) \right] dxdy \end{aligned} \tag{3.3}$$

$$\begin{aligned} \mathrm{B2} &= \delta \iint \left[t - P(x,y) \right] e^{-2\pi j(x\xi + y\eta)} dxdy \Big|_{\xi=0,\eta=0}, \\ &= \delta \iint \left[t - P(x,y) \right] dxdy \end{aligned} \tag{3.4}$$

$$\mathrm{B} = \mathrm{B1} - \mathrm{B2} = 2\delta \iint P(x,y) dxdy. \tag{3.5}$$

where $j = \sqrt{-1}$, (x,y) denotes the coordinate in spatial domain, (ξ,η) denotes the coordinate in frequency domain, $t+P(x,y)$ and $t-P(x,y)$ denote 2D random patterns (512×512 pixels), B1 and B2 denote the recorded intensity values, B denotes the retrieved signal, and δ denotes a scaling factor. In the proposed method, scaling factors exist between the retrieved data and original data, as shown in Eqs. (3.3) and (3.4). In the proposed method, each pixel value of original signal has been encoded into two random amplitude-only patterns, and a subtraction operation between the two corresponding intensity points recorded by single-pixel detector can be directly used for retrieving each pixel value of original signal as described in Eq. (3.5).

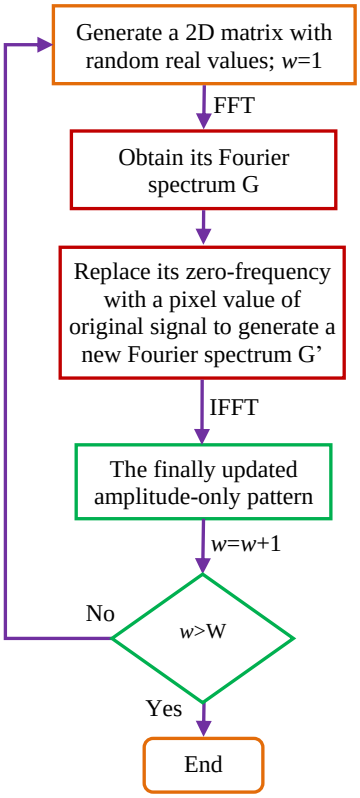

Figure 3.2 Flow chart for the generation of a series of 2D random amplitude-only patterns: *w* denotes each pixel (1, 2, 3,…); W, the total number of pixels in original signal.

3.3 Experimental Results and Discussion

A series of optical experiments are carried out to illustrate feasibility and effectiveness of the proposed NLOS free-space optical information transmission through turbid water around a corner. In Fig. 3.1, He-Ne laser with 17.0 mW and wavelength of 633.0 nm is used. A beam expander with a magnification of 40 is used to adjust size of the laser beam followed by the collimation using a converging lens with focal length of 100.0 mm. The collimated laser beam is reflected by a mirror and illuminates the surface of an amplitude-only SLM (Holoeye, LC-R720) with pixel size of 20.0 μm. In this study, a modulation rate of 1.25 Hz is used to conduct a proof-of-principle experiment and verify the proposed method. The angle between the incident beam and the reflected beam on the SLM is 45°. The water tank in Fig. 3.1 is made from PMMA, and has a dimension of 60 mm (L) × 110

mm (W) × 300 mm (H). In this study, axial distance between the SLM and water tank is 100 mm, and axial distance between water tank and scattering wall is 50 mm. Axial distance between the scattering wall and single-pixel detector is 100 mm. A single-pixel detector (Newport, 918D-UVOD3R) and a power meter (Newport, 1936-R) are used to record light intensity at the receiving end. Temperature in the laboratory is set as 24℃ for optical experiments.

3.3.1 Turbidity of Water

The optical wave dramatically attenuates, when it propagates through turbid water. Scattering is a form of accumulation, which means that the bigger the turbidity is, the heavier its impact on quality of the retrieved signal. The effect of different turbidities of turbid water on the accuracy of the proposed free-space optical signal transmission is experimentally tested here. In the optical experimental setup shown in Fig. 3.1, 850 mL clean water is first prepared and placed into the water tank, and then skimmed milk in which molecules have diameters ranging from 10 to 600 nm is used to emulate turbidity. When particles have a size of 10 nm, they can lead to the forward and backward scattering effect. Therefore, skimmed milk is an optimal option to emulate all kinds of scattering effects in seawater conditions. Then, skimmed milk is added to the water tank in order to increase the turbidity. The volume of skimmed milk starts from 20 mL with an increase of 5 mL each time, and this process is repeated for five times. Three significantly different analog signals are randomly selected and tested in each milk concentration case. The wave propagation distance through turbid water is 60 mm, and separation distance around the corner, i.e., between scattering wall and protective screen, is set as 45 mm. In addition, the power just before water tank is 0.93 mW in optical experiments. To quantify turbidity level of the scattering medium, an optical power meter can be utilized to record the light

intensity after propagating through the turbid water. In Eq. (3.2), Beer's coefficient $c(\lambda)$ can be calculated based on the light intensity before water tank, the light intensities after water tank and the propagation distance through turbid water. Beer's coefficient $c(\lambda)$ can be calculated using Eq. (3.2) and is employed to represent the turbidity level [170,171].

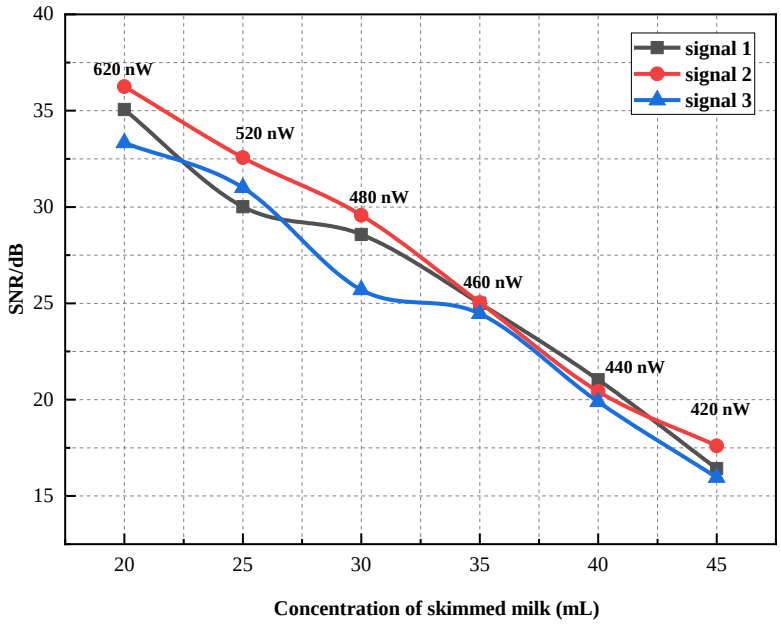

Figure 3.3 A relationship between the concentration of skimmed milk and the quality of retrieved signals at the receiving end. Turbid water in the water tank consists of 850 mL clean water and different volumes of skimmed milk.

To quantitatively evaluate performance of the proposed method, signal-to-noise ratio (SNR) is calculated and defined by

$$\mathrm{SNR} = 10 \times \log_{10}\left[\frac{\sum S_{ori}^2}{\sum \left(S_{ori} - S_{re}\right)^2}\right], \tag{3.6}$$

where S_{ori} denotes original signal and S_{re} denotes the retrieved signal. Quantitative results about the SNR variation with different concentrations of skimmed milk are shown in Fig. 3.3. The typically retrieved signals are shown in Figs. 3.4(a)–3.4(f), when different concentrations of skimmed milk are added to the water tank. It can be seen in Fig. 3.3 that

the SNR values decline with the incremental of skimmed milk concentration. When the volume of skimmed milk is increased to be 40 mL, SNR values for the three retrieved analog signals are close to 20 dB.

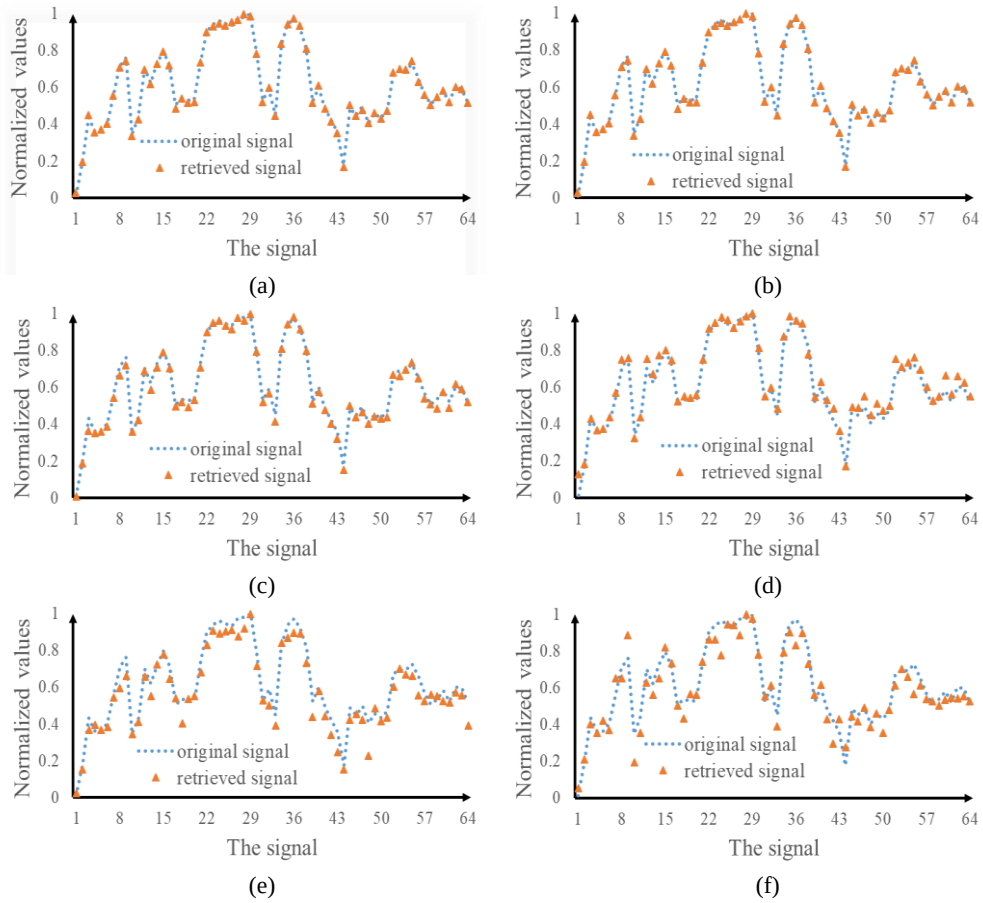

Figure 3.4 (a)–(f) Comparisons between original signal and the experimentally retrieved signals at the receiving end when different concentrations of skimmed milk (i.e., 20 mL, 25 mL, 30 mL, 35 mL, 40 mL and 45 mL) are respectively used in the water tank. The signal 2 in Fig. 3.3 is used and typically presented here.

The signals retrieved at the receiving end are shown in Figs. 3.4(e) and 3.4(f), when 40 mL and 45 mL skimmed milk is respectively used. When the concentrations of skimmed milk are smaller than 40 mL, the retrieved signals have high SNR values as shown in Fig. 3.3 and nearly overlap with original signals as shown in Figs. 3.4(a)–3.4(d). Due to the accumulation feature of scattering, scattering becomes stronger as the skimmed milk concentration increases, which will have the heavier influence on the quality of retrieved

signals. It is also illustrated in Figs. 3.3 and 3.4 that there is a steady decrease in the SNR values and light power when skimmed milk concentration is increased, and quality of the retrieved signals has a relationship with the light power. From the optical powers given in Fig. 3.3, it can be further observed that water turbidity significantly affects the propagating light wave, and lead to high scattering and high absorption in the free-space optical transmission channel. In addition, the optical experimental results in Figs. 3.3 and 3.4 demonstrate that the proposed method is able to directly retrieve high-fidelity and high-SNR analog signals in free-space optical transmission through turbid water around a corner.

3.3.2 Separation Distances Around the Corner

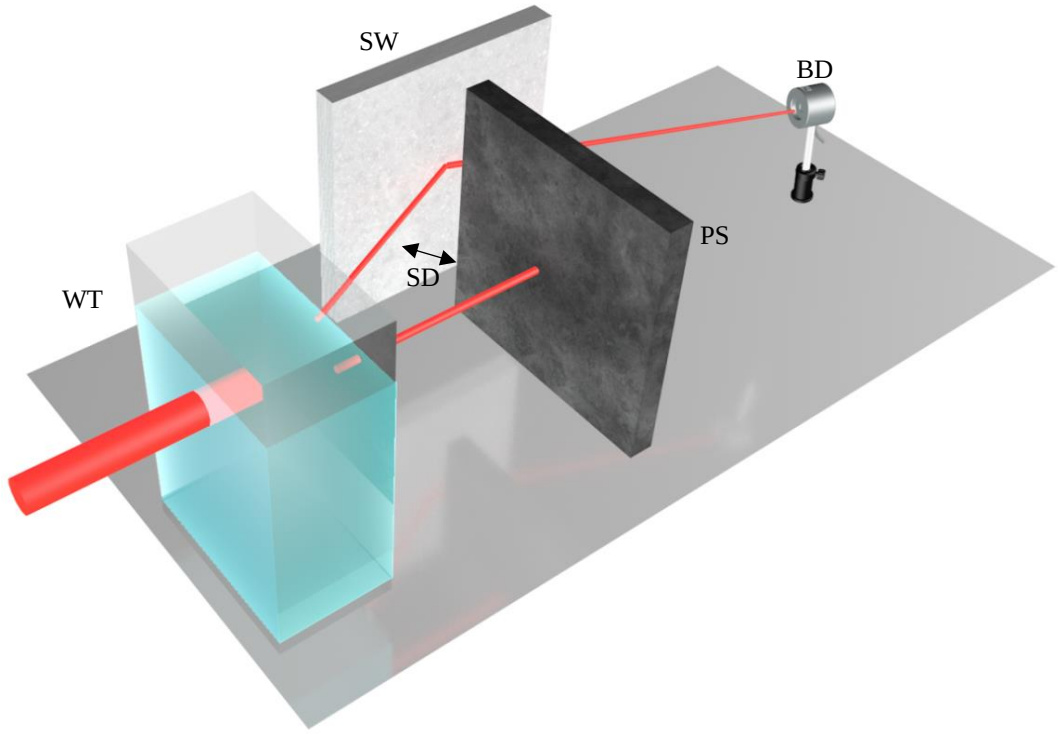

Figure 3.5 A schematic optical experimental setup for wave propagation around a corner behind turbid water: SD: separation distance. WT: Water tank; SW: Scattering wall; PS: Protective screen to block the beam; BD: Single-pixel (bucket) detector.

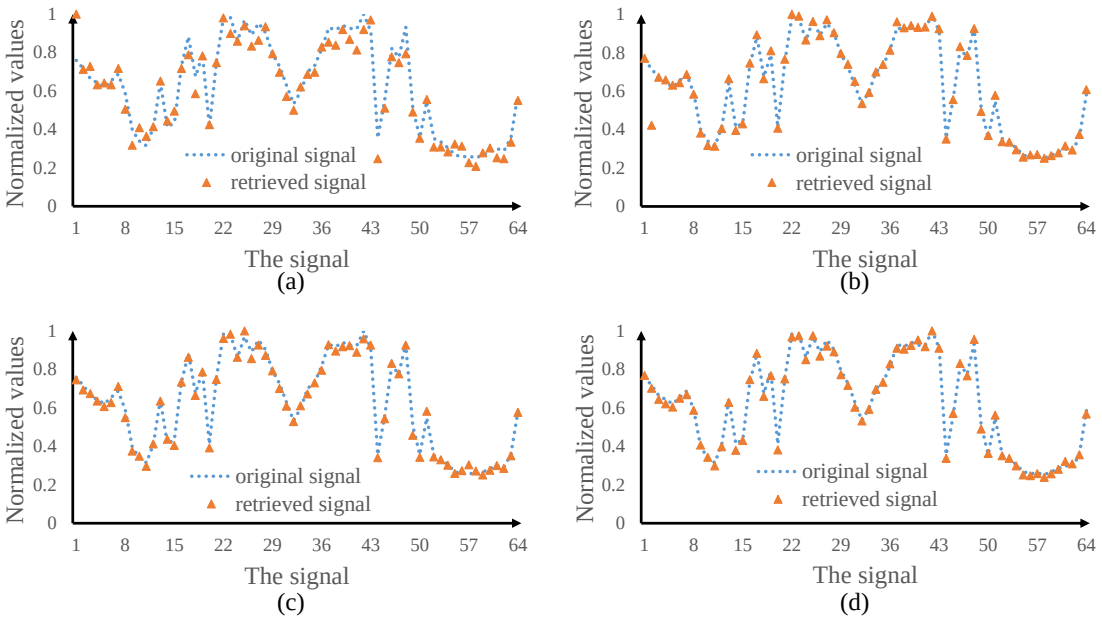

Figure 3.6 (a)–(d) Comparisons between the retrieved analog signals at the receiving end in optical experiments and original signal when different separation distances are used around the corner, i.e., SD= 3, 5, 15 and 30 mm. SNR values of the retrieved analog signals in (a)–(d) are 21.04 dB, 24.78 dB, 31.75 dB and 33.44 dB, respectively. MSE values of the retrieved analog signals in (a)–(d) are 3.55×10^{-3}, 1.50×10^{-3}, 3.01×10^{-4} and 2.04×10^{-4}, respectively.

In addition to water turbidity, the separation distance SD around the corner (i.e., between scattering wall and protective screen) in Fig. 3.5 can also affect optical power detected at the receiving end. In the optical experiment, a protective screen is placed between the transmitter and the receiver to block the wave, and the scattering wall is used to further reflect the diffused wave after turbid water.

In optical experiments, the scattering wall is opaque. In Fig. 3.5, an ordinarily white paper is used to emulate the scattering wall. In this optical experiment, 850 mL clean water is mixed with 20 mL skimmed milk to be placed into the water tank. The separation distance SD has an impact on the optical power detected at the receiving end, and a relationship between the separation distance SD and optical power detected at the receiving end is studied here. In this case, the loss is calculated by [172,173]

$$PL = 10\times\log_{10}\left(\frac{P_t}{P_r}\right), \tag{3.7}$$

where PL denotes the loss (dB), P_t denotes the power just before water tank, and P_r denotes optical power just before single-pixel detector. The power P_t just before water tank is 1.5 mW in the optical experiments. Optical experimental results are shown in Figs. 3.6(a)–3.6(d) and 3.7.

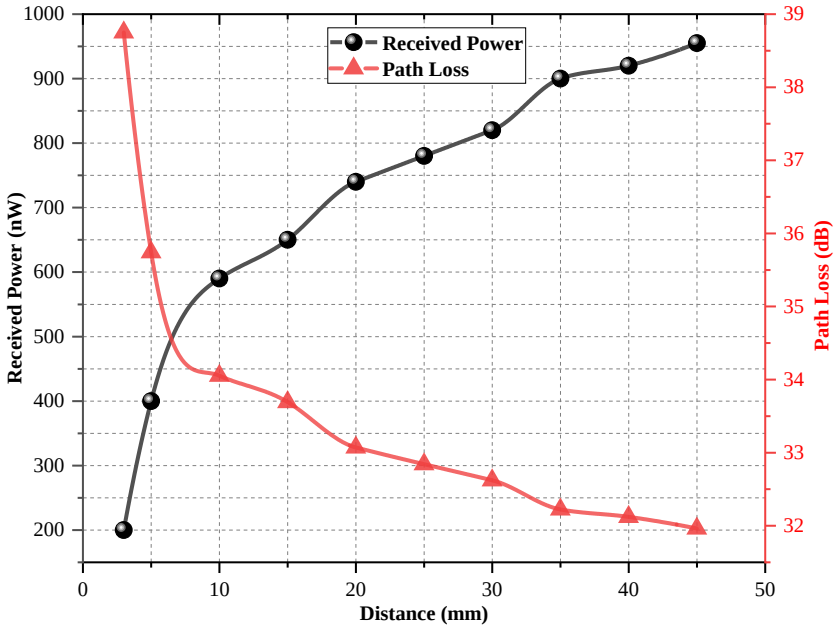

Figure 3.7 The detected optical power and the loss when optical wave propagates through turbid water (850 mL clean water with 20 mL skimmed milk) and further propagates around a corner respectively with the separation distance SD of 3, 5, 10, 15, 20, 25, 30, 35, 40 and 45 mm.

It can be seen in Figs. 3.6 and 3.7 that when the separation distance SD increases, optical power detected at the receiving end increases and power loss decreases. In addition, accuracy of the retrieved analog signals is enhanced. These optical experimental results illustrate the high-robustness feature of the proposed NLOS free-space optical transmission method through turbid water around a corner. There is a sharply downward trend in the detected power when the separation distance is lower than 3 mm, since only a small part of optical wave is reflected by the scattering wall and others are blocked by the protective screen. When the separation distance SD is lower than 3 mm, MSE values are larger than 3.55×10^{-3} and SNR values are smaller than 21.04 dB. Therefore, it can be

seen in Figs. 3.6 and 3.7 that when the separation distance SD is not smaller than 5 mm, the retrieved signals are always of high fidelity.

3.3.3 The Detection Range of Single-Pixel Detector

In conventional free-space optical transmission systems through complex media, the acquisition, tracking and pointing can be difficult, and pointing errors cannot be effectively mitigated. In addition, the alignment process is complicated when there are turbid water and obstacles in the wave propagation path. In the proposed NLOS free-space optical transmission system, there is no need to accurately place the single-pixel detector at the receiving end, and pointing errors can be fully suppressed.

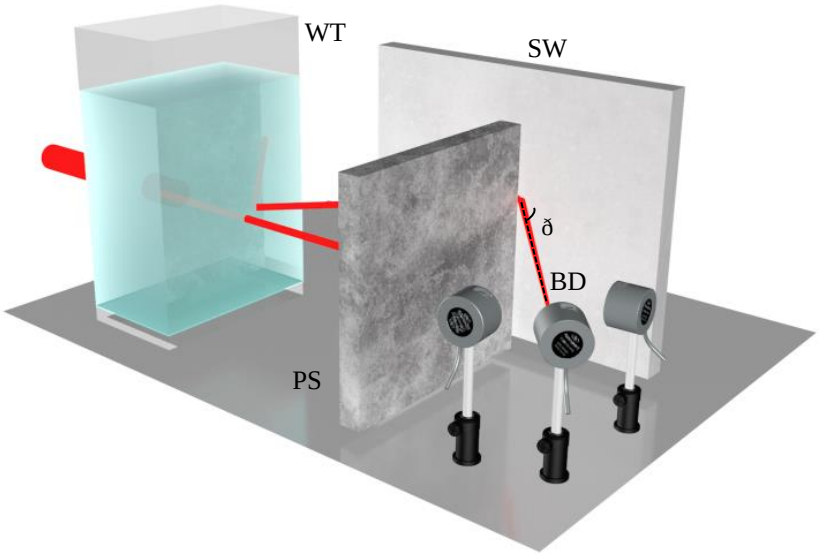

Figure 3.8 A schematic setup for testing the detection range of single-pixel detector: normal direction denotes zero degree as indicated by the dotted line. ð denotes different positions of single-pixel detector. Clockwise direction denotes positive degree, and counterclockwise direction denotes negative degree.

In Fig. 3.8, the optical wave propagates through turbid water, and then the diffused wave is further reflected by the scattering wall. The reflected wave is detected by using a single-pixel detector placed at an arbitrary position (ð). Here, the detection angle (ð) range of single-pixel detector is further studied. In optical experiments, 850 mL clean water is

mixed with 20 mL skimmed milk, and an ordinarily white paper is used as the scattering wall. The power loss is calculated to investigate performance of the developed NLOS free-space optical transmission system.

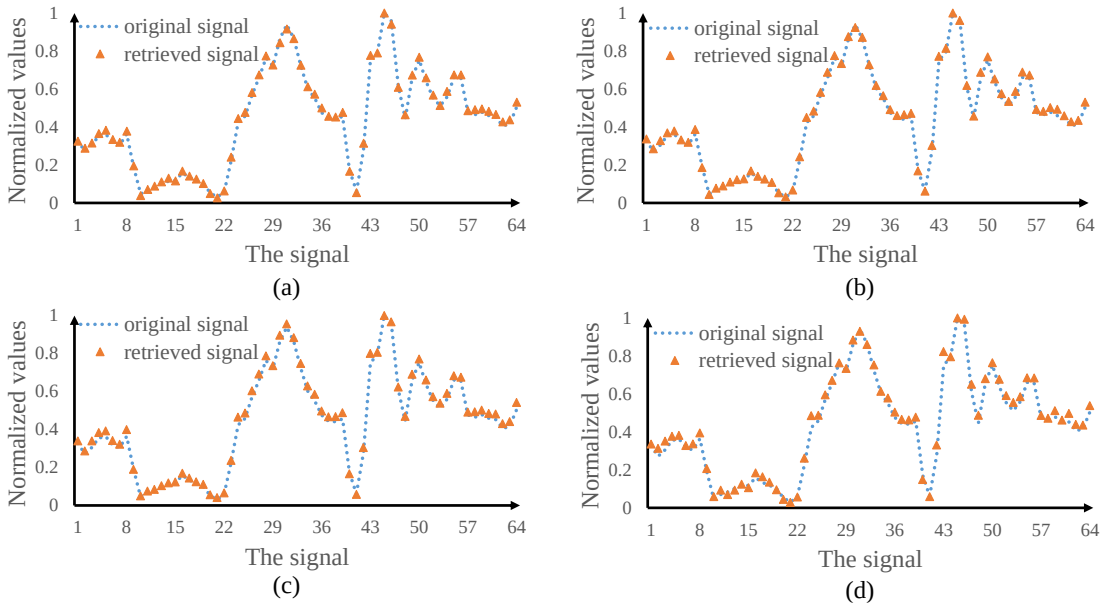

Figure 3.9 (a–d) Comparisons between analog signals retrieved at the receiving end in optical experiments and the original signal when different detection angles ð={0°, 15°, 35°, 45°} of single-pixel detector at the receiving end are respectively used.

It can be seen in Figs. 3.9 and 3.10 that when the single-pixel detector is arbitrarily moved and placed in a detection angle ranging from -45° to 45°, the proposed method can always realize high-fidelity free-space optical data transmission. In other words, the proposed method can realize a large angular coverage at the receiving end, and high mobility is achieved. Optical experimental results demonstrate that the proposed method is robust, and pointing errors existing in conventional methods are effectively suppressed. The single-pixel detector is a high-sensitivity device, and can be applied in low-light detection environment. The proposed method can realize a multi-point connection, and can mitigate the workload of multiple carriers on each sensor.

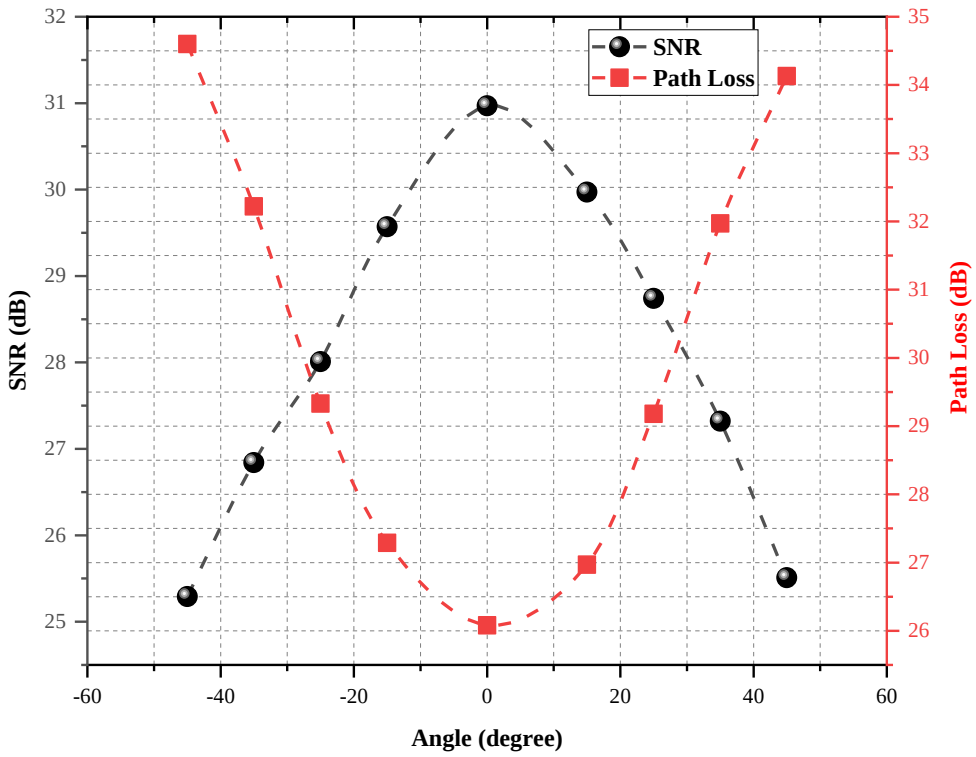

Figure 3.10 SNR values of the retrieved signals and power loss obtained when different detection angles ð of -45°, -35°, -25°, -15°, 0°, 15°, 25°, 35° and 45° are respectively used.

3.3.4 Two-Dimensional Grayscale-Image Transmission

In addition to one-dimensional analog signals, the proposed method is also feasible to transmit grayscale images. In optical experiments, the turbid water consists of 850 mL clean water and 25 mL skimmed milk. In this case, the separation distance SD around the corner is 25 mm, and the detection angle of single-pixel detector is set as 0°.

(a) (b) (c)

Figure 3.11 Optical experimental results obtained by using single-pixel bucket detector: (a)–(c) 2D images (64×64 pixels) typically retrieved at the receiving end. The PSNR and SSIM values are given.

To quantitatively evaluate quality of the retrieved images at the receiving end, two evaluation parameters, i.e., PSNR [174–176] and SSIM [174], are calculated. The maximum SSIM value is 1, and the calculated SSIM value shows the similarity between original image and the retrieved image obtained at the receiving end.

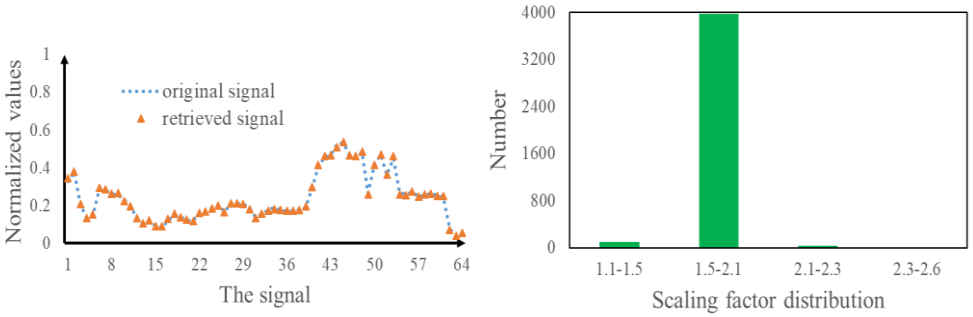

(a) (b)

Figure 3.12 (a) A comparison between pixel values along the 55th row of the retrieved image in Fig. 3.11(c) and those along the 55th row of original image, and (b) a scaling factor distribution (magnitude of the coefficients: 2×10^{-12}) corresponding to that in Fig. 3.11(c).

In optical experiments, the typically retrieved images are shown in Figs. 3.11(a)–3.11(c). It can be seen in Figs. 3.11(a)–3.11(c) that the three retrieved images are of high fidelity, and PSNR values are 40.53 dB, 37.13 dB and 41.90 dB, respectively. The SSIM values for Figs. 3.11(a)–3.11(c) are 0.9929, 0.9893, and 0.9920, respectively. To clearly show the quality of retrieved images, the pixel values along the 55th row in Fig. 3.11(c) are shown in Fig. 3.12(a), and the experimentally retrieved data overlap with original data. It is also found that scaling factor between the retrieved image and original image can be further calculated to evaluate the quality. As can be in Fig. 3.12(b), the scaling factors are within a small range. It is illustrated that high-fidelity grayscale image can be retrieved in the proposed NLOS free-space optical data transmission method.

3.4 Summary

In Chapter 3, a new and robust method has been proposed for NLOS free-space optical data transmission through complex media, and high-fidelity free-space optical data transmission through turbid water around a corner has been realized. Optical experiments have been conducted to verify the proposed method using different turbid water conditions, different separation distances around the corner and different detection angles of single-pixel detector. Optical experimental results demonstrate that the proposed method possesses high feasibility and high robustness when there are turbid water and obstacles in the wave propagation path. In addition, different signals, e.g., analog signals and grayscale images, are widely tested by using the proposed method. The proposed approach can effectively overcome the challenges in conventional NLOS free-space optical data transmission methods, i.e., low-fidelity analog signal retrieval through turbid water, low light detection, low mobility and high pointing errors.

Chapter 4 Optical Data Transmission through Highly Dynamic and Turbid Water Using Dynamic Scaling Factors and Single-Pixel Detector

4.1 Introduction

Free-space optical communication is promising for versatile, secure and high-bandwidth data transmission in various applications, e.g., underwater [177–180]. Recently, there has been much research interest in using light as information carrier in underwater transmission links, since the light can provide the larger bandwidth, higher capacity, and lower power consumption compared to other communication techniques [181–185]. A challenging scenario is free-space optical data transmission through dynamic and turbid water, and it is well recognized that complex water environment could hinder applications of optical wireless communication. There is a severe power loss of optical wave in highly dynamic and turbid water environment, and the power loss is mainly due to absorption, scattering and turbulence [186–190]. Absorption and scattering depend on the wavelength of light and water properties, e.g., density and particles. The turbulence also imposes a limit on the propagating wave due to the fluctuation in refractive index of water in the presence of air bubbles, temperature and salinity [191–194], and could induce beam wandering and wavefront distortion. Until now, much research was focused on the enhancement of data rate and working distance [195–197] in free-space optical communication. However, real situations related to free-space optical data transmission in water environment, e.g., strong turbulence and dynamic water, are always overlooked in previous work. This issue is still open for research. In addition, much research work used a tank filled with clean water in optical experiments. However, in real water environment, attenuation coefficient is significantly high due to particles, air bubbles and

turbulence. Therefore, it is desirable to develop new approaches to retrieving accurate signals, when optical wave propagates through highly dynamic and turbid water.

In this Chapter, a new approach is proposed to establish a high-fidelity and high-robustness optical wireless transmission channel through highly dynamic and turbid water using a series of dynamic scaling factors to correct light intensities recorded by a single-pixel bucket detector. This is the first investigation of utilizing dynamic scaling factors to realize high-fidelity and high-robustness free-space optical data transmission in highly dynamic and turbid water environment. A signal to be transmitted is considered as a series of independent pixels, and each pixel value is encoded into a 2D random amplitude-only pattern. The series of generated random amplitude-only patterns, called illumination patterns, is sequentially embedded into a SLM, and a fixed reference pattern, i.e., a pre-generated random amplitude-only pattern, is used before each illumination pattern to correct the recorded light intensities. Optical wave is diffused through highly dynamic and turbid water, and a single-pixel bucket detector [198–200] is used to record a series of light intensities. The proposed method is experimentally verified by using different turbid water conditions, different strengths of water-flow-induced turbulence and a laser with different wavelengths. Experimental results demonstrate that high-fidelity irregular analog signals can be retrieved by using the proposed method, and high robustness against turbulence generated by water flow is achieved. The corresponding publication is as follows:

Zilan Pan, Y. Xiao, Y. Cao, L. Zhou, and W. Chen, "Optical data transmission through highly dynamic and turbid water using dynamic scaling factors and single-pixel detector," Opt. Express 30(24), 43480–43490 (2022).

4.2 Methodology

In the developed free-space optical data transmission system, a signal to be transmitted is first encoded into a series of 2D random amplitude-only patterns to be sequentially embedded into the SLM in Fig. 4.1.

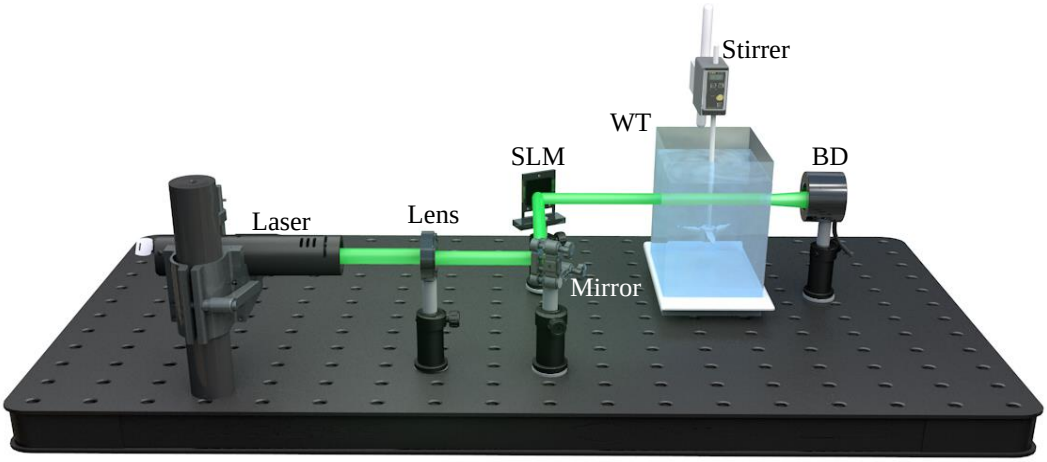

Figure 4.1 A schematic experimental setup to verify the proposed method.

The optical data encoding process is as follows:

(1) generate a 2D random matrix (512×512 pixels) with real and positive values;

(2) apply FFT to the 2D random matrix generated in Step (1) to obtain its spectrum;

(3) replace zero frequency of the generated spectrum in Step (2) by a pixel value of original signal, and then a new Fourier spectrum is obtained;

(4) apply inverse IFFT to the new Fourier spectrum obtained in Step (3) to generate an updated random amplitude-only pattern (P);

(5) repeat the above Steps (1)-(4) until every pixel of original signal is encoded into a 2D random amplitude-only pattern. The series of generated random amplitude-only patterns (P) can be sequentially embedded into the SLM in Fig. 4.1. Since it is impossible to use the SLM to directly display the generated pattern that contains negative values, a

positive and real constant m is further used to divide each generated pattern (P) into two separate patterns ($m+P$) and ($m-P$), called illumination patterns.

In Fig. 4.1, the propagating wave is distorted by highly dynamic and turbid water, i.e., via scattering, absorption and turbulence. Attenuation coefficient $u(\lambda)$ consists of absorption and scattering which are related to wavelength of the laser, respectively denoted by $c_a(\lambda)$ and $c_s(\lambda)$. In the optical transmission through turbid water, absorption leads to a large power loss in the wave propagation path, and absorption coefficient depends on light wavelength and water properties (e.g., different chemical compositions of dissolved materials). Scattering deflects the photons in random directions, and leads to beam wandering and wavefront distortion. These attenuations [201–205] affect the light intensities recorded at the receiving end, and according to Beer-Lambert law [206–209] the process can be described by

$$I = I_0 \exp(-\mu l), \tag{4.1}$$

$$\mu = \mu_s + \mu_a, \tag{4.2}$$

where I_0 denotes incident light intensity, $I(l)$ denotes output light intensity, and l denotes the path length. In addition, the turbulence is also induced by random changes of refractive index in the wave propagation path due to salinity, temperature and pressure.

To obtain dynamic scaling factors in highly dynamic and turbid water environment, a fixed reference pattern $R(x,y)$, i.e., a random amplitude-only pattern, is further proposed here and embedded into the SLM before each illumination pattern, i.e., ($m+P$) and ($m-P$). At the receiving end, light intensities are recorded by using the single-pixel bucket detector in Fig. 4.1. The recording process is described by

$$\mathrm{B}_{ir} = k_i(t_i) \iint R(x,y) e^{-2\pi j(x\xi + y\eta)} dxdy \Big|_{\xi=0,\eta=0} + noise, \tag{4.3}$$

$$\mathrm{B}_{i1} = k_i\,(t_{i+1}) \iint \left[m + P(x,y) \right] e^{-2\pi j(x\xi + y\eta)} dxdy \Big|_{\xi=0,\eta=0} + noise, \tag{4.4}$$

$$\bar{\mathrm{B}}_{ir} = k_{i+1}(t_{i+2}) \iint R(x,y) e^{-2\pi j(x\xi + y\eta)} dxdy \Big|_{\xi=0,\eta=0} + noise, \tag{4.5}$$

$$\mathrm{B}_{i2} = k_{i+1}(t_{i+3}) \iint \left[m - P(x,y) \right] e^{-2\pi j(x\xi + y\eta)} dxdy \Big|_{\xi=0,\eta=0} + noise, \tag{4.6}$$

where $j = \sqrt{-1}$, (x,y) denotes coordinate in spatial domain, (ξ,η) denotes coordinate in frequency domain, B_{i1} and B_{i2} denote the recorded intensity values corresponding to the ith pixel of the transmitted signal, B_{ir} and $\bar{\mathrm{B}}_{ir}$ denote the recorded intensity values corresponding to the reference pattern, and $k(t)$ denotes time-varying (dynamic) scaling factors. In the free-space optical data transmission system, environmental and shot noise is always induced. Since every time interval between the reference pattern and each illumination pattern (e.g., t_{i+1}-t_i or t_{i+3}-t_{i+2}) is short, adjacent scaling factors can be assumed to be the same, i.e., $k_i(t_i) \approx k_i(t_{i+1})$ and $k_{i+1}(t_{i+2}) \approx k_{i+1}(t_{i+3})$.

Therefore, each pixel value B_i of a signal obtained at the receiving end is retrieved by

$$\begin{aligned}
\mathrm{B}_i &= \frac{\mathrm{B}_{i1}}{\mathrm{B}_{ir}} - \frac{\mathrm{B}_{i2}}{\bar{\mathrm{B}}_{ir}} \\
&= \frac{k_i\,(t_{i+1}) \iint \left[m + P(x,y) \right] dxdy + noise}{k_i(t_i) \iint R(x,y) dxdy + noise} - \frac{k_{i+1}(t_{i+3}) \iint \left[m - P(x,y) \right] dxdy + noise}{k_{i+1}(t_{i+2}) \iint R(x,y) dxdy + noise} \\
&\approx \frac{1}{\iint R(x,y) dxdy + noise} \left\{ \iint \left[m + P(x,y) \right] dxdy - \iint \left[m - P(x,y) \right] dxdy \right\} \\
&= \frac{2}{\iint R(x,y) dxdy + noise} \iint P(x,y) dxdy \\
&\propto \iint P(x,y) dxdy
\end{aligned} \quad . \tag{4.7}$$

Based on Eq. (4.7), the noise part is eliminated, and noise magnitude is far smaller than that of signal which is also verified by our experimental results. Therefore, the noise can be fully suppressed, and the retrieved intensity value is proportional to original signal

pixel. Therefore, high-fidelity signals can be retrieved at the receiving end in the proposed free-space optical data transmission through highly dynamic and turbid water.

4.3 Experimental Results and Discussion

A schematic experimental setup is shown in Fig. 4.1 to verify the developed free-space optical data transmission through highly dynamic and turbid water. In Fig. 4.1, a laser is controlled by using a laser diode mount (Thorlabs, LDM56/M) in a range of 0-500 mA, and three different wavelengths are individually used, i.e., 658.0 nm, 520.0 nm and 405.0 nm. A lens with focal length of 100.0 mm is utilized to collimate the laser beam, and then the collimated optical wave illuminates an amplitude-only SLM (Holoeye, LC-R720) with pixel size of 20.0 μm. The modulated optical wave propagates through highly dynamic and turbid water tank, and a stirrer is used to generate dynamic water environment. In this study, a water tank with size of 10.0 cm (L) × 25.0 cm (W) × 30.0 cm (H) is used to conduct a proof-of-principle experiment and verify the proposed method. The longer transmission distances can also be used in the proposed scheme, and the estimated propagation distance through dynamic and turbid water could be approximately 120.0 m in the proposed scheme according to Beer-Lambert law. A single-pixel bucket detector (Newport, 918D-UV-OD3R) with optical power meter (Newport, 1936-R) is applied to record a series of light intensities at the receiving end. In optical experiments, axial distance between the SLM and water tank is 10.0 cm, and axial distance between water tank and single-pixel bucket detector is 5.0 cm.

4.3.1 The Turbidity

To verify the proposed method, different volumes of milk are mixed with clean water to be placed in the water tank in Fig. 4.1. Dissolving milk in clean water creates particle

suspension, and can change attenuation coefficients. To emulate the turbidity, different volumes of milk are added to clean water with volume of 3.0 L, resulting in a variation of attenuation coefficients. Beer's coefficient μ(λ) is calculated based on Eq. (4.1), and is used to describe turbidity level [206,207] in this study. Performance of the developed free-space optical data transmission system through highly dynamic and turbid water can be evaluated, and experimental results are shown in Figs. 4.2 and 4.3.

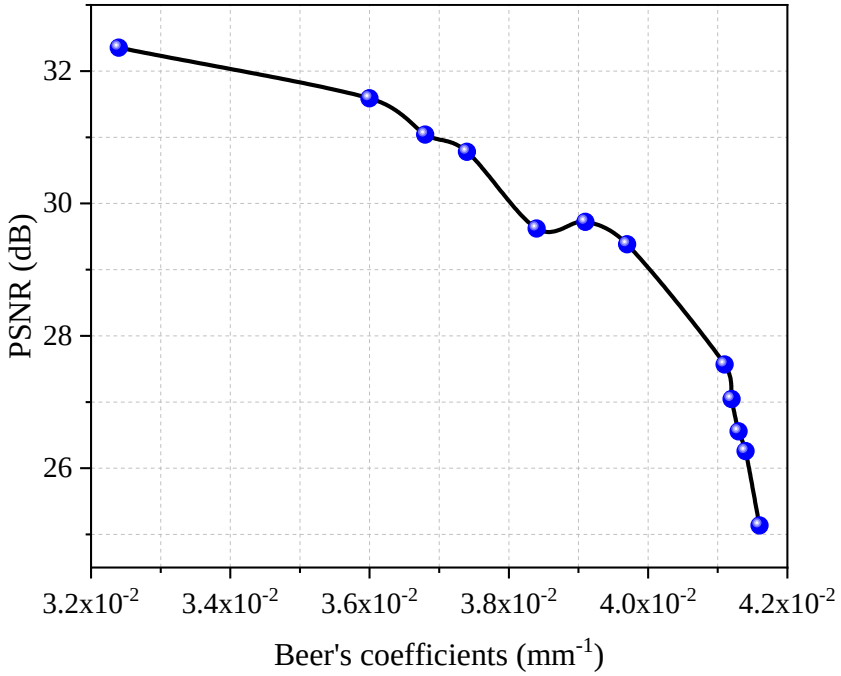

Figure 4.2 PSNR values of the retrieved signals using the proposed method in the free-space optical data transmission through highly dynamic and turbid water when different water turbidities are used and tested. In this experiment, speed of the stirrer is 900.0 rpm.

To quantitatively evaluate quality of the signals retrieved at the receiving end, PSNR [208,209] is calculated. Fig. 4.2 shows PSNR values of the retrieved signals, when turbidity of water in the tank, i.e., attenuation coefficients, is 3.24×10^{-2}, 3.60×10^{-2}, 3.68×10^{-2}, 3.74×10^{-2}, 3.84×10^{-2}, 3.91×10^{-2}, 3.97×10^{-2}, 4.11×10^{-2}, 4.12×10^{-2}, 4.13×10^{-2}, 4.14×10^{-2} and 4.16×10^{-2}, respectively. It can be seen in Fig. 4.2 that PSNR decreases with the increase of water turbidity level. When the turbidity is not larger than 3.97×10^{-2}, the

retrieved signals are of high fidelity as shown in Figs. 4.3(a)–4.3(c). It is illustrated that the proposed method is feasible and effective. When attenuation coefficients are larger than 3.97×10^{-2}, PSNR values of the retrieved analog signals decrease dramatically as shown in Fig. 4.3(d). Due to the accumulation feature, scattering becomes stronger as milk concentration increases. It is also demonstrated in Figs. 4.2 and 4.3 that quality of the retrieved signals has a strong relationship with the detected light power, and highly dynamic and turbid water leads to a power loss of the propagating wave via scattering and absorption.

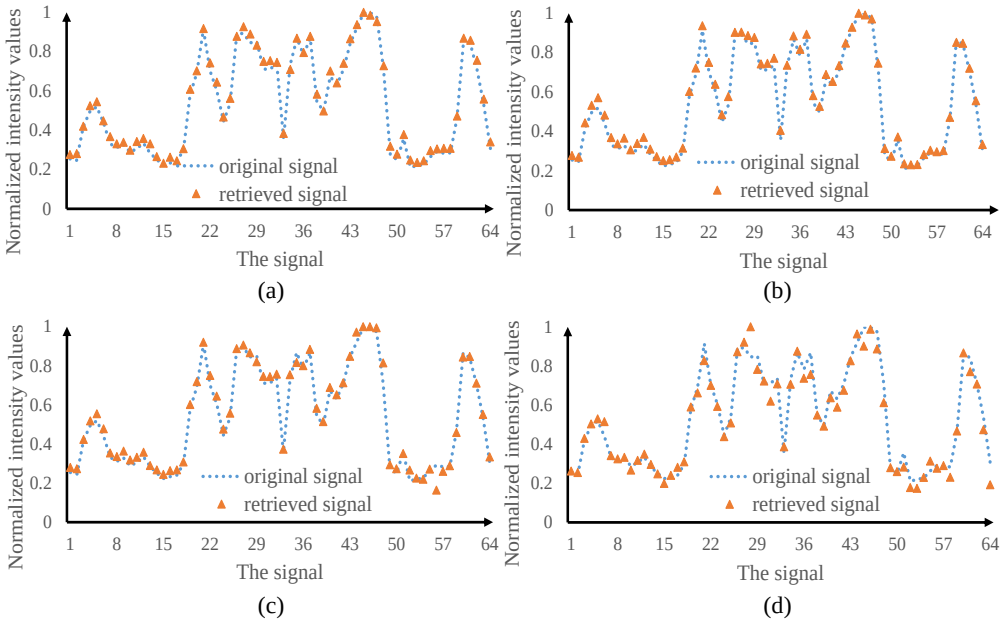

Figure 4.3 Comparisons between original signal and the experimentally retrieved signals at the receiving end when different volumes of milk are used in the water tank to have an attenuation coefficient of (a) 3.24×10^{-2}, (b) 3.74×10^{-2}, (c) 3.97×10^{-2} and (d) 4.13×10^{-2}.

4.3.2 Water-Flow-Induced Turbulence

A real water environment is always not static, and could be complex. A real water environment also produces turbulence. Therefore, we also investigate effect of water-flow-induced turbulence on the performance of the proposed method. In our study, dynamic water flow is generated by using a stirrer in Fig. 4.1, and different turbulence

strengths are obtained by using different speeds of the stirrer in the water tank. The turbulences result in beam distortion and beam wandering, which cause large fluctuations of light intensities recorded at the receiving end.

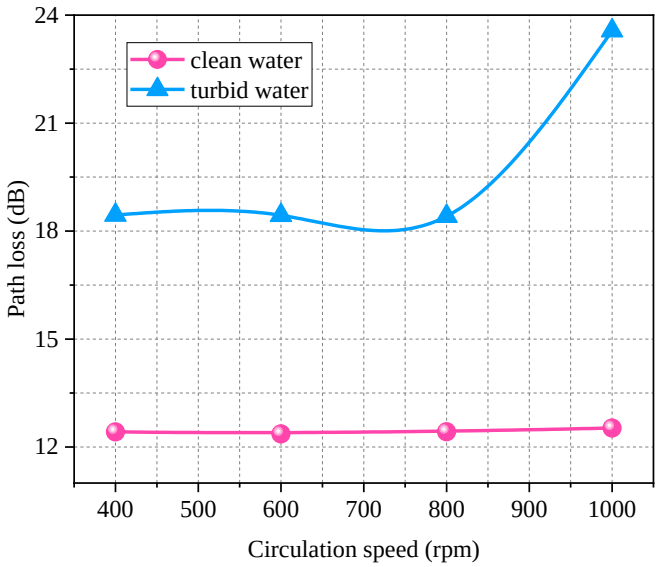

Figure 4.4 Path loss due to wave propagation through clean water and turbid water in the tank when speed of the stirrer is 400.0, 600.0, 800.0 and 1000.0 rpm, respectively.

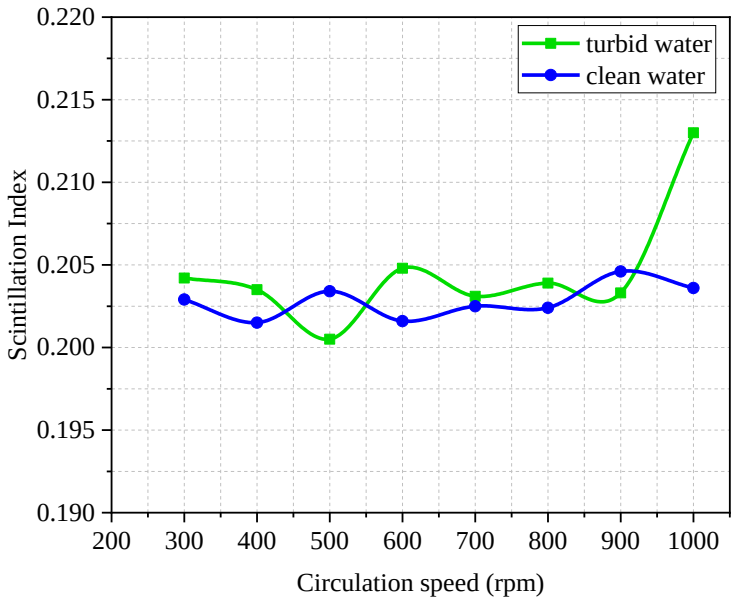

Figure 4.5 A relationship between speed of the stirrer and average scintillation index obtained when clean water and turbid water are respectively used.

In highly dynamic water environment, clean water and turbid water are respectively studied here. Turbid water is obtained by a mixture of clean water of 3.0 L and milk of 10.0 mL to be placed in the water tank in Fig. 4.1. The stirrer is used in optical experiments, and path loss and scintillation index are also calculated. The path loss is calculated by [210,211]

$$PL = 10 \times \log_{10}\left(\frac{P_t}{P_r}\right), \tag{4.8}$$

where PL denotes the loss (unit: dB), P_t denotes optical power just before water tank, and P_r denotes optical power collected by the single-pixel bucket detector. The optical power P_t just before water tank is 80.0 μW in our optical experiments. A relationship between speed of the stirrer and path loss is shown in Fig. 4.4. In addition, scintillation index is used and defined by [212,213]

$$\sigma_I^2 = \frac{\langle I^2 \rangle}{\langle I \rangle^2} - 1, \tag{4.9}$$

where $\langle \cdot \rangle$ denotes ensemble average, and I denotes the measured beam intensity by the single-pixel bucket detector at the receiving end. A relationship between speed of the stirrer and average scintillation index is shown in Fig. 4.5.

It can be seen in Fig. 4.4 that path loss in clean water is smaller than that in turbid water, and the path loss increases dramatically in turbid water environment when speed of the stirrer approaches 1000.0 rpm. It can be seen in Fig. 4.5 that the range of scintillation index is 0.201-0.205 in clean water and 0.200-0.213 in turbid water, which is larger than that used in other work [214].

The typically retrieved analog signals are shown in Figs. 4.6(a)–4.6(h). It is demonstrated that the retrieved signals are of high fidelity, and the proposed method is feasible and effective. When speed of the stirrer increases, PSNR values of the retrieved

signals declines as shown in Fig. 4.7. When speed of the stirrer is not higher than 900.0 rmp, the retrieved signals are always of high quality as shown in Figs. 4.6(a)–4.6(f) and 4.7.

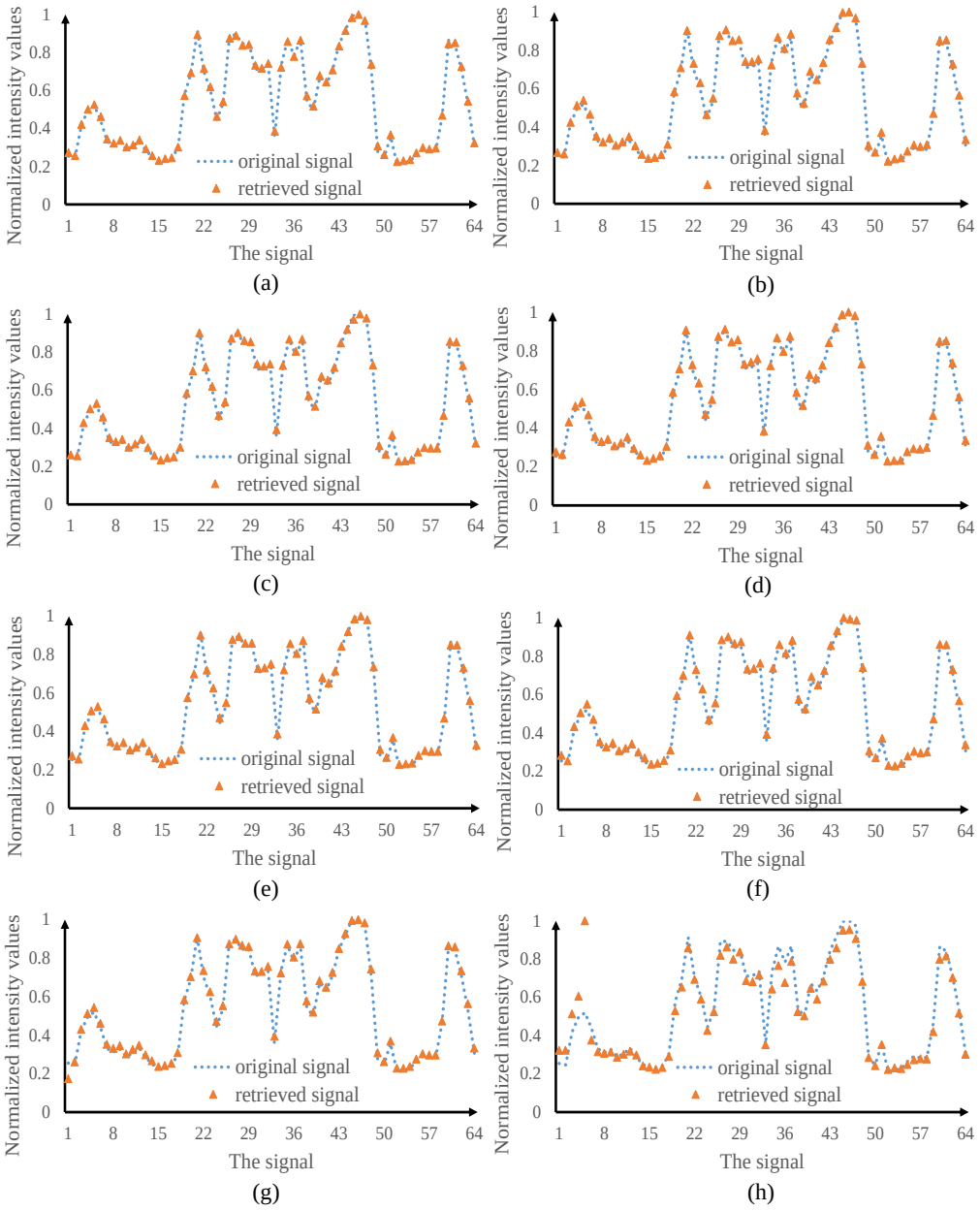

Figure 4.6 (a)–(h) Comparisons between the retrieved analog signals at the receiving end and original signals respectively in clean water and turbid water when different speeds of the stirrer are used: i.e., (a), (b) 400 rpm; (c), (d) 600 rpm; (e), (f) 800 rpm; and (g), (h) 1000 rpm. (a), (c), (e) and (g) in clean water; (b), (d), (f) and (h) in turbid water.

It is also indicated that as velocity of dynamic scattering medium increases, there are severe and harsh turbulences. When water flow increases, particles in the water move

rapidly which results in the larger power loss and wave distortion. It is verified that high-fidelity irregular analog signals can always be retrieved at the receiving end using the proposed method, and high robustness against highly dynamic and turbid water is achieved.

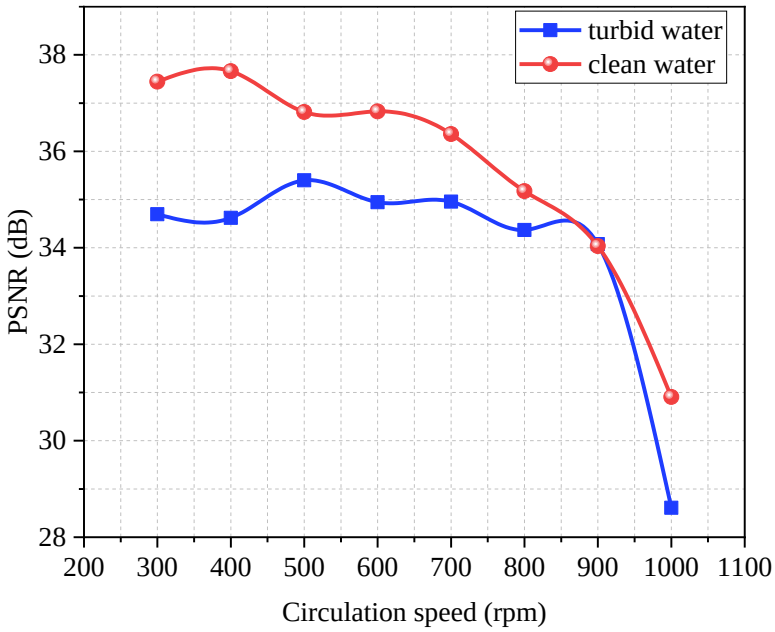

Figure 4.7 A relationship between speed of the stirrer and quality of the retrieved signals.

4.3.3 The Laser with Different Wavelengths

The laser with different wavelengths, i.e., 405.0 nm blue laser (Thorlabs, DL5146-101S), 520.0 nm green laser (Thorlabs, L520P50) and 658.0 nm red laser (Thorlabs, L658P040), is individually used to further verify the proposed method. Turbid water is prepared by a mixture of clean water of 3.0 L and milk of 10.0 mL to be placed in water tank as shown in Fig. 4.1. Milk serves as a strongly scattering material, which has spheroidically-shaped particles floating in water. According to Mie scattering for spheroids, there is a linear downward trend on the percent of scattering light with an increment of the wavelength [215]. Therefore, light with the longer wavelength can propagate longer in turbid water. Fig. 4.8 shows PSNR values of the retrieved signals, when different speeds of the stirrer

and a laser beam with three different wavelengths are used. It can be seen in Fig. 4.8 that high-fidelity free-space optical information transmission is also realized by using the proposed method at wavelengths of 658.0 nm and 520.0 nm, and it is impossible to realize high-fidelity data transmission at wavelength of 405.0 nm. It is illustrated that a laser with long wavelengths (e.g., 658.0 nm and 520.0 nm) is feasible in the proposed method compared with short wavelength (e.g., 405 nm), when there is highly dynamic and turbid water in the wave propagation path.

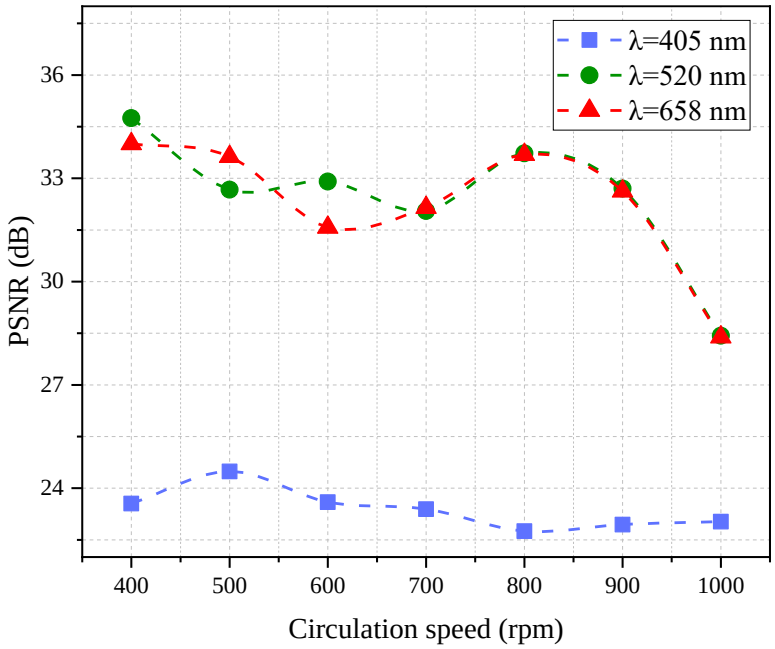

Figure 4.8 PSNR values of the retrieved signals obtained when different speeds of the stirrer and a laser beam with three different wavelengths are respectively used. The irregular analog signal in Fig. 4.3 is tested.

4.4 Summary

In Chapter 4, a new approach has been proposed to establish a high-fidelity and high-robustness optical wireless transmission channel through highly dynamic and turbid water using a series of dynamic scaling factors to correct the light intensities recorded by a single-pixel bucket detector. A series of generated 2D random amplitude-only patterns are sequentially embedded into the SLM, and a fixed reference pattern is used before each

illumination pattern to correct the series of recorded light intensities. The optical wave is severely diffused through highly dynamic and turbid water, and a single-pixel bucket detector is used to record a series of light intensities. The proposed method is experimentally verified by using different turbid water conditions, different strengths of water-flow-induced turbulence and a laser with different wavelengths. It is demonstrated that high-fidelity irregular analog signals can always be retrieved at the receiving end using the proposed method, and high robustness against highly dynamic and turbid water is achieved. The proposed method could open up a novel research perspective for the development of high-fidelity and high-robustness free-space optical data transmission through highly dynamic and turbid water. The proposed method is also feasible to realize high-fidelity data transmission in other environment, such as biological tissues, around corner and smoke [136, 216–218].

Chapter 5 Accurate Optical Information Transmission Through Thick Tissues Using Zero-Frequency Modulation and Single-Pixel Detection

5.1 Introduction

With ever-increasing concerns on life quality, there is much fast-growing interest in developing new technologies for medical devices and applications. In recent years, wireless communication offers a reliable and portable means for medical devices [219,220]. Technological developments over the past decades have made possible not only to monitor health conditions but also to diagnose and react to numerous onsets. Novel health-related technologies allow to enhance the quality of life and save lives in critical health conditions. Nowadays, medical devices and various sensors play a significant role in medical information communication [221–224]. The communications can be conducted by using radio frequency (RF) and acoustic waves. RF technology provides an attractive solution by powering wireless devices with continuous and stable energy over the air. However, when body sensors using the same RF spectrum operate in close vicinity, safety threats exist [225,226] and interference could become a challenge. Since data integrity also plays a vital role in medical information communication, any undesired interference may lead to information impotence. Moreover, there is also a concern of vital RF signals being accessed by unintended parties. Ultrasonic communication produces a wireless connection between remote communication nodes using elastic waves. Ultrasonic waves can also be generated to propagate through biological tissues, and ultrasound techniques have been widely used to diagnose the onsets. However, penetration depth of ultrasonic communication is limited [226,227]. A major disadvantage of ultrasound methods is their

incompetence to propagate in free space. The RF and ultrasounds dissipate energy while propagating through the tissues, indicating that an increased amount of energy could be absorbed and dispersed by biological tissues [228,229]. Optical wireless transmission (OWT) has emerged as a promising means in recent years, and optical light source has some remarkable advantages. For instance, the OWT is secure, private and safe. In many medical applications, it is feasible to transmit data using optical light source, and it is highly desirable that delivering accurate information through thick tissues can be fully explored by using optical light source with low illumination power.

In this Chapter, a new method based on zero-frequency modulation is proposed to realize accurate optical information transmission through thick tissues at low light intensities. This is the first investigation of encoding data information into 2D random amplitude-only patterns to realize accurate optical information transmission through thick tissues. In the proposed zero-frequency modulation-based encoding scheme, information to be transmitted is considered as a series of independent pixel values, and each pixel value is encoded into one 2D random amplitude-only pattern. Subsequently, the generated 2D random amplitude-only patterns are sequentially embedded into SLM to be modulated. Then, the modulated light projects onto the tissue and propagates through biological tissues, i.e., chicken breast tissues used in this study. The optical beams are scattered and absorbed through chicken breast tissues, and a single-pixel detector [230–238] is used to record light intensity without using a lens. A differential detection approach is further developed to suppress noise and enhance quality of the detected signals (e.g., PSNR). Accurate information is retrieved by using the collected light intensity without any complex post-processing algorithms. The proposed method is experimentally verified by

using different thicknesses of chicken breast tissues and a laser beam with different wavelengths. The corresponding publications are as follows:

(1) **Zilan Pan**, Yin Xiao, Yonggui Cao, Lina Zhou, and Wen Chen, "Accurate optical information transmission through thick tissues using zero-frequency modulation and single-pixel detection," Optics and Lasers in Engineering, 158, 107133(7pp), 2022.

(2) **Zilan Pan**, Yin Xiao, Lina Zhou, and Wen Chen, "Optical transmission through thick biological tissue using optical modulation," International Conference on Optical and Photonic Engineering (icOPEN 2022), Proceedings of SPIE, 24–27 November 2022, Nanjing, China.

5.2 Samples and Methods

5.2.1 Experimental Preparation

A schematic optical setup is shown in Fig. 5.1. The laser diode current is controlled by using a laser driver (Thorlabs, LDC205C) in a range of 0-500 mA using a laser diode mount (Thorlabs, LDM56/M). The laser is stabilized at room temperature with a controller (Thorlabs, TED200C). In optical experiments, laser diodes with three different wavelengths are individually used, i.e., 658.0 nm (Thorlabs L658P040), 520.0 nm (Thorlabs L520P50) and 405.0 nm (Thorlabs DL5146-101S). The laser beam is expanded and collimated by a converging lens with a focal length of 100.0 mm. The collimated laser beam is reflected by a mirror, and then illuminates the surface of an amplitude-only spatial light modulator (Holoeye, LC-R720) with pixel size of 20.0 μm. In this study, a modulation rate of 1.25 Hz is used to conduct a proof-of-principle experiment and verify the proposed method. The angle between the incident beam and the reflected beam on the surface of SLM is 45°. Then, the modulated optical wave propagates through biological

tissues. At the receiving end, a single-pixel detector (Newport, 918D-UV-OD3R) with a power meter (Newport, 1936-R) is used to record light intensity. In this study, laboratory temperature is set as 20℃ for a series of optical experiments.

The sample used in this study is frozen and raw chicken breast tissues, since chicken breast has good muscle orientation whose characteristic is similar to human tissues. In our optical experiments, the samples are purchased from a local supermarket, and the skin and fat of chicken breast are removed. The chicken breast is cut to be placed into a transparent container. The container is filled with a small amount of microscope oil to avoid water evaporation in optical experiments. Optical properties of chicken breast tissues might be slightly variable due to biological variations and other conditions, e.g., the freezing and thawing period that can cause cell rupture. All optical experiments are performed within 3 days after phantom preparation. Optical powers illuminated onto the samples are monitored and measured and are in accordance with the safety requirement.

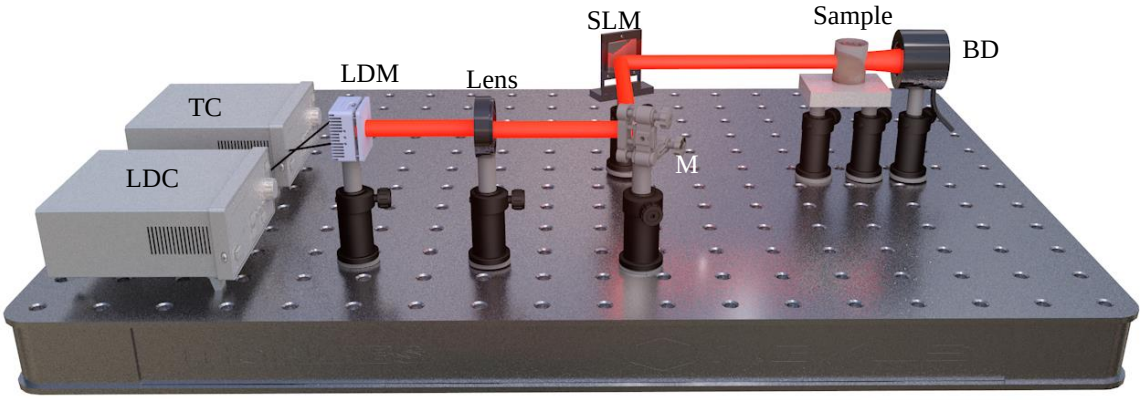

Figure 5.1 A schematic experimental setup for the proposed zero-frequency modulation-based optical information transmission through thick biological tissues: LDC: Laser driver controller; TC: Temperature controller; LDM: Laser diode mount; Chicken breast tissue is used as a sample in this study, and single-pixel detector is placed close to the sample.

5.2.2 Principle

A series of 2D random amplitude-only patterns are first generated to encode original information to be transmitted. Then, a laser diode generates spatially coherent

monochromatic beam to illuminate the SLM which sequentially displays the series of generated 2D random amplitude-only patterns as schematically shown in Fig. 5.1.

The proposed approach to generating 2D random amplitude-only patterns for encoding original information is described as follows: A 2D random matrix with real and nonnegative values is first generated. Then, FFT is applied to the 2D random matrix to obtain its corresponding Fourier spectrum. Zero frequency of the generated Fourier spectrum is replaced by one pixel value of original information, and a new Fourier spectrum is correspondingly generated. Subsequently, IFFT is applied to the new Fourier spectrum to obtain an updated 2D random amplitude-only pattern (P). The above steps are repeated until each pixel value of original information is encoded into one 2D random amplitude-only pattern. It is worth noting that size of the generated 2D random amplitude-only pattern (P) can be flexibly designed in the proposed zero-frequency modulation method, e.g., 256×256 or 512×512 pixels. The process of the proposed zero-frequency modulation-based encoding scheme is further shown in Fig. 5.2. In the optical experiments, negative values existing in the generated 2D random patterns (P) cannot be displayed by the SLM, and each generated 2D random pattern (P) is further transformed into two separate patterns, i.e., patterns (t+P) and (t-P) where t denotes a positive constant.

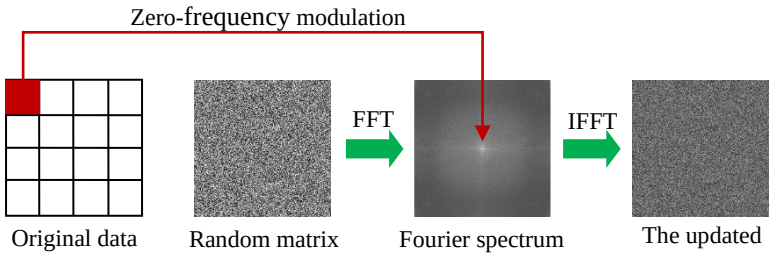

Figure 5.2 A flow chart to schematically illustrate the proposed zero-frequency modulation-based encoding method for accurate optical information transmission through thick biological tissues. In the proposed method, a 2D random amplitude-only pattern is generated for each pixel value of original information.

The interaction between the light and biological tissues is an important topic, and optical wave propagation through thick biological tissues is a complex process. When optical lightwave propagates through thick biological tissues, it generally undergoes reflection and refraction at the interface of inner tissues. The biotissues, e.g., chicken breast tissues, could be considered as high anisotropy media with strong absorption and scattering. Therefore, optical light source attenuates dramatically by the absorption and scattering, and the total light attenuation coefficient μ can be described by

$$\mu = \mu_s + \mu_a, \tag{5.1}$$

where μ_s denotes scattering coefficient and μ_a denotes absorption coefficient. In the biotissues, hemoglobin, melanin, bilirubin and betacarotene are the main absorbers [239], and optical wave propagation through the biotissues can be described by Beer-Lambert law [240] as follows:

$$I = I_0 \exp(-\mu l), \tag{5.2}$$

where I_0 denotes the incident light intensity just before the sample, I denotes the transmitted light intensity just after the sample, and l denotes optical path length. A schematic is shown in Fig. 5.3 to describe the transmittance rate, and the transmittance T is described by

$$T = \frac{I}{I_0}. \tag{5.3}$$

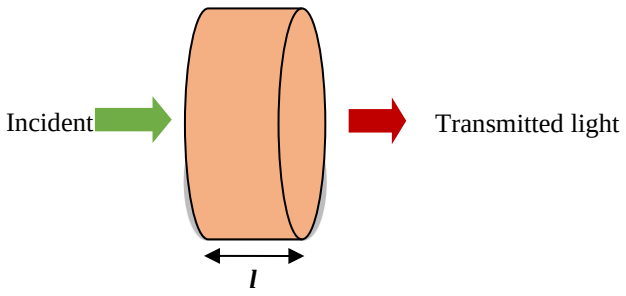

Figure 5.3 A schematic of the transmittance.

Optical scattering is caused by the mismatch of refractive indices through biological tissues. Scattering coefficients and anisotropy factor can approximate the scattered light in the biotissues [241]. The light can be scattered in various directions through the biotissues, and anisotropy factor *g* is defined by

$$g = \langle \cos\theta \rangle, \tag{5.4}$$

where θ denotes photon scattering angle and < > denotes an ensemble average. The range of anisotropy parameter is [-1, 1]. Here, backward scattering is represented by -1, and forward scattering is represented by 1. Biotissues undergo Rayleigh scattering and Mie scattering due to the heterogeneous structures. For most biotissues, anisotropy factor *g* is approximately 0.9 [242], which means that forward scattering dominates over backward scattering.

After optical waves propagate through thick tissues, optical light intensity is recorded by using a single-pixel detector [230–238] at the receiving end as shown in Fig. 5.1. Single-pixel detection process is described by

$$\begin{aligned} \mathrm{B1} &= \delta \iint [t + P(x,y)] e^{-2\pi j(x\xi + y\eta)} dxdy \Big|_{\xi=0,\eta=0}, \\ &= \delta \iint [t + P(x,y)] dxdy \end{aligned} \tag{5.5}$$

$$\begin{aligned} \mathrm{B2} &= \delta \iint [t - P(x,y)] e^{-2\pi j(x\xi + y\eta)} dxdy \Big|_{\xi=0,\eta=0}, \\ &= \delta \iint [t - P(x,y)] dxdy \end{aligned} \tag{5.6}$$

where $j = \sqrt{-1}$, (x,y) denotes a coordinate in spatial domain, (ξ, η) denotes a coordinate in frequency domain, $t+P(x,y)$ and $t-P(x,y)$ denote 2D random patterns with 256×256 pixels embedded into the SLM, δ denotes a scaling factor related to free-space wave propagation environment, and B1 and B2 denote the recorded intensity values which are related to one pixel value of original information. Each pixel value of information is finally transformed

into two 2D amplitude-only patterns ($t+P(x,y)$) and ($t-P(x,y)$), and a differential operation between two neighboring intensity measurements is carried out to retrieve accurate information. The differential operation process is described by

$$\mathrm{B}=\mathrm{B1}-\mathrm{B2}=2\delta\iint P(x,y)dxdy. \tag{5.7}$$

5.3 Experimental Results and Discussion

The capabilities of light to penetrate the biotissues, interact with the biotissues and transmit through the biotissues are critical in practical applications. Therefore, the light penetration depth through biotissues is first studied at low light levels in the designed optical wireless transmission. Subsequently, optical light source with different wavelengths is investigated, and absorption and scattering through biotissues are studied to determine the transmitted light intensity. Here, a series of optical experiments are conducted, and experimental results are presented and discussed to verify feasibility and effectiveness of the proposed method.

5.3.1 Light Penetration Depth through Chicken Breast Tissues

The penetration depth through biological tissues is important, and efficiency and fidelity of the designed optical wireless transmission setup are studied. A laser diode with wavelength of 658.0 nm is used as light source shown in Fig. 5.1, and a chicken breast sample with different thicknesses is prepared and placed in the optical path to investigate feasibility and effectiveness of the proposed method. Low light intensities are used for sample illumination. Experimental results are shown in Figs. 5.4 and 5.5. To quantitatively evaluate experimental results, PSNR is calculated and defined by

$$\mathrm{PSNR}=10\log_{10}\left(\frac{MAX_{ori}^{2}}{\mathrm{MSE}}\right), \tag{5.8}$$

$$\mathrm{MSE} = \frac{1}{N}\sum\left(S_{ori} - S_{re}\right)^2, \tag{5.9}$$

where MAX_{ori} denotes the maximum value of original information, S_{ori} denotes original information, S_{re} denotes the retrieved information, and N denotes the total number of pixels in original information.

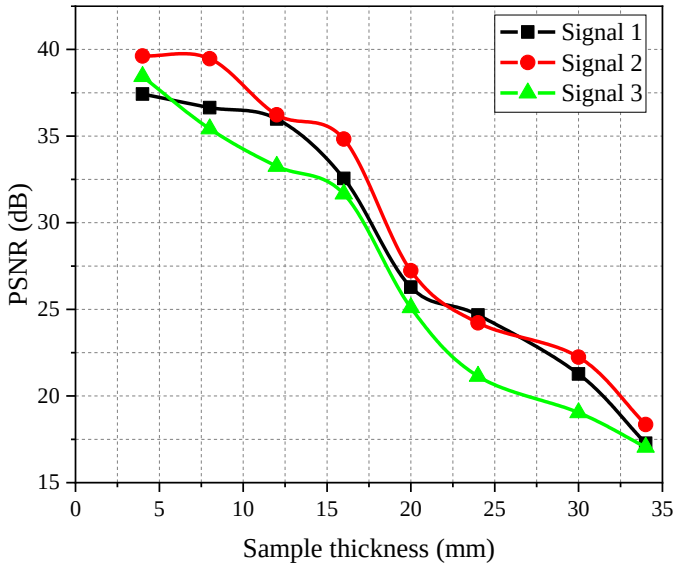

Figure 5.4 A relationship between sample thickness (i.e., chicken breast tissues) and quality of the experimentally retrieved analog signals using the proposed zero-frequency modulation method.

Table 5.1 Transmittance rate for optical information transmission through biotissues with different thicknesses using the proposed zero-frequency modulation method. The light power detection area is 1.0 cm^2.

Thickness (mm)	Incident light power I_0 (mW)	Transmitted light power I (mW)	Transmittance rate (%)
4.0	0.08	4.54×10^{-3}	5.68
8.0	0.08	4.02×10^{-3}	5.03
12.0	0.08	1.58×10^{-3}	1.98
16.0	0.08	1.28×10^{-3}	1.60
20.0	0.08	1.01×10^{-3}	1.26
24.0	0.08	0.76×10^{-3}	0.95
30.0	0.08	0.64×10^{-3}	0.80
34.0	0.08	0.52×10^{-3}	0.65

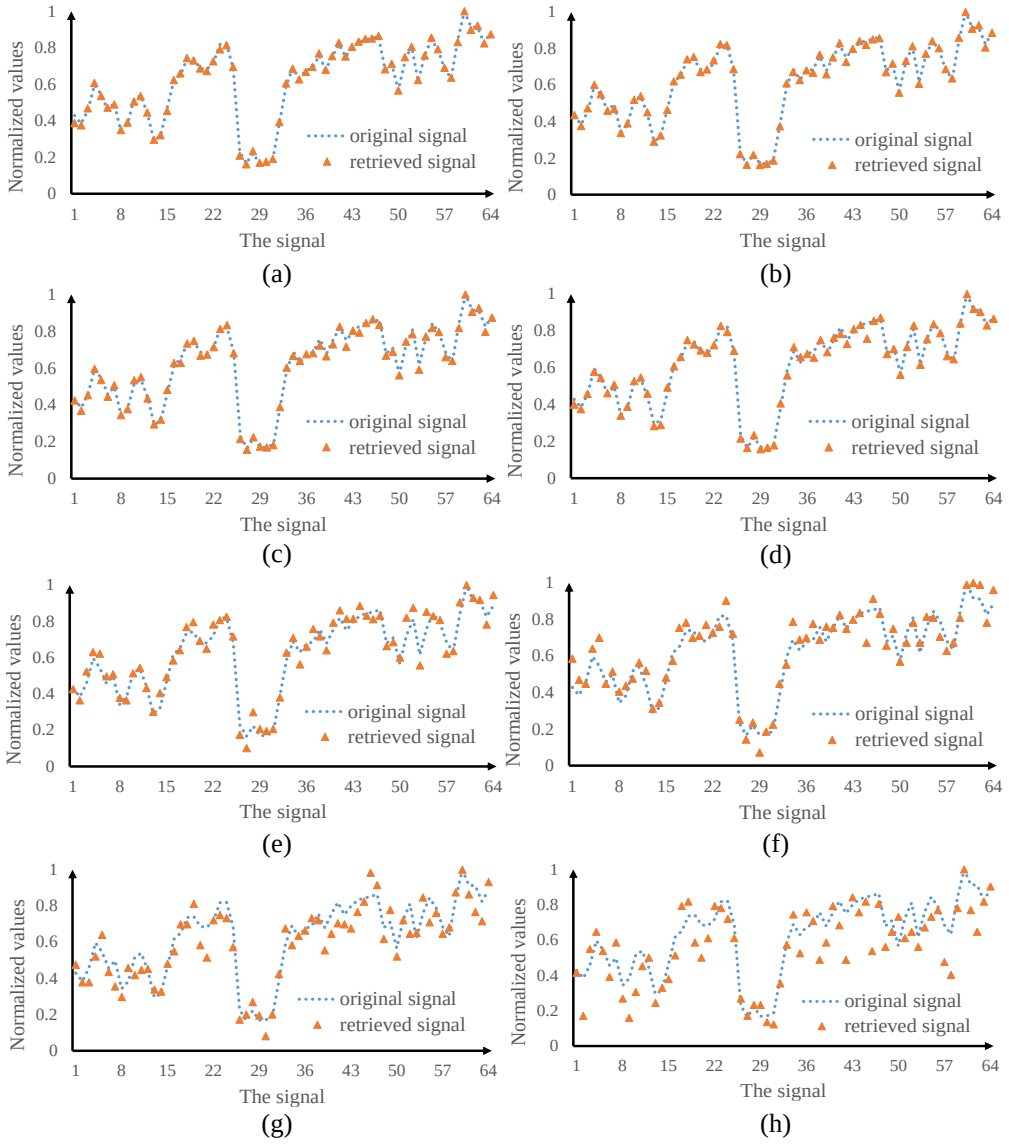

Figure 5.5 Comparisons between original signal and the experimentally retrieved signals when different sample thicknesses of (a) 4.0 mm, (b) 8.0 mm, (c) 12.0 mm, (d) 16.0 mm, (e) 20.0 mm, (f) 24.0 mm, (g) 30.0 mm, and (h) 34.0 mm are respectively applied in optical experiments using the proposed zero-frequency modulation method at low light illumination levels. Here, the signal 2 in Fig. 5.4 is tested and typically presented.

Experimental results are shown in Fig. 5.4, when chicken breast tissues with different thicknesses are used as sample. Three typically irregular analog signals are tested in this case. The typically retrieved analog signals are shown in Fig. 5.5. It can be seen in Fig. 5.4 that PSNR values decrease with the increased sample thickness. When the thickness

of biotissues is not larger than 16.0 mm, the retrieved signals are always of high quality as shown in Fig. 5.4 and Figs. 5.5(a)–5.5(d).

The accurate information transmission through biological tissues is realized by using the proposed method. Here, a low laser power of only 0.08 mW/cm^2 has been used to illuminate the sample, and the transmittance rate is calculated and given in Table 5.1. Compared with conventional methods [243], the proposed method realizes accurate optical information transmission through biological tissues with a thickness of 16.0 mm, when a low laser power of only 0.08 mW/cm^2 is used. It is demonstrated that the proposed method is effective and robust for accurate optical information transmission through thick tissues using a low illumination power.

5.3.2 Laser Beam with Different Wavelengths

In visible light spectrum, average absorption coefficients and reduced scattering coefficients through biological tissues could be different. We further investigate the proposed method using a laser beam with different wavelengths for optical information transmission through thick tissues, and experimental results are shown in Figs. 5.6 and 5.7. In this case, a low laser power of only 0.08 mW/cm^2 has been used just before the sample.

It can be seen in Fig. 5.6 that accurate optical information transmission through chicken breast tissues is realized by using red and green laser beams in the proposed method, but quality of the retrieved signal is low when a blue laser is used as the illumination light source. It has also been demonstrated [228,242] that two absorption peaks could exist when light source with the wavelengths of 430.0 nm and 540.0 nm is used, and a reduced scattering coefficient peak exists at the wavelength of 450.0 nm. The

peaks in the measured absorption spectra are generated due to the absorbers like hemoglobin, melanin, myoglobin, bilirubin and carotene in chicken breast tissues. In addition, scattering through chicken breast tissues originates from cell and cellular organelles, e.g., membranes, nuclei and mitochondria [244].

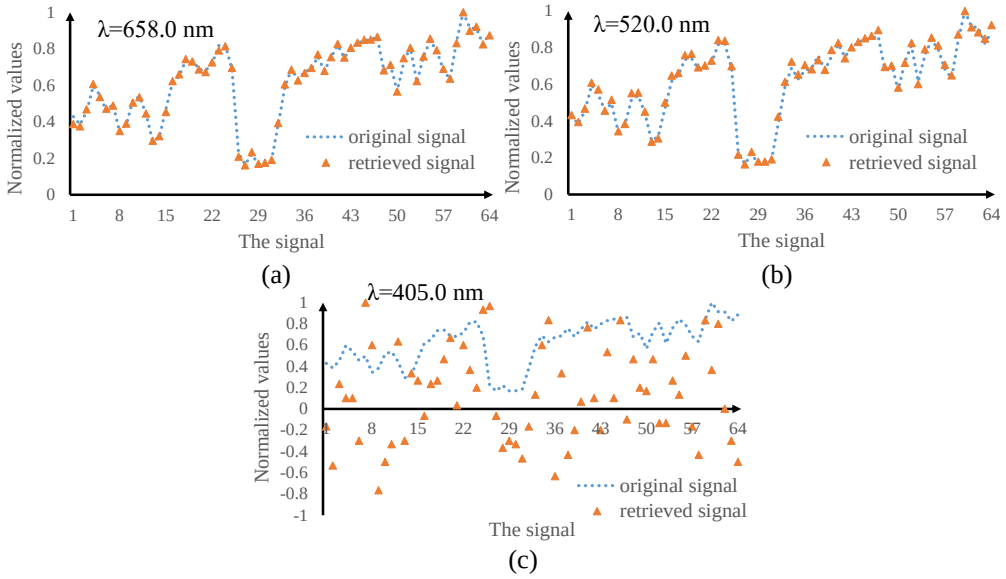

Figure 5.6 Comparisons between original signal and the experimentally retrieved signals when a laser beam with different wavelengths of (a) 658.0 nm, (b) 520.0 nm and (c) 405.0 nm is respectively applied in optical experiments using the proposed zero-frequency modulation method. The thickness of biological tissue is 4.0 mm in this case.

Breast chicken tissue with different thicknesses is used to further investigate performance of the proposed method using red, green and blue lasers, and quality of the retrieved signals is quantitatively evaluated and shown in Fig. 5.7. High transmission accuracy is always achieved at the wavelength of 658.0 nm when the thickness of chicken breast tissues is not larger than 16.0 mm, and the blue laser with wavelength of 405.0 nm is not suitable to be applied as illumination light source for accurate optical information transmission through biological tissues using the proposed method. It can be seen in Figs. 5.6 and 5.7 that when light source with the longer wavelength is used in the proposed method, there are less absorption and scattering through chicken breast tissues.

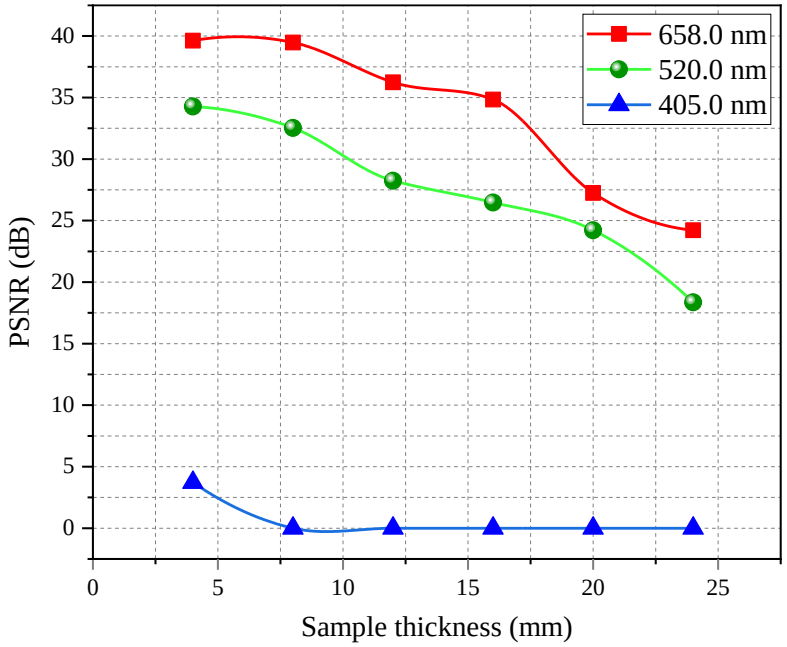

Figure 5.7 Effect of light source with different wavelengths (i.e., red, green and blue) on quality of the retrieved signals when a sample with different thicknesses (i.e., 4.0 mm, 8.0 mm, 12.0 mm, 16.0 mm, 20.0 mm and 24.0 mm) is applied in optical experiments using the proposed zero-frequency modulation method.

5.3.3 Scattering Effect

The attenuation of light depends on scattering and absorption when traversing chicken breast tissues, and we further uncouple the effect of scattering and absorption in order to explain the findings in Section 5.3.2 using the proposed zero-frequency modulation method. Here, a ratio (r) between scattering and absorption is described by

$$r = \frac{\mu_s}{\mu_s + \mu_a}, \tag{5.10}$$

To quantitatively evaluate the proposed method, three cascaded diffusers (Thorlabs, DG10-1500-MD) are used to emulate only the scattering (i.e., r=1) as shown in Fig. 5.8, and each diffuser has a diameter of 25.4 mm and a thickness of 2.0 mm. It has been well recognized that through the biotissues, Mie scattering dominates over Rayleigh scattering [245–248]. In our optical experiments, a laser beam with different wavelengths is applied, and free space without and with scattering media is studied. Experimental results are

shown in Figs. 5.9(a)–5.9(f), and quality of the experimentally retrieved signals is quantitatively evaluated and given in Table 5.2.

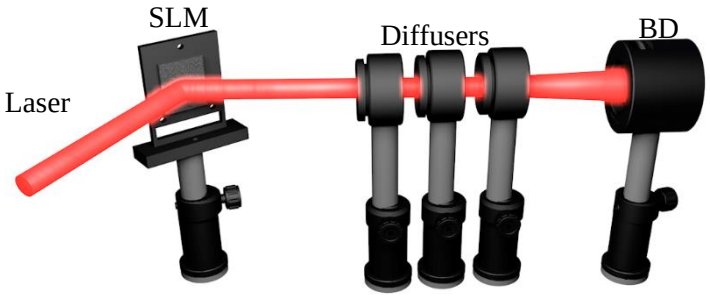

Figure 5.8 A schematic experimental setup for testing the proposed method against scattering using three cascaded diffusers.

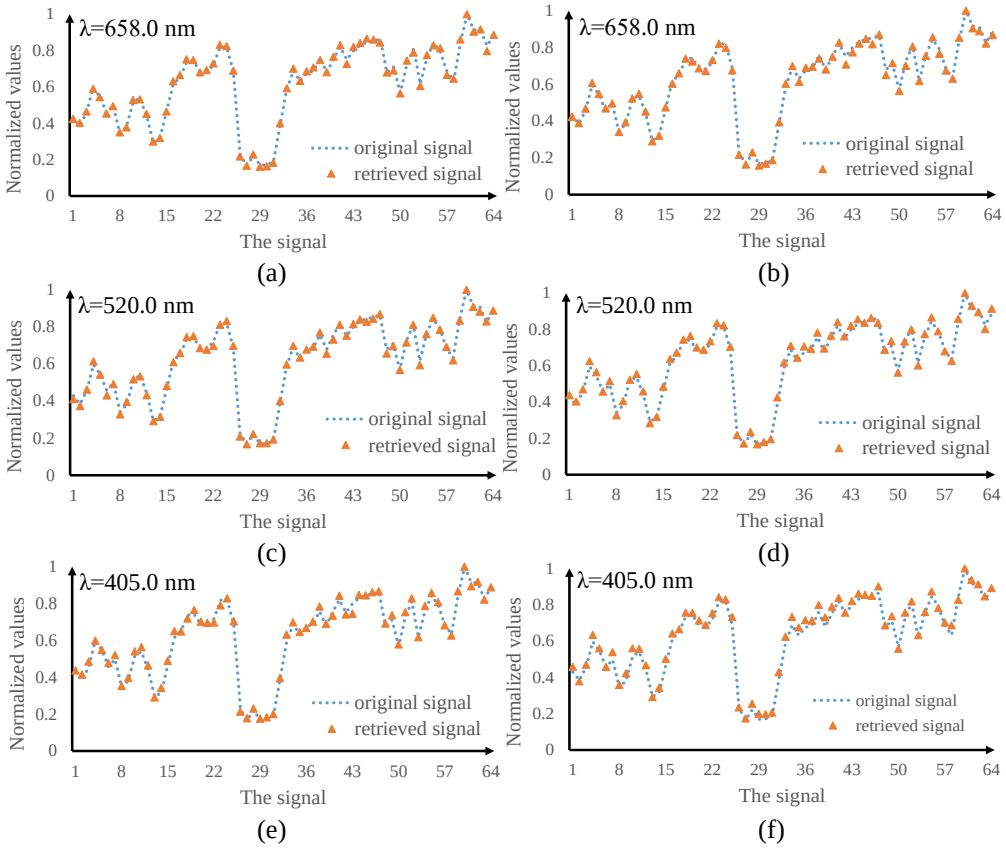

Figure 5.9 The effect of scattering on quality of the experimentally retrieved signals when a laser beam with wavelengths of 658.0 nm, 520.0 nm and 405.0 nm is respectively applied in optical experiments using the proposed zero-frequency modulation method. (a), (c), (e) Comparison between original analog signal and the experimentally retrieved analog signals when free space environment without scattering media is used; (b), (d), (f) comparison between original analog signal and the experimentally retrieved analog signals when a scattering medium with three cascaded diffusers is used in free space.

Table 5.2 Optical information transmission accuracy in free space without and with scattering media using the proposed zero-frequency modulation method with a laser beam of different wavelengths corresponding to those in Figs. 5.9(a)–5.9(f).

Wavelength (nm)	PSNR (dB)	
	Without scattering	With scattering
405.0	34.63	31.46
520.0	38.63	35.32
658.0	38.08	37.51

It can be seen in Table 5.2 and Fig. 5.9 that high-fidelity analog signal is always obtained at the receiving end using the proposed method. It is demonstrated that the proposed method has high robustness against scattering, and the low quality of the retrieved signals, i.e., the finding described in Section 5.3.2, is mainly due to absorption through chicken breast tissues rather than scattering when the blue laser with wavelength of 405.0 nm is used as illumination light source.

5.4 Summary

In Chapter 5, a new method using zero-frequency modulation-based optical data encoding scheme has been proposed to realize accurate optical information transmission through thick tissues at low light intensities. Optical experiments have been conducted to verify the proposed method using different thicknesses of chicken breast tissues and the laser beam with different wavelengths. Experimental results demonstrate that the proposed method can realize accurate optical information transmission through thick biological tissues, and is able to overcome the existing challenges (i.e., small penetration depth and low transmission accuracy). It is illustrated that the proposed method can realize accurate optical information (i.e., analog signals rather than only binary signals) transmission through biological tissues with a thickness of 16.0 mm, when a low laser power of only 0.08 mW/cm^2 is used to illuminate the biological sample at wavelength of 658.0 nm. The

proposed method can apply to biomedical field for medical diagnosis. There is limitation for application due to the large size of the optical devices, such as SLM. In the near future, it can be integrated by applying with metamaterials or other devices to achieve deep information transmission. The proposed method provides a promising means for accurate optical information transmission through deep biological tissues.

Chapter 6 Conclusions and Future Work

6.1 Research Findings

This Ph.D. thesis devotes to tackling the challenges existing in optical information transmission in free space through complex scattering media including static and dynamic disordered media.

It is found that the ubiquitous difficulties encountered in this topic are usually complex and unknown environments. The scattering induced by inhomogeneous media impedes effective delivery of information, resulting in energy degradation and information loss. Conventional methods for information transmission and retrieval in scattering media are demonstrated to be effective in relatively weak conditions, and are unable to cope with the increased complexity and inhomogeneity of the scattering media. In addition, it is challenging for these methods to achieve high-fidelity and high-robustness information transmission in highly dynamic and complex environment. Furthermore, the existing methods suffer from huge computational load, low accuracy, complicated experimental setup, and high sensitivity to noise. This Ph.D. thesis proposes zero-frequency modulation-based optical information transmission through complex scattering media. Each pixel of original analog-signal is sequentially encoded into random amplitude-only patterns as an information carrier, and the proposed method can realize a kind of pixel-to-plane optical analog-signal transmission with high fidelity and high efficiency. Furthermore, by exploiting single-pixel detector at the receiver to record the total light intensity and utilizing a differential operation to recover optical analog signal, it has an unsurpassed advantage that the proposed method has high robustness to the changes of complex environment (e.g., changeable distances and various water conditions). The

proposed method is easy to implement and shows a virtue of avoiding wearisome pre-processing algorithms, enabling direct retrieval of optical information with unprecedented flexibility. In addition, the proposed method can realize a wide range of detection free-space optical information transmission when there are obstacles. The proposed method provides a new avenue to analog-signal transmission through turbid water, and has high robustness against noise which could contribute to evolutionary developments of optical data transmission in harsh environments.

Since dynamic scattering medium poses a severe threat to free-space optical information transmission, a new method using a series of dynamic scaling factors has been proposed to correct light intensities. A fixed reference pattern is utilized to obtain the series of dynamic scaling factors during optical data transmission in free space. The light intensity is recorded by a single-pixel detector. The complicated pre-processing algorithm is not required in the data retrieval process. In this study, the proposed method is experimentally verified by using different turbid water conditions, different strengths of water-flow-induced turbulence and a laser with different wavelengths. The proposed method is easy to operate and is cost-effective. The proposed method could open up a novel research perspective for the development of high-fidelity and high-robustness free-space optical data transmission through highly dynamic and turbid water. It can be expected that the proposed method is feasible to realize free-space optical data transmission in various environment.

Owing to the complicated structures and strong scattering characteristics of biological tissues, it is expected to develop an effective method to realize high-fidelity information transmission through thick biological tissues with low light intensity. The main principle in the developed optical information transmission system is by transmitting information

using a 2D random amplitude-only patterns and consider it as information carriers. Optical experiments have been conducted to verify the proposed method using different thicknesses of chicken breast tissues and the laser beam with different wavelengths. It is experimentally demonstrated that the proposed method can realize accurate optical information transmission through thick biological tissues, and is able to overcome the existing challenges (i.e., small penetration depth and low transmission accuracy). It is illustrated that the proposed method can realize accurate optical information (i.e., analog signals rather than only binary signals) transmission through thick biological tissues with low laser power using visible light. Hence, the proposed method provides a new avenue to develop optical wireless transmission with deep penetration in biology.

In these research findings, zero-frequency modulation and single-pixel detection for optical analog-signal transmission through complex scattering media can be effectively implemented, and its applications in static or dynamic and complex environment (e.g., turbid and dynamic water, thick biological tissues) can shed some light on optical wireless information transmission. It is hoped that it will inspire more researchers to develop ideas to solve key scientific problems in this research area.

6.2 Contributions of the Thesis

The main contributions of my Ph.D. thesis are summarized as follows:

(1). In static and turbid water, a new and robust method to encode analog signals into random amplitude-only patterns is proposed to realize high-robustness and high-fidelity optical data transmission. A number of experimental results have demonstrated that for different kinds of analog signals, the proposed method is able to realize high-fidelity optical information transmission through turbid water. Compared with conventional methods [159–162], the proposed method is easier to implement, and prior knowledge

about turbid water is not required. In addition, a NLOS free-space optical data transmission system through complex media is built to realize high-fidelity optical data transmission through turbid water when there are obstacles between the transmitter and receiver. Compared with conventional NLOS free-space optical data transmission methods [156], the proposed approach can effectively transmit analog signals with high fidelity, high robustness, and a wide detection range.

(2). In dynamic and turbid water, a new approach using a series of generated 2D random amplitude-only patterns, i.e., illumination pattern, is proposed, and a fixed reference pattern is used before each illumination pattern to correct the series of recorded light intensities. It is demonstrated that high-fidelity irregular analog signals can always be retrieved at the receiving end using the proposed method, and high robustness against highly dynamic and turbid water is achieved. The proposed method could open up a novel research perspective for the development of high-fidelity and high-robustness free-space optical data transmission through highly dynamic and turbid water.

(3). A new method using zero-frequency modulation-based optical data encoding scheme has been proposed to realize accurate optical information transmission through thick tissues at low light intensities. Optical experiments have been conducted to verify the proposed method using different thicknesses of chicken breast tissues and the laser beam with different wavelengths. Compared with conventional methods [243], the proposed method realizes accurate optical information transmission through biological tissues with a thickness of 16.0 mm, when a low laser power of only 0.08 mW/cm^2 is used. The proposed method provides a promising means for accurate optical information transmission through deep biological tissues.

6.3 Future Work

This Ph.D. thesis utilizes zero frequency modulation and single-pixel detection to realize high-fidelity and high-robustness optical information transmission through complex scattering media including static and turbid water, dynamic and turbid water and biological tissue. However, transmission rate in the proposed optical wireless transmission system is limited by optical devices, i.e., SLM. High transmission rate is necessary to achieve, such as underwater wireless optical transmission and biomedical field.

Possible potentialities and recommendations are given as follows:

(1). In Chapter 4, dynamic scaling factors are corrected to realize optical information transmission through highly dynamic and turbid water. The proposed method works effectively in turbid media with dynamic scattering. With an exponential increase of data in a digital era and the need for fast transmission, it is necessary to minimize storage space and the transmission cost. It is imperative to design a high-efficiency and low-cost image compression and transmission system.

For instance, a compression and transmission model based on QR code and discrete wavelet transform (DWT) can be designed as shown in Fig. 6.1. Data compression before optical transmission is an attractive alternative as minimal hardware resources are performed. At the transmitter, original information (e.g., image) can be encoded into a QR code which is compressed using DWT. Then the compressed wavelet spectrum coefficients are obtained and can serve as the transmitted data through complex scattering media in free space. A series of random amplitude-only patterns which are generated by encoding the transmitted data in the wavelet spectrum coefficients based on zero-

frequency modulation are sequentially projected onto the SLM.

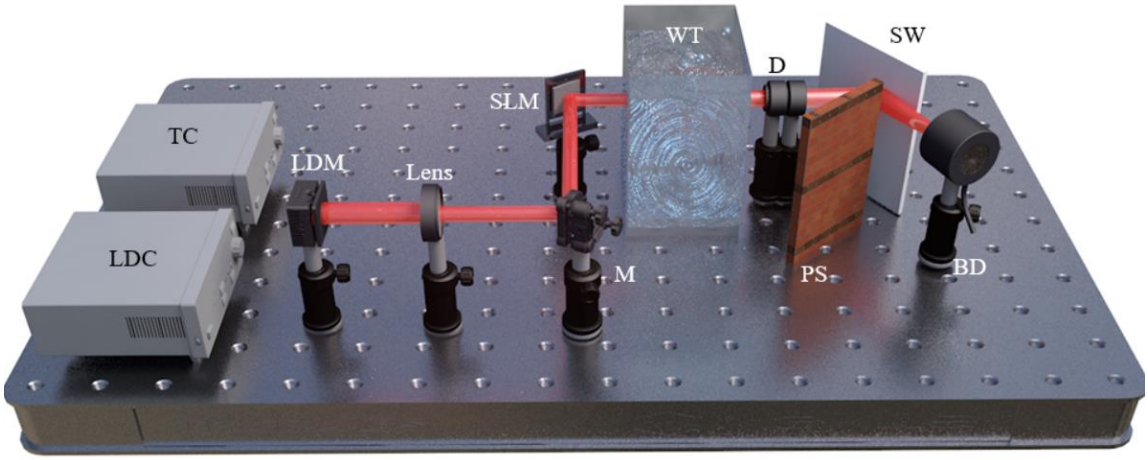

Figure 6.1 A schematic experimental setup for the proposed joint optical information compression and transmission system.

(2). In Chapter 5, zero-frequency modulation is used to realize accurate optical information transmission through thick tissues at low light intensities. The proposed method works effectively in biological tissue (i.e., chicken breast tissue). For zero-frequency modulation-based optical information transmission in tissue, the enhancement is possible with a usage of extremely fast light modulators that have been developed. For instance, multiplexing algorithm, e.g., Orthogonal Frequency Division Multiplexing (OFDM), is alternative to achieve high transmission rate and enhance information capacity.

Bibliography

[1]. F. A. Jenkins and H. E. White, Fundamentals of Optics (McGraw-Hill Kogaskusha, Tokyo, 1957).

[2]. M. Born and E. Wolf, Principles of Optics, sixth ed. (Pergamon Press, Oxford, England, 1993).

[3]. J. W. Goodman, Statistical Optics (Wiley, New York, 2000), p. 550.

[4]. S. F. Ray, Applied photographic optics, (Focal Press, New York 2002).

[5]. W. Smith, Modern optical engineering, 4th Ed. (McGraw-Hill, New York 2007).

[6]. P. Mouroulis, and J. Macdonald, Geometrical optics and optical design (Oxford University Press, New York 1997).

[7]. A. Miks, Applied optics (Czech Technical University Press, Prague 2009). 6. M. Herzberger, Modern geometrical optics (Interscience Publishers, Inc., New York 1958).

[8]. A. D. Clark, Zoom lenses (Adam Hilger, London, 1973).

[9]. K. Yamaji, Progres in optics, Vol.VI (North-Holland Publishing Co., Amsterdam 1967).

[10]. A. Mikš, J. Novák, and P. Novák, "Method of zoom lens design," Appl. Opt. 47(32), 6088–6098 (2008).

[11]. D. Huang, E. A. Swanson, C. P. Lin, J. S. Schuman, W. G. Stinson, W. Chang, M. R. Hee, T. Flotte, K. Gregory, C. A. Puliafito, and J. G. Fujimoto, "Optical coherence tomography," Science 254, 1178–1181 (1991).

[12]. J. W. Lichtman and J. A. Conchello, "Fluorescence microscopy," Nat. Methods 2(12), 910–919 (2005).

[13]. S. W. Hell, "Microscopy and its focal switch," Nat. Methods 6(1), 24–32 (2009).

[14]. S. W. Hell and J. Wichmann, “Breaking the diffraction resolution limit by stimulated emission: stimulated-emission-depletion fluorescence microscopy,” Opt. Lett. 19(11), 780–782 (1994).

[15]. T. N. Rescigno and C. W. McCurdy, “Numerical grid methods for quantum-mechanical scattering problems,” Physical Review A, 62(3), 032706 (2000).

[16]. J. H. Richmond, “Digital computer solutions of the rigorous equations for scattering problems,” Proceedings of the IEEE, 53(8), 796–804 (1965).

[17]. S. M. Day, “Finite element analysis of seismic scattering problems,” University of California, San Diego. (Ph. D. in Oceanography), (1977).

[18]. B. Borden, “Mathematical problems in radar inverse scattering,” Inverse Problems, 18(1), R1 (2001).

[19]. D. Colton and R. Kress, “Inverse acoustic and electromagnetic scattering theory,” Springer Nature, (2019).

[20]. J. L. Volakis, A. Chatterjee and L C. Kempel, “Finite element method electromagnetics: antennas, microwave circuits, and scattering applications,” John Wiley & Sons, (1998).

[21]. M. N. Vesperinas, “Scattering and diffraction in physical optics,” World Scientific Publishing Company, (2006).

[22]. X. Liu and B. Zhang, “Direct and inverse obstacle scattering problems in a piecewise homogeneous medium,” SIAM Journal on Applied Mathematics, 70(8), 3105–3120 (2010).

[23]. K. Umashankar, A. Taflove and S. Rao, “Electromagnetic scattering by arbitrary shaped three-dimensional homogeneous lossy dielectric objects,” IEEE Transactions on Antennas and Propagation, 34(6), 758–766 (1986).

[24]. P. Latimer, “Light scattering by a homogeneous sphere with radial projections,” Applied optics, 23(3), 442–447 (1984).

[25]. J. R. Wait, “Electromagnetic scattering from a radially inhomogeneous sphere,” Applied Scientific Research, Section B, 10(5-6), 441–450 (1962).

[26]. A. Aubry and A. Derode, “Multiple scattering of ultrasound in weakly inhomogeneous media: Application to human soft tissues,” The Journal of the Acoustical Society of America, 129(1), 225–233 (2011).

[27]. D. Colton and P. Monk, “The inverse scattering problem for time-harmonic acoustic waves in an inhomogeneous medium,” The Quarterly Journal of Mechanics and Applied Mathematics, 41(1), 97–125 (1988).

[28]. P. A. Martin, “Acoustic scattering by inhomogeneous obstacles,” SIAM Journal on Applied Mathematics, 64(1), 297–308 (2003).

[29]. T. N. Rescigno and C. W. McCurdy, “Numerical grid methods for quantum-mechanical scattering problems,” Physical Review A, 62(3), 032706 (2000).

[30]. F. H. L. Koppens, D. E. Chang, and F. J. G. De Abajo, “Graphene plasmonics: a platform for strong light-matter interactions,” Nano Lett.11, 3370–3377 (2011).

[31]. N. Rivera and I. Kaminer, “Light–matter interactions with photonic quasiparticles,” Nat. Rev. Phys. 2(10), 538–561(2020).

[32]. L. Britnell, et al., “Strong light-matter interactions in heterostructures of atomically thin films,” Science, vol. 340, no. 6138, pp. 1311–1314, 2013.

[33]. L. D. Barron and A. D. Buckingham, “Rayleigh and Raman scattering from optically active molecules,” Mol. Phys. 20, 1111–1119(1971).

[34]. L. D. Barron and A. D. Buckingham, “Rayleigh and Raman optical activity,” Annu. Rev. Phys. Chem. 26, 381–396 (1975).

[35]. G. A. Jones and D. S. Bradshaw, “Resonance energy transfer: from fundamental theory to recent applications,” Front. Phys. 7, 100 (2019).

[36]. C. F. Bohren and D. R. Huffman, Absorption and scattering of light by small particles (Wiley, New York, 1983).

[37]. H. C. Van de Hulst, Light scattering by small particles (Wiley, New York, 1957).

[38]. M. Kerker, The scattering of light and other electromagnetic radiation (Academic, New York, 1969).

[39]. L. V. Wang and H.-I. Wu, Biomedical optics: principles and imaging (Wiley, 2007), Chap. 12, pp. 283–321.

[40]. J. C. Dainty, Laser Speckle and Related Phenomena (Springer-Verlag, 1984).

[41]. J. M. Schmitt, S. H. Xiang, and K. M. Yung, “Speckle in optical coherence tomography,” J. Biomed. Opt. 4(1), 95–105 (1999).

[42]. D. A. Boas and A. K. Dunn, “Laser speckle contrast imaging in biomedical optics,” J. Biomed. Opt. 15(1), 011109 (2010).

[43]. J. W. Goodman, Speckle phenomena in optics: theory and applications (Roberts and Company, 2007).

[44]. J. W. Goodman, “Some fundamental properties of speckle,” J. Opt. Soc. Am. 66(11), 1145–1150 (1976).

[45]. I. M. Vellekoop, “Controlling the propagation of light in disordered scattering media,” Ph.D. thesis, University of Twente (2008).

[46]. I. M. Vellekoop and A. P. Mosk, “Focusing coherent light through opaque strongly scattering media,” Opt. Lett. 32(16), 2309 (2007).

[47]. H. B. de Aguiar, S. Gigan, and S. Brasselet, “Enhanced nonlinear imaging through scattering media using transmission-matrix-based wave-front shaping,” Phys. Rev. A 94, 043830 (2016).

[48]. J. Bertolotti and O. Katz, “Imaging in complex media,” Nat. Phys. 18, 1008–1017 (2022).

[49]. I. M. Vellekoop and A. P. Mosk, “Universal optimal transmission of light through disordered materials,” Phys. Rev. Lett. 101(12), 120601 (2008).

[50]. D. B. Conkey, A. M. Caravaca-Aguirre, and R. Piestun, “High-speed scattering medium characterization with application to focusing light through turbid media,” Opt. Express 20(2), 1733–1740 (2012).

[51]. O. Tzang, E. Niv, S. Singh, S. Labouesse, G. Myatt, and R. Piestun, “Wavefront shaping in complex media with a 350 kHz modulator via a 1D-to-2D transform,” Nat Photon 13, 788-793 (2019).

[52]. H. Yu, J. Park, K. Lee, J. Yoon, K. Kim, S. Lee, and Y. Park, “Recent advances in wavefront shaping techniques for biomedical applications,” Curr. Appl. Phys. 15(5), 632–641 (2015).

[53]. I. M. Vellekoop, “Feedback-based wavefront shaping,” Opt. Express 23(9), 12189–12206 (2015).

[54]. S. Gigan, O. Katz, H. B. de Aguiar, E. Andresen, A. Aubry, J. Bertolotti, E. Bossy, D. Bouchet, J. Brake, and S. Brasselet, “Roadmap on Wavefront Shaping and deep imaging in complex media,” J. Phys. Photonics 4(4), 042501 (2022).

[55]. J. Yoon, K. Lee, J. Park, and Y. Park, “Measuring optical transmission matrices by wavefront shaping,” Opt. Express 23(8), 10158–10167 (2015).

[56]. R. Horstmeyer, H. Ruan, and C. Yang, “Guidestar-assisted wavefront-shaping methods for focusing light into biological tissue,” Nat. Photonics 9(9), 563–571 (2015).

[57]. Z. Yaqoob, D. Psaltis, M. S. Feld, and C. Yang, “Optical phase conjugation for turbidity suppression in biological samples,” Nat. Photonics 2(2), 110–115 (2008).

[58]. C.-L. Hsieh, Y. Pu, R. Grange, and D. Psaltis, “Digital phase conjugation of second harmonic radiation emitted by nanoparticles in turbid media,” Opt. Express 18(12), 12283–12290 (2010).

[59]. M. Cui and C. Yang, “Implementation of a digital optical phase conjugation system and its application to study the robustness of turbidity suppression by phase conjugation,” Opt. Express 18(4), 3444–3455 (2010).

[60]. J. Ryu, M. Jang, T. J. Eom, C. Yang, and E. Chung, “Optical phase conjugation assisted scattering lens: variable focusing and 3D patterning,” Sci. Rep. 6, 23494 (2016).

[61]. T. R. Hillman, T. Yamauchi, W. Choi, R. R. Dasari, M. S. Feld, Y. Park, and Z. Yaqoob, “Digital optical phase conjugation for delivering two-dimensional images through turbid media,” Sci. Rep. 3, 1909 (2013).

[62]. O. Katz, E. Small, and Y. Silberberg, “Looking around corners and through thin turbid layers in real time with scattered incoherent light,” Nat. Photonics 6(8), 549–553 (2012).

[63]. S. Popoff, G. Lerosey, M. Fink, A. C. Boccara, and S. Gigan, “Image transmission through an opaque material,” Nat. Commun. 1(6), 81 (2010).

[64]. D. B. Conkey and R. Piestun, “Color image projection through a strongly scattering wall,” Opt. Express 20(25),27312–27318 (2012).

[65]. M. Kim, Y. Choi, C. Yoon, W. Choi, J. Kim, Q. H. Park, and W. Choi, “Maximal energy transport through disordered media with the implementation of transmission eigenchannels,” Nat. Photonics 6(9), 583–587 (2012).

[66]. F. Helmchen and W. Denk, “Deep tissue two-photon microscopy,” Nat. Methods 2(12), 932–940 (2005).

[67]. D. Wang, E. H. Zhou, J. Brake, H. Ruan, M. Jang, and C. Yang, “Focusing through dynamic tissue with millisecond digital optical phase conjugation,” Optica 2(8), 728–735 (2015).

[68]. I. Freund, “Looking through walls and around corners,” Physica A 168(1), 49–65 (1990).

[69]. M. Vellekoop and C. M. Aegerter, “Scattered light fluorescence microscopy: imaging through turbid layers,” Opt. Lett. 35(8), 1245–1247 (2010).

[70]. I. M. Vellekoop and C. M. Aegerter, “Focusing light through living tissue,” Proc. SPIE 7554, 755430 (2010).

[71]. A. P. Mosk, A. Lagendijk, G. Lerosey, and M. Fink, “Controlling waves in space and time for imaging and focusing in complex media,” Nature Photon.6, 283 (2012).

[72]. S. Feng, C. Kane, P. A. Lee, and A. D. Stone, “Correlations and fluctuations of coherent wave transmission through disordered media,” Phys. Rev. Lett. 61(7), 834–837 (1988).

[73]. H. Hui-Ling, C. Zi-Yang, S. Cun-Zhi, L. Ji-Lin, and P. Ji-Xiong, “Light focusing through scattering media by particles warm optimization,” Chin. Phys. Lett.32(10), 104202 (2015).

[74]. Q. Feng, B. Zhang, Z. Liu, C. Lin, and Y. Ding, “Research on intelligent algorithms for amplitude optimization of wavefront shaping,” Appl. Opt.56(12), 3240–3244 (2017).

[75]. L. Fang, H. Zuo, Z. Yang, X. Zhang, J. Du, and L. Pang, “Binary wavefront optimization using particle swarm algorithm,” Laser Phys.28(7), 076204 (2018).

[76]. L. Fang, H. Zuo, Z. Yang, X. Zhang, J. Du, and L. Pang, “Binary wavefront optimization using a simulated annealing algorithm,” Appl. Opt.57(8), 1744–1751 (2018).

[77]. Z. Fayyaz, N. Mohammadian, F. Salimi, A. Fatima, M. R. R. Tabar, and M. R. Avanaki, “Simulated annealing optimization in wavefront shaping controlled transmission,” Appl. Opt.57(21), 6233–6242 (2018).

[78]. I. M. Vellekoop and A. Mosk, “Phase control algorithms for focusing light through turbid media,” Opt. Commun.281(11), 3071–3080 (2008).

[79]. Z. Fayyaz, N. Mohammadian, M. Reza Rahimi Tabar, R. Manwar, and K. Avanaki, “A comparative study of optimization algorithms for wavefront shaping,” J. Innovative Opt. Health Sci.,12(2019).

[80]. H. Li, C. M. Woo, T. Zhong, Z. Yu, Y. Luo, Y. Zheng, X. Yang, H. Hui, and P. Lai, “Adaptive optical focusing through perturbed scattering media with a dynamic mutation algorithm,” Photonics Res. 9(2), 202–212 (2021).

[81]. Choi, A. P. Mosk, Q. H. Park, and W. Choi, “Transmission eigenchannels in a disordered medium,” Phys. Rev. B 83(13), 134207 (2011).

[82]. W. Choi, Q. H. Park, and W. Choi, “Perfect transmission through Anderson localized systems mediated by a cluster of localized modes,” Opt. Express 20(18), 20721–20729 (2012).

[83]. M. Kim, W. Choi, C. Yoon, G. H. Kim, and W. Choi, “Relation between transmission eigenchannels and single-channel optimizing modes in a disordered medium,” Opt. Lett. 38(16), 2994–2996 (2013).

[84]. C. W. J. Beenakker, “Random-matrix theory of quantum transport,” Rev. Mod. Phys. 69(3), 731–808 (1997).

[85]. J. G. Rivas, R. Sprik, C. M. Soukoulis, K. Busch, and A. Lagendijk, “Optical transmission through strong scattering and highly polydisperse media,” Europhys. Lett. 48(1), 22–28 (1999).

[86]. B. Payne, J. Andreasen, H. Cao, and A. Yamilov, “Relation between transmission and energy stored in random media with gain,” Phys. Rev. B 82(10), 104204 (2010).

[87]. B. Gérardin, J. Laurent, A. Derode, C. Prada, and A. Aubry, “Full transmission and reflection of waves propagating through a maze of disorder,” Phys. Rev. Lett. 113(17), 173901 (2014).

[88]. T. Schwartz, G. Bartal, S. Fishman, and M. Segev, “Transport and Anderson localization in disordered two-dimensional photonic lattices,” Nature 446(7131), 52–55 (2007).

[89]. Y. M. Wang, B. Judkewitz, C. A. Dimarzio, and C. Yang, “Deep-tissue focal fluorescence imaging with digitally time-reversed ultrasound-encoded light,” Nat. Commun. 3, 928 (2012).

[90]. J. B. Pendry, “Quasi-extended electron-states in strongly disordered-systems,” J. Phys. C: Solid State Phys. 20(5), 733–742 (1987).

[91]. O. Katz, E. Small, Y. Bromberg, and Y. Silberberg, “Focusing and compression of ultrashort pulses through scattering media,” Nat. Photonics 5(6), 372–377 (2011).

[92]. S. John, “Electromagnetic absorption in a disordered medium near a photon mobility edge,” Phys. Rev. Lett. 53(22), 2169–2172 (1984).

[93]. D. S. Wiersma, P. Bartolini, A. Lagendijk, and R. Righini, “Localization of light in a disordered medium,” Nature 390(6661), 671–673 (1997).

[94]. K. Si, R. Fiolka, and M. Cui, “Fluorescence imaging beyond the ballistic regime by ultrasound pulse guided digital phase conjugation,” Nat. Photonics 6(10), 657–661 (2012).

[95]. I. N. Papadopoulos, S. Farahi, C. Moser, and D. Psaltis, “Focusing and scanning light through a multimode optical fiber using digital phase conjugation,” Opt. Express 20(10), 10583–10590 (2012).

[96]. T.Čižmár, M. Mazilu, and K. Dholakia, “In situ wavefront correction and its application to micromanipulation,” Nat. Photonics 4(6), 388–394 (2010).

[97]. I. M. Vellekoop, M. Cui, and C. Yang, “Digital optical phase conjugation of fluorescence in turbid tissue,” Appl. Phys. Lett. 101(8), 081108 (2012).

[98]. A. Drémeau, A. Liutkus, D. Martina, O. Katz, C. Schülke, F. Krzakala, S. Gigan, and L. Daudet, “Reference-less measurement of the transmission matrix of a highly scattering material using a dmd and phase retrieval techniques,” Opt. Express23(9), 11898–11911 (2015)

[99]. T. Ikeda, G. Popescu, R. R. Dasari, and M. S. Feld, “Hilbert phase microscopy for investigating fast dynamics in transparent systems,” Opt. Lett. 30(10), 1165–1167 (2005).

[100]. W. Choi, C. Fang-Yen, K. Badizadegan, S. Oh, N. Lue, R. R. Dasari, and M. S. Feld, “Tomographic phase microscopy,” Nat. Methods 4(9), 717–719 (2007).

[101]. M. C. Pitter, C. W. See, and M. G. Somekh, “Full-field heterodyne interference microscope with spatially incoherent illumination,” Opt. Lett. 29(11), 1200–1202 (2004).

[102]. Y. Park, W. Choi, Z. Yaqoob, R. Dasari, K. Badizadegan, and M. S. Feld, “Speckle-field digital holographic microscopy,” Opt. Express 17(15), 12285–12292 (2009).

[103]. Y. Choi, T. D. Yang, K. J. Lee, and W. Choi, “Full-field and single-shot quantitative phase microscopy using dynamic speckle illumination,” Opt. Lett. 36(13), 2465–2467 (2011).

[104]. A. P. Mosk. Wavefront shaping in complex optics. https://amolf.nl/wp-content/uploads/2019/06/4-Optical-wavefront-shaping-Prof.-Allard-Mosk-Utrecht-University-small.pdf.

[105]. F. Kong, R. H. Silverman, L. Liu, P. V. Chitnis, K. K. Lee, and Y.-C. Chen, “Photoacoustic-guided convergence of light through optically diffusive media,” Opt. Lett. 36(11), 2053–2055 (2011).

[106]. A. M. Caravaca-Aguirre, D. B. Conkey, J. D. Dove, H. Ju, T. W. Murray, and R. Piestun, “High contrast three-dimensional photoacoustic imaging through scattering media by localized optical fluence enhancement,” Opt. Express 21(22), 26671–26676 (2013).

[107]. J. Aulbach, B. Gjonaj, P. Johnson, and A. Lagendijk, “Spatiotemporal focusing in opaque scattering media by wave front shaping with nonlinear feedback,” Opt. Express 20(28), 29237–29251 (2012).

[108]. I. M. Vellekoop, E. G. van Putten, A. Lagendijk, and A. P. Mosk, “Demixing light paths inside disordered metamaterials,” Opt. Express 16(1), 67–80 (2008).

[109]. E. G. van Putten, A. Lagendijk, and A. P. Mosk, “Optimal concentration of light in turbid materials,” J. Opt. Soc. Am. B 28(5), 1200–1203 (2011).

[110]. T. J. Huisman, S. R. Huisman, A. P. Mosk, and P. W. Pinkse, “Controlling single-photon fock-state propagation through opaque scattering media,” Appl. Phys. B 3, 1–5 (2013).

[111]. A. Yariv, “Phase conjugate optics and real-time holography [invited paper],” IEEE J. Quantum Electron. 14(9), 650–660 (1978).

[112]. P. Günter, “Holography, coherent light amplification and optical phase conjugation with photorefractive materials,” Phys. Rep. 93, 199–299 (1982).

[113]. H. Ruan, J. Xu, and C. Yang, “Optical information transmission through complex scattering media with optical-channel-based intensity streaming,” Nat. Commun. 12, 2411 (2021).

[114]. J. Seeds and K. J. Williams, “Microwave photonics,” J. Lightw. Technol. 24(12), 4628–4641 (2006).

[115]. J. Capmany and D. Novak, “Microwave photonics combines two worlds,” Nat. Photonics 1(6), 319–330 (2007).

[116]. X. Zhu and J. M. Kahn, “Free-space optical communication through atmospheric turbulence channels,” IEEE Trans. Commun. 50(8), 1293–1300 (2002).

[117]. H. Kaushal and G. Kaddoum, “Optical communication in space: Challenges and mitigation techniques,” IEEE Commun. Surv. Tut., 19(1), 57–96 (2017).

[118]. M. Guan, Z. Wu, Y. Cui, C. X. Mei, L. Wang, J. F. Ye, and B. Peng, “Efficiency evaluations based on artificial intelligence for 5G massive MIMO communication

systems on high-altitude platform stations," IEEE Trans. Ind. Informat. 16(10), 6632–6640 (2019).

[119]. J. Bertolotti, E. G. van Putten, C. Blum, A. Lagendijk, W. L. Vos, and A. P. Mosk, "Non-invasive imaging through opaque scattering layers," Nature 491(7423), 232–234 (2012).

[120]. O. Katz, P. Heidmann, M. Fink, and S. Gigan, "Non-invasive single-shot imaging through scattering layers and around corners via speckle correlations," Nat. Photonics 8(10), 784–790 (2014).

[121]. J. C. Stover, Optical Scattering, Measurement and Analysis, 2nd ed. (SPIE Press, 1995).

[122]. I. M. Vellekoop, A. Lagendijk, and A. P. Mosk, "Exploiting disorder for perfect focusing," Nat. Photonics 4, 320–322 (2010).

[123]. S. M. Popoff, G. Lerosey, R. Carminati, M. Fink, A. C. Boccara, and S. Gigan, "Measuring the transmission matrix in optics: An approach to the study and control of light propagation in disordered media," Phys. Rev. Lett. 104, 100601 (2010).

[124]. Y. Zhao, C. Cai, J. Zhang, X. Cao, L. Wang, S. Li, and J. Wang, "Feedback-enabled adaptive underwater twisted light transmission link utilizing the reflection at the air-water interface," Opt. Express 26, 16102–16112 (2018).

[125]. H. Huang, Y. Cao, G. Xie, Y. Ren, Y. Yan, C. Bao, N. Ahmed, M. A. Neifeld, S. J. Dolinar, and A. E. Willner, "Crosstalk mitigation in a free-space orbital angular momentum multiplexed communication link using 4 × 4 MIMO equalization," Opt. Lett. 39, 4360–4363 (2014).

[126]. J. Jiang, G. Han, L. Shu, S. Chan, and K. Wang, “A trust model based on cloud theory in underwater acoustic sensor networks,” IEEE Trans. Ind. Informat. 13(1), 342–350 (2017).

[127]. M. Chitre, S. Shahabudeen, and M. Stojanovic, “Underwater acoustic communications and networking: Recent advances and future challenges,” Mar. Technol. Soc. J. 42(1), 103–116(2008).

[128]. T. Oberg, B. Nilsson, N. Olofsson, M. L. Nordenvaad, and E. Sangfelt, “Underwater communication link with iterative equalization,” in Proc. IEEE OCEANS Conf. 1–6 (2006).

[129]. H. Kaushal and G. Kaddoum, “Underwater optical wireless communication,” IEEE Access 4, 1518–1547 (2016).

[130]. I. Jawhar, N. Mohamed, J. Al-Jaroodi, and S. Zhang, “An architecture for using autonomous underwater vehicles in wireless sensor networks for underwater pipeline monitoring,” IEEE Trans. Ind. Informat. 15(3), 1329–1340 (2018).

[131]. T. Qiu, Z. Zhao, T. Zhang, C. Chen, and C. L. P. Chen, “Underwater Internet of Things in smart ocean: system Architecture and open issues”, IEEE Trans. Ind. Informat. 16(7), 1–13 (2019).

[132]. E. Tajahuerce, V. Durán, P. Clemente, E. Irles, F. Soldevila, P. Andrés, and J. Lancis, “Image transmission through dynamic scattering media by single-pixel photodetection,” Opt. Express 22(14), 16945–16955 (2014).

[133]. Y. Xiao, L. Zhou, and W. Chen, “Experimental demonstration of ghost-imaging-based authentication in scattering media,” Opt. Express 27(15), 20558–20566 (2019).

[134]. Y. Xiao, L. Zhou, and W. Chen, “Wavefront control through multi-layer scattering media using single-pixel detector for high-PSNR optical transmission,” Opt. Lasers Eng. 139, 106453 (2021).

[135]. Y. Xiao, L. Zhou, and W. Chen, “High-fidelity ghost diffraction and transmission in free space through scattering media,” Appl. Phys. Lett. 118(10), 104001 (2021).

[136]. Z. Pan, Y. Xiao, L. Zhou, Y. Cao, M. Yang, and W. Chen, “Non-line-of-sight optical information transmission through turbid water,” Opt. Express 29(24), 39498–39510 (2021).

[137]. J. A. Myers, B. S. Curtis, and W. R. Curtis, “Improving accuracy of cell and chromophore concentration measurements using optical density,” BMC Biophys. 6(1), 4 (2013).

[138]. X. Liu, S. Yi, X. Zhou, Z. Fang, Z. J. Qiu, L. Hu, C. Cong, L. Zheng, R. Liu, and P. Tian, “34.5 m underwater optical wireless communication with 2.70 Gbps data rate based on a green laser diode with NRZ-OOK modulation,” Opt. Express 25(22), 27937–27947 (2017).

[139]. R. Joshi, T. O’Connor, X. Shen, M. Wardlaw, and B. Javidi, “Optical 4D signal detection in turbid water by multidimensional integral imaging using spatially distributed and temporally encoded multiple light sources,” Opt. Express 28(7), 10477–10490 (2020).

[140]. S. Komatsu, A. Markman, and B. Javidi, “Optical sensing and detection in turbid water using multidimensional integral imaging,” Opt. Lett. 43(14), 3261–3264 (2018).

[141]. R. Joshi, G. Krishnan, T. O'Connor, and B. Javidi, "Signal detection in turbid water using temporally encoded polarimetric integral imaging," Opt. Express 28(24), 36033–36045 (2020).

[142]. M. Dehshiri, S. G Sabouri, and A. Khorsandi, "Structural similarity assessment of an optical coherence tomographic image enhanced using the wavelet transform technique," J. Opt. Soc. Am. A 38(1), 1–9 (2021).

[143]. T. D. Dickey, "Emerging ocean observations for interdisciplinary data assimilation systems," J. Mar. Syst. 40-41, 5–48 (2003).

[144]. M. A. Khalighi and M. Uysal, "Survey on free space optical communication: a communication theory perspective," IEEE Comm. Surv. and Tutor. 16(4), 2231–2258 (2014).

[145]. Z. Zeng, S. Fu, H. Zhang, Y. Dong, and J. Cheng, "A survey of underwater optical wireless communications," IEEE Comm. Surv. and Tutor. 19(1), 204–238 (2017).

[146]. C.-C. Kao, Y.-S. Lin, G.-D. Wu, and C.-J. Huang, "A comprehensive study on the internet of underwater things: applications, challenges, and channel models," Sensors 17(7), 1477 (2017).

[147]. B. Cochenour, L. J. Mullen, and A. E. Laux, "Characterization of the beam-spread function for underwater wireless optical communications links," IEEE J. Oceanic Eng. 33(4), 513–521 (2008).

[148]. J. H. Fischer, K. R. Bennett, S. A. Reible, J. H. Cafarella, and Iwen Yao, "A high data rate, underwater acoustic data-communications transceiver," in Proc. OCEANS: Mastering Oceans Through Technol., 2, 571–576 (1992).

[149]. J. Wang, J. Y. Yang, I. M. Fazal, N. Ahmed, Y. Yan, H. Huang, Y. Ren, Y. Yue, S. Dolinar, M. Tur, and A. E. Willner, "Terabit free-space data transmission

employing orbital angular momentum multiplexing," Nat. Photonics 6, 488–496 (2012).

[150]. G. Gibson, J. Courtial, M. J. Padgett, M. Vasnetsov, V. Pas'ko, S. M. Barnett, and S. Franke-Arnold, "Free-space information transfer using light beams carrying orbital angular momentum," Opt. Express 12(22), 5448–5456 (2004).

[151]. H. M. Oubei, C. Li, K. H. Park, T. K. Ng, M. S. Alouini, and B. S. Ooi, "2.3 Gbit/s underwater wireless optical communications using directly modulated 520 nm laser diode," Opt. Express 23(16), 20743–20748 (2015).

[152]. K. Nakamura, I. Mizukoshi, and M. Hanawa, "Optical wireless transmission of 405 nm, 1.45 Gbit/s optical IM/DD-OFDM signals through a 4.8 m underwater channel," Opt. Express 23(2), 1558–1566 (2015).

[153]. A. Trichili, M. A. Cox, B. S. Ooi, and M. S. Alouini, "Roadmap to free space optics," J. Opt. Soc. Am. B 37(11), A184–A201 (2020).

[154]. C. C. Davis, I. I. Smolyaninov, and S. D. Milner, "Flexible optical wireless links and networks," IEEE Commun. Mag. 41, 51–57 (2003).

[155]. S. Arnon and D. Kedar, "Non-line-of-sight underwater optical wireless communication network," J. Opt. Soc. Am. A 26(3), 530–539 (2009).

[156]. X. Sun, W. Cai, O. Alkhazragi, E.-N. Ooi, H. He, A. Chaaban, C. Shen, H. M. Oubei, M. Z. M. Khan, T. K. Ng, M.-S. Alouini, and B. S. Ooi, "375-nm ultraviolet-laser based non-line-of-sight underwater optical communication," Opt. Express 26(10), 12870–12877 (2018).

[157]. G. Chen, Z. Xu, and B. M. Sadler, "Experimental demonstration of ultraviolet pulse broadening in short-range non-line-of-sight communication channels," Opt. Express 18(10), 10500–10509 (2010).

[158]. S. Zhu, X. Chen, X. Liu, G. Zhang, and P. Tian, “Recent progress in and perspectives of underwater wireless optical communication,” Prog. Quantum Electron.73, 100274 (2020).

[159]. D. Wiersma, “Disordered photonics,” Nat. Photonics 7(3), 188–196 (2013).

[160]. S. Yu, C.-W. Qiu, Y. Chong, S. Torquato, and N. Park, “Engineered disorder in photonics,” Nat. Rev. Mater. 6, 226–243 (2021).

[161]. X. Xu, H. Liu, and L. V. Wang, “Time-reversed ultrasonically encoded optical focusing into scattering media,” Nat. Photonics 5(3), 154–157 (2011).

[162]. J. Tang, R. N. Germain, and M. Cui, “Superpenetration optical microscopy by iterative multiphoton adaptive compensation technique,” Proc. Natl. Acad. Sci. U.S.A. 109(22), 8434–8439 (2012).

[163]. A. Liutkus, D. Martina, S. Popoff, G. Chardon, O. Katz, G. Lerosey, S. Gigan, L. Daudet, and I. Carron, “Imaging with nature: compressive imaging using a multiply scattering medium,” Sci. Rep. 4, 5552 (2014).

[164]. K. L. C. Seow, P. Torok, and M. R. Foreman, “Single pixel polarimetric imaging through scattering media,” Opt. Lett.45(20), 5740–5743 (2020).

[165]. K. Soltanlou and H. Latifi, “Three-dimensional imaging through scattering media using a single pixel detector,” Appl. Opt. 58(28), 7716–7726 (2019).

[166]. L. X. Lin, J. Cao, D. Zhou, H. Cui, and Q. Hao, “Ghost imaging through scattering medium by utilizing scattered light,” Opt. Express 30(7), 11243–11253 (2022).

[167]. V. Durán, F. Soldevila, E. Irles, P. Clemente, E. Tajahuerce, P. Andrés, and J. Lancis, “Compressive imaging in scattering media,” Opt. Express 23(11), 14424–14433 (2015).

[168]. P. Udabage, R. Sharma, D. Murphy, I. Mckinnon, and R. Beckett, “Size distribution of reconstituted skim milk using field-flow fractionation,” J. Microcolumn Sep. 9(7), 557–563 (1997).

[169]. L. Wind and W. W. Szymanski, “Quantification of scattering corrections to the Beer-Lambert law for transmittance measurements in turbid media,” Meas. Sci. Technol. 13(3), 270–275 (2002).

[170]. B. Javidi, A. Carnicer, J. Arai, T. Fujii, H. Hua, H. Liao, M. Martínez-Corral, F. Pla, A. Stern, L. Waller, Q. H. Wang, G. Wetzstein, M. Yamaguchi, and H. Yamamoto, “Roadmap on 3D integral imaging: sensing, processing, and display,” Opt. Express 28(22), 32266–32293 (2020).

[171]. S. Komatsu, A. Markman, and B. Javidi, “Optical sensing and detection in turbid water using multi-dimensional integral imaging,” Opt. Lett. 43(14), 3261–3264 (2018).

[172]. S. Tang, Y. Dong, and X. Zhang, “On path loss of NLOS underwater wireless optical communication links,” in Proceedings of IEEE Conference on Oceans, IEEE Xplore, 1–3 (2013).

[173]. Y. Zuo, H. Xiao, J. Wu, Y. Li, and J. Lin, “A single-scatter path loss model for non-line-of-sight ultraviolet channels,” Opt. Express 20(9), 10359–10369 (2012).

[174]. A. Hore and D. Ziou, “Image quality metrics: PSNR vs. SSIM,” in 2010 20th International Conference on Pattern Recognition (IEEE, 2010), pp. 2366–2369.

[175]. Y.-F. Zhang, P. J. Thorburn, W. Xiang, and P. Fitch, “SSIM–a deep learning approach for recovering missing time series sensor data,” IEEE Internet of Things Journal, 6 (4), 6618–6628 (2019).

[176]. S. Becker, J. Bobin, and E. Candes, “NESTA: a fast and accurate first-order method for sparse recovery,” SIAMJ. Imaging Sciences 4(1), 1–39 (2011).

[177]. P. Pathak, X. Feng, P. Hu, and P. Mohapatra, “Visible light communication, networking, and sensing: A survey, potential and challenges,” IEEE Commun. Surveys Tuts., 17(4), 2047–2077 (2015).

[178]. V. W. S. Chan, “Free-space optical communications,” J. Lightwave Technol. 24(12), 4750–4762 (2006).

[179]. A. K. Majumder and J. C. Ricklin, Free-Space Laser Communications: Principles and Advances (Springer, 2008), Chap.1.

[180]. G. Gibson, J. Courtial, M. J. Padgett, M. Vasnetsov, V. Pas’ko, S. M. Barnett, and S. Franke-Arnold, “Free space information transfer using light beams carrying orbital angular momentum,” Opt. Express 12 (22), 5448–5456 (2004).

[181]. M. Jahanbakht, W. Xiang, L. Hanzo, and M. R. Azghadi, “Internet of underwater things and big marine data analytics–a comprehensive survey,” IEEE Trans. Inform. Forensic Secur. 23(2), 904–956 (2021).

[182]. M. Kong, J. Wang, Y. Chen, T. Ali, R. Sarwar, Y. Qiu, S. Wang, J. Han, and J. Xu, “Security weaknesses of underwater wireless optical communication,” Opt. Express 25(18), 21509–21518 (2017).

[183]. Y. Pan, P. Wang, W. Wang, S. Li, M. Cheng, and L. Guo, “Statistical model for the weak turbulence-induced attenuation and crosstalk in free space communication systems with orbital angular momentum,” Opt. Express 29(8), 12644–12662 (2021).

[184]. D. B. Kilfoyle and A. B. Baggeroer, “State of the art in underwater acoustic telemetry,” IEEE J. Ocean. Eng., 25(1) 4–27, (2000).

[185]. D. O'Brien, G. E. Faulkner, E. B. Zyambo, K. Jim, D. J. Edwards, P. Stavrinou, G. Parry, J. Bellon, M. J. Sibley, V. A. Lalithambika, V. M. Joyner, R. J. Samsudin, D. M. Holburn, and R. J. Mears, "Integrated transceivers for optical wireless communication," IEEE J. Sel. Top. Quantum Electron. 11(1), 173–183 (2005).

[186]. P. Sebbah, eds. Waves and Imaging Through Complex Media (Kluwer Academic, 2001).

[187]. M. Nixon, O. Katz, E. Small, Y. Bromberg, A. A. Friesem, Y. Silberberg, and N. Davidson, "Real-time wavefront shaping through scattering media by all-optical feedback," Nat. Photonics 7, 919 (2013).

[188]. A. Ishimaru, "Wave propagation and scattering in random media and rough surfaces," Proc. IEEE 79, 1359–1366 (1991).

[189]. Y. Weng, Y. Guo, O. Alkhazragi, T. K. Ng, J.-H. Guo, and B. S. Ooi, "Impact of turbulent-flow-induced scintillation on deep-ocean wireless optical communication," J. Lightwave Technol. 37(19), 5083–5090 (2019).

[190]. L. E. M. Matheus, A. B. Vieira, L. F. M. Vieira, M. A. M. Vieira, and O. Gnawali, "Visible light communication: concepts, applications and challenges," IEEE Commun. Surveys Tuts. 21, 3204–3237 (2019).

[191]. H. M. Oubei, E. Zedini, R. T. ElAfandy, A. Kammoun, M. Abdallah, T. K. Ng, M. Hamdi, M.-S. Alouini, and B. S. Ooi, "Simple statistical channel model for weak temperature-induced turbulence in underwater wireless optical communication systems," Opt. Lett. 42(13), 2455–2458 (2017).

[192]. P. Qiu, G. Cui, Z. Qian, S. Zhu, X. Shan, Z. Zhao, X. Zhou, X. Cui, and P. Tian, "4.0 Gbps visible light communication in a foggy environment based on a blue laser diode," Opt. Express 29(9), 14163–14173 (2021).

[193]. Y. Zhao, A. Zhao, L. Zhu, W. Lv, J. Xu, S. Li, and J. Wang, "Performance evaluation of underwater optical communications using spatial modes subjected to bubbles and obstructions," Opt. Lett. 42(22), 4699–4702 (2017).

[194]. M. V. Jamali, A. Mirani, A. Parsay, B. Abolhassani, P. Nabavi, A. Chizari, P. Khorramshahi, S. Abdollahramezani, and J. A. Salehi, "Statistical studies of fading in underwater wireless optical channels in the presence of air bubble, temperature, and salinity random variations," IEEE Trans. Commun. 66(10), 4706–4723 (2018).

[195]. X. Yang, Z. Tong, Y. Dai, X. Chen, H. Zhang, H. Zou, and J. Xu, "100 m full-duplex underwater wireless optical communication based on blue and green lasers and high sensitivity detectors," Opt. Commun. 498, 127261 (2021).

[196]. C. H. Kang, A. Trichili, O. Alkhazragi, H. Zhang, R. C. Subedi, Y. Guo, S. Mitra, C. Shen, I. S. Roqan, N. G. Tien Khee, M.-S. Alouini, and B. S. Ooi, "Ultraviolet-to-blue color-converting scintillating-fibers photoreceiver for 375-nm laser-based underwater wireless optical communication," Opt. Express 27(21), 30450–30461 (2019).

[197]. J. Wang, C. Lu, S. Li, and Z. Xu, "100 m/500 Mbps underwater optical wireless communication using an NRZ-OOK modulated 520 nm laser diode," Opt. Express 27(9), 12171–12181 (2019).

[198]. Y.-K. Xu, W.-T. Liu, E.-F. Zhang, Q. Li, H.-Y. Dai, and P.-X. Chen, "Is ghost imaging intrinsically more powerful against scattering?" Opt. Express 23(26), 32993–33000 (2015).

[199]. M. P. Edgar, G. M. Gibson, and M. J. Padgett, "Principles and prospects for single-pixel imaging," Nat. Photonics 13(1), 13–20 (2019).

[200]. Z. Zhang, X. Ma, and J. Zhong, “Single-pixel imaging by means of Fourier spectrum acquisition,” Nat. Commun. 6(1), 6225 (2015).

[201]. N. Enghiyad and A. G. Sabbagh, “Impulse response of underwater optical wireless channel in the presence of turbulence, absorption, and scattering employing Monte Carlo simulation,” J. Opt. Soc. Am. A 39 (1), 115–126 (2022).

[202]. L. Lu, X. Ji, and Y. Baykal, “Wave structure function and spatial coherence radius of plane and spherical waves propagating through oceanic turbulence,” Opt. Express 22(22), 27112–27122 (2014).

[203]. L. Lu, P. Zhang, C. Fan, and C. Qiao, “Influence of oceanic turbulence on propagation of a radial Gaussian beam array,” Opt. Express 23(3), 2827–2836 (2015).

[204]. H. Song, R. Zhang, N. Hu, H. Zhou, X. Su, H. Song, K. Zou, K. Pang, C. Liu, D. Park, B. Lynn, G. Gbur, A. Dogariu, R. Watkins, J. Miller, E. Johnson, M. Tur, and A. Willner, “Dynamic aerosol and dynamic air-water interface curvature effects on a 2-Gbit/s free-space optical link using orbital-angular-momentum multiplexing,” Nanophotonics 11(4), 885–895 (2022).

[205]. Z. Y. Zhu, M. Janasik, A. Fyffe, H. Darrick, Y. Y. Zhou, B. Kantor, T. Winder, R. W. Boyd, G. Leuchs, and Z. M. Shi, “Compensation-free high-dimensional free-space optical communication using turbulence-resilient vector beams,” Nat. Commun. 12(1), 1–8 (2021).

[206]. D. F. Swinehart, “The beer-lambert law,” J. Chem. Educ. 39(7), 333–335 (1962).

[207]. R. Gordon, “Light in a subwavelength slit in a metal: propagation and reflection,” Phys. Rev. B 73(15), 153405 (2006).

[208]. Y. Huang, B. Niu, H. Guan and S. Zhang, “Enhancing image watermarking with adaptive embedding parameter and psnr guarantee,” IEEE Trans. Multimedia, 21(10) 2447–2460 (2019).

[209]. Z. Pan, Y. Xiao, Y. Cao, L. Zhou, and W. Chen, “Optical analog-signal transmission and retrieval through turbid water,” Appl. Opt. 60(34), 10704–10713 (2021).

[210]. W. Tang, M Z. Chen, X. Chen, J. Dai, Y. Han, M. D. Renzoet, Y. Zeng, S. Jin, Q. Cheng, and T. J. Cui, “Wireless communications with reconfigurable intelligent surface: path loss modeling and experimental measurement,” IEEE Trans. Wireless Commun. 20, 421–439 (2021).

[211]. P. Xu, J. Zheng, J. K. Doylend, and A. Majumdar, “Low-loss and broadband nonvolatile phase-change directional coupler switches,” ACS Photon. 6, 553–557 (2019).

[212]. L. C. Andrews, R. L. Phillips, and C. Y. Hopen, Laser Beam Scintillation with Applications (SPIE, 2001).

[213]. Y. Gu, O. Korotkova, and G. Gbur, “Scintillation of nonuniformly polarized beams in atmospheric turbulence,” Opt. Lett. 34(15), 2261–2263 (2009).

[214]. Y.Guo, M. Kong, M. Sait, S. Marie, O. Alkhazragi, T. K. Ng, and B. S. Ooi, “Compact scintillating-fiber/450-nm-laser transceiver for full-duplex underwater wireless optical communication system under turbulence,” Opt. Express 30 (1), 53–69 (2022).

[215]. T. M. P. Cattaneo and S. E. Holroyd, “The use of near infrared spectroscopy for determination of adulteration and contamination in milk and milk powder: updating knowledge,” J. Near Infrared Spectrosc. 21(5), 341–349 (2013).

[216]. Z. Pan, Y. Xiao, Y. Cao, L. Zhou, and W. Chen, “Accurate optical information transmission through thick tissues using zero-frequency modulation and single-pixel detection,” Opt. Lasers Eng. 158, 107133 (2022).

[217]. Y. Xiao and W. Chen, “High-fidelity optical transmission around the corner,” IEEE Photon. Technol. Lett. 33 (1), 3–6 (2021).

[218]. Y. Cao, Y. Xiao, Z. Pan, L. Zhou, and W. Chen, “High-fidelity temporally-corrected transmission through dynamic smoke via pixel-to-plane data encoding,” Opt. Express 30(20), 36464–36477 (2022).

[219]. M. R. Yuce, “Implementation of wireless body area networks for healthcare systems,” Sens. Actuators A Phys. 162(1), 116–129 (2010).

[220]. Q. H. Abbasi, M. U. Rehman, K. Qaraqe, and A. Alomainy, Advances in Body Centric Wireless Communication: Applications and State-of-the-Art, IET, London (2016).

[221]. M. Mujeeb-U-Rahman et al., “Optical power transfer and communication methods for wireless implantable sensing platforms,” J. Biomed. Opt. 20(9), 095012 (2015).

[222]. A. Abou-Elnour, A. Safi, and A. N. Aldalu, “A reliable wireless monitoring network for healthcare applications,” Health Monitoring of Structural and Biological Systems, Proc. of SPIE 7984, pp. 79841C-1, San Diego, California, United States (2011) [doi:10.1117/12.880997].

[223]. A. Kiourti and K. S. Nikita, “A review of in-body biotelemetry devices: implantables, ingestibles, and injectables,” IEEE Trans. Biomed. Eng. 64(7), 1422–1430 (2017).

[224]. C. Camara, P. Peris-Lopeza, and J. E. Tapiadora, “Security and privacy issues in implantable medical devices: a comprehensive survey,” J. Biomed. Inform. 55, 272–289 (2015).

[225]. L. Mucchi, S. Jayousi, A. Martinelli, S. Caputo, and P. Marcocci, “An overview of security threats, solutions and challenges in WBANs for healthcare,” in Proc. 13th Int. Symp. Med. Inf. Commun. Technol. pp. 1–6, IEEE, Oslo, Norway, (2019) [doi:10.1109/ISMICT.2019.8743798].

[226]. T. Bos, W. Dehaene, and M. Verhelst, “Ultrasound in-body communication with OFDM through multipath realistic channels,” in Proc. IEEE Biomed. Circuits Syst. Conf, pp. 1–4, IEEE, Nara, Japan (2019).

[227]. F. Mazzilli, M. Peisino, R. Mitouassiwou, B. Cotté, P. Thoppay, C. Lafon, P. Favre, E. Meurville, and C. Dehollain, “In-vitro platform to study ultrasound as source for wireless energy transfer and communication for implanted medical devices,” in Proc. Annu. Int. Conf. IEEE Eng. Med. Biol, pp. 3751–3754, IEEE, Buenos Aires, Argentina (2010).

[228]. G. Marquez et al., “Anisotropy in the absorption and scattering spectra of chicken breast tissue,” Appl. Opt. 37(4), 798–804 (1998).

[229]. P. Taroni et al., “In vivo absorption and scattering spectroscopy of biological tissues,” Photochem. Photobiol. Sci. 2(2), 124–129 (2003).

[230]. R. I. Stantchev, B. Sun, S. M. Hornett, P. A. Hobson, G. M. Gibson, M. J. Padgett, and E. Hendry, “Noninvasive, near-field terahertz imaging of hidden objects using a single-pixel detector,” Sci. Adv. 2(6), e1600190 (2016).

[231]. R. Dutta et al., “Single-pixel imaging of the retina through scattering media,” Biomed. Opt. Express 10(8), 4159–4167 (2019).

[232]. G. M. Gibson, B. Sun, M. P. Edgar, D. B. Phillips, N. Hempler, G. T. Maker, G. P. Malcolm, and M. J. Padgett, “Real-time imaging of methane gas leaks using a single-pixel camera,” Opt. Express 25(4), 2998–3005 (2017).

[233]. P. Clemente, V. Durán, E. Tajahuerce, P. Andrés, V. Climent, and J. Lancis, “Compressive holography with a single-pixel detector,” Opt. Lett. 38(14), 2524–2527 (2013).

[234]. N. Radwell, K. J. Mitchell, G. M. Gibson, M. P. Edgar, R. Bowman, and M. J. Padgett, “Single-pixel infrared and visible microscope,” Optica 1(5), 285–289 (2014).

[235]. M.-J. Sun, M. P. Edgar, G. M. Gibson, B. Sun, N. Radwell, R. Lamb, and M. J. Padgett, “Single-pixel three-dimensional imaging with time-based depth resolution,” Nat. Commun. 7(1), 12010 (2016).

[236]. D. B. Phillips, M.-J. Sun, J. M. Taylor, M. P. Edgar, S. M. Barnett, G. M. Gibson, and M. J. Padgett, “Adaptive foveated single-pixel imaging with dynamic supersampling,” Sci. Adv. 3(4), e1601782 (2017).

[237]. N. Yu, P. Genevet, M. A. Kats, F. Aieta, J.-P. Tetienne, F. Capasso, and Z. Gaburro, “Light propagation with phase discontinuities: generalized laws of reflection and refraction,” Science 334(6054), 333–337 (2011).

[238]. R. I. Stantchev, X. Yu, T. Blu, and E. Pickwell-MacPherson, “Real-time terahertz imaging with a single-pixel detector,” Nat. Commun. 11(1), 2535 (2020).

[239]. S. L. Jacques, “Optical properties of biological tissues: a review,” Phys. Med. Biol. 58(11), R37–R61 (2013).

[240]. D.-H. Kim, “Fundamentals of propagation of light in tissue,” Theory Appl. Heat Transf. Humans 1, 153–166 (2018).

[241]. H. Key et al., “Optical attenuation characteristics of breast tissues at visible and near-infrared wavelengths,” Phys. Med. Biol. 36(5), 579–590 (1991).

[242]. S. E. Trevlakis, A. A. A Boulogeorgos, and N. D. Chatzidiamantis, “Pathloss modeling for in-body optical wireless communications,” 10th International Conference on Modern Circuits and Systems Technologies (MOCAST). Thessaloniki, Greece: IEEE; 1–6 (2021).

[243]. P. Jin, J. Fu, F Wang, Yingchao Zhang, Peng Wang, Xin Liu, Yang Jiao, Hangfei Li, Ying Chen, Yinji Ma, Xue Feng, “A flexible, stretchable system for simultaneous acoustic energy transfer and communication,” Sci. Adv. 7(40), 2507 (2021).

[244]. V. V. Tuchin, Tissue Optics: Light Scattering Methods and Instruments for Medical Diagnostics, 2nd ed., SPIE Press, Bellingham, WA (2009).

[245]. H. Senjuti, “Measurements and Characterization of Optical Wireless Communications through Biological Tissues,” Master. thesis, University of Oulu (2020).

[246]. A. J. Welch and M. J. C. van Gemert, Optical-Thermal Response of Laser-Irradiated Tissue, Plenum Press, New York (1995).

[247]. J. Ripoll, D. Yessayan, G. Zacharakis, and V. Ntziachristos, “Experimental determination of photon propagation in highly absorbing and scattering media,” J. Opt. Soc. Am. A 22(3), 546–551 (2005).

[248]. D. D. Nolte, Optical Interferometry for Biology and Medicine, Springer, New York (2012).